Structures and Dynamics of Disclinations and Inversion Walls in Nematic Polymers

by

Ding-Kuo Ding

SUBMITTED TO THE DEPARTMENT OF MATERIALS SCIENCE AND ENGINEERING
IN PARTIAL FULFILLMENT OF THE REQUIREMENTS FOR THE DEGREE OF

DOCTOR OF PHILOSOPHY
in Polymers

at the

MASSACHUSETTS INSTITUTE OF TECHNOLOGY

May 1994

Signature of Author _____
Department of Materials Science and Engineering
April 29,1994

Certified by _____
Professor Edwin L. Thomas
Thesis Supervisor

Accepted by _____
Carl V. Thompson II
Professor of Electronic Materials, Chair, Departmental Committee on Graduate Students

Structures and Dynamics of Disclinations and Inversion Walls in Nematic Polymers

by

Ding-Kuo Ding

Submitted to the Department of Materials Science and Engineering on April 29, 1994
in partial fulfilment of the requirements for the degree of Doctor of Philosophy

Abstract

The structures and dynamics of disclinations and inversion walls in nematic thermotropic liquid crystal polymers (TLCPs) are studied principally by polarized light optical microscopy and by atomic force microscopy via a lamellar decoration technique.

A schlieren texture composed of only integer strength point disclinations was created by thermal quenching from the isotropic state to the nematic state in a polyester TLCP based on methyl hydroquinone and 1,10-decane bisterephthaloyl chloride (MHDT). A first order red plate and quarterwave plate were used to determine the sign and structure of integer point disclinations. The annihilation behavior of disclination pairs was found to be similar to that for point defects in small molecule liquid crystals. The coarsening behavior of the schlieren textures was in good agreement with the scaling prediction of asymptotic behavior of disclination density $\rho(t) \sim t^{-1}$.

A solution for director orientation across Néel inversion walls in a liquid crystal placed in a magnetic field for different values of the elastic anisotropy was determined. This analysis redefined the appropriate characteristic length, containing the bend, k_{33}, and splay, k_{11}, elastic constants, for the Néel type inversion walls as $1/H((k_{11}+k_{33})/\chi_a)^{0.5}$. The elastic anisotropy of liquid crystal polymers may be obtained directly from microscopic images of inversion walls by measuring the director orientation with the lamellar decoration technique. Combined with the measurement of the wall width, the absolute value of elastic

constants, k_{11} and k_{33}, can be obtained with knowledge of the magnetic susceptibility anisotropy. Values of bend elastic constant, $k_{11}=2.8\cdot10^{-6}$ dyne, and splay elastic constant, $k_{33}=0.9\cdot10^{-6}$ dyne, of a polyether TLCP, based on 1-(4-hydroxy-4′-biphenyl)-2-(4-hydroxyphenyl)propane and α,ω-dibromopentane (TPP5), were obtained, and the measured elastic anisotropy is approximately 0.5 (i.e. $k_{11}=3k_{33}$).

The director patterns of Néel splay and Néel bend walls, which are formed via magnetic field alignment, of TPP5 were characterized and identified by optical and atomic force microscopy. The Néel inversion walls form irregularly shaped loops or terminate in disclinations of half integral strength. The inversion walls are metastable, and may shrink, smooth, coalesce, and/or split into a wall terminated by two opposite sign disclinations. These mechanisms lead to the uniform equilibrium state with the director parallel to the field direction. Our calculation of the energy of inversion walls with elastic anisotropy provided insight to the inversion wall dynamics and the shape of isolated shrinking loops.

Thesis Supervisor: Professor Edwin L. Thomas
Title: Morris Cohen Professor of Materials Science and Engineering

Acknowledgements

I would like to express my deep appreciation to my thesis supervisor, Professor Edwin L. Thomas, for his freedom, guidance, support and helpful discussion throughout this thesis. This freedom, which I could not learn from outside, creates many ideas to try out.

I am grateful to the members of my thesis committee, Professor Robert Armstrong, Professor Peggy Cebe and Professor Chris K. Ober, for their helpful discussion in the research.

I am indebted to Professor Vigil Percec for providing the TPP5 polymer sample and to Prefessor Chris K. Ober for helping the synthesis of MHDT polyester at Cornell University. I gratefully acknowledge use of the superconducting magnet facility at the Bitter National Magnet Laboratory, Cambridge, MA, and the help of Dr. L. Rubin and D. Lynch.

I would like to thank all those who gave me help in my doctoral years and in research work: Steven D. Hudson, Mary Jane O'Rourke, Debbie Vezie, Stephanie Simmons, Janelle Gunther, Bruce Carvalho, John Chen, Christian Honeker, Robert Lescanec, Marcelo Villar, Martha Himes, Alick Chang, Hwaping Chang, Chen-an Chen, Hui-Ching Hsieh, Linda Lee, Susan Kam, and Mei-Rong Wu.

Financial support from the Ministry of Education, Taiwan, ROC, and AFOSR grants 90-0150 and 91-0078 are greatly appreciated.

Table of Contents

List of Figures

etched sample in figure 4a showing the detailed director fields of a positive integer defect and negative integer defect. The director fields of the schlieren texture are directly seen due to lamellar decoration.

Figure 2.5: (a)The schlieren texture under cross polars. (b) The schlieren texture with first order red plate. (c) Sample stage rotated 45° from (b). (d) The schlieren texture with quarterwave plate. (e) Defects are identified by positive and negative sign.

Figure 2.6: A typical pair annihilation sequence with experimental time shown on the left side. A pair of defects are pinned at the right side.

Figure 2.7: OM between crossed polars of overall isothermal coarsening sequences of schlieren textures, created by a thermal quench.

Figure 2.8: The pair distance D vs time before annihilation for three sets of data. The slope fits the scaling prediction by Pargellis et al.

Figure 2.9 : Defect density vs annealing time at 160°C using data as in figure 2.7.

Figure 3.1: (a) Schematics of the molecular director across three types of π Helfrich inversion walls, including Néel bend (bend-splay), Néel splay (splay-bend), and Bloch (twist) walls. (b) The planar director field of Néel inversion wall loops and extinction regions under cross polars. There are two parallel-like extinction lines along the inversion wall when the polarizer is oriented 45° to the direction of the magnetic field. The wall appears as a bright region with a single central dark extinction line when the polarizer is parallel to the field.

Figure 3.2: PLM images of transient textures at short time response during magnetic reorientation before the Néel walls well developed.

Figure 3.3: AFM image of transient texture with the developing Néel bend and Néel splay walls.

Figure 3.4: Two possible reponses upon magnetic reorientation: (a) developing walls along the field, and (b) normal to the field.

Figure 3.5: Schematic mechanism for formation of a Néel inversion wall loop. (a) A magnetic field is applied normal to the initial direction of molecules, n_0. (b) The molecules tend to reorient parallel or antiparallel to the field. (c) The molecules in region A reorient by clockwise rotation and the molecules in regions B and C reorient by counterclockwise rotation, a Néel bend wall is formed parallel to the field and a Néel splay wall normal to the field. (d) A Néel inversion loop is formed.

Figure 3.6: PLM images of inversion wall loops in TPP5 indicating Néel type inversion walls. Not only elliptical shaped but irregular inversion wall loops are formed. (a) The polarizer is oriented 45° to the direction of the magnetic field. (b) The polarizer is parallel to the field.

Figure 3.7: (a) PLM image and AFM micrograph of a portion of Néel bend inversion wall terminated at -1/2 disclination and a Néel inversion wall loop in TPP5. (b) AFM micrograph of a Néel splay wall terminated at a -1/2 disclination and a distorted +1/2 disclination.

Figure 3.8: The coalescence of two inversion wall loops into one inversion wall and the collapse of the inversion wall with production of a disclination line pair.

Figure 3.9: Shrinkage and smoothness of the Néel inversion wall evolution at a subsequent time.

Figure 3.10: (a) AFM image of two coalescing Néel bend walls. (b) Suggested coalescent mechanism of molecular trajectories between two bend walls.

Figure 3.11: The processes of coalesce and anisotropic shrinkage of Néel wall loops with various ellipticities.

Figure 3.12: (a) Schematic of the movement of disclinations along a circular Néel inversion wall loop. (b) The magnitude of forces with respect to the azithumal angle θ.

Figure 4.1: Schematics of the molecular director across π inversion walls : (a) Néel bend-splay walls parallel to the field at different values of elastic anisotropy, and (b) Néel splay-bend walls normal to the field at different values of elastic anisotropy. These figures are based on the numerical solutions in figure 4.2.

Figure 4.2: (a) Numerical solutions of director fields across Néel bend and Néel splay walls at different values of elastic anisotropy. Curves 1 to 7 are the solutions of ε=1, 0.9, 0.5, 0, -0.5, -0.9, -1 for Néel bend walls, while curves 1 to 7 correspond to ε=-1, -0.9, -0.5, 0, 0.5, 0.9, 1, respectively, for Néel splay walls. Open circles and stars represent the measured values utilizing the lamellar decoration method for a AFM and HRSEM[2] image. Best fit of the experimental data for TPP5 (open circles) is $\varepsilon \approx 0.5$ and for HBA/HQ/PA (stars) is $\varepsilon \approx 0$. (b) Calculated director orientation across Néel bend walls. (c) Calculated director orientation across Néel splay walls. Curve 1 is the molecular trace for the easy splay case in Néel splay walls. Curve 1 also represents the lamellar image of a Néel bend wall for the easy bend case.

Figure 4.3: (a) AFM micrograph of a portion of Néel splay inversion wall in TPP5. The observed lamellae are perpendicular to the local molecular director and the deformation is approximately two dimensional. (b) Height variation across the Néel bend invresion wall indicating a small amount of out of plane (twist) deformation.

List of Table

CHAPTER 1

INTRODUCTION TO LIQUID CRYSTAL TEXTURES

In recent years scientists and engineers have become interested in thermotropic liquid crystal polymers (TLCPs) because of their attractive properties, combining both virtues from polymers and from liquid crystals, such as excellent mechanical strength, processability (low melt viscosities), and optical anisotropy. Their unusual physical properties have made them exciting materials for more fundamental research. The study of defects in ordered media has become an important subject in materials science, since defects play an important role in determining the relationship between structure and properties of materials. Liquid crystals exhibit a variety of striking textures, such as the schlieren texture of the nematic phase, the fingerprint texture of the cholesteric phase, and the focal conic texture of the smectic phase. These patterns arise due to the influence of defect structure on the long range molecular order of liquid crystals, and these characteristic textures may be used as indicators of mesophase identity.

Thermotropic liquid crystal polymers can be used in applications such as high strength fibers, field-active display and waveguide modulators. Understanding and controlling the defect textures becomes an important issue in these applications. The molecules in the liquid crystal phase are free to move as in a liquid, but they tend to remain oriented in a certain direction call the *director*. In this introductory chapter, the basics of defects in nematic liquid crystals and the concept of the *director*, which guides the understanding of defect textures, will be discussed. The underlying physics of defect structures and their dynamics in nematic polymers derives essentially from the distortional free energy of defects in liquid crystals, which is described in the following sections. Chapter 2 is devoted to defect structures in thermotropic liquid crystal polyesters. A schlieren texture with only $s=\pm1$ point defects formed by special boundary conditions is

investigated. This integer point defect texture has not previously been reported and identified in nematic thermotropic liquid crystal polymers (TLCPs). The point defect dynamics are also observed and compared to defect annihilation in small molecule liquid crystals (SMLCs).

Although the transient textures and inversion walls formed by a magnetic field have been studied in small molecule liquid crystals, the detailed molecular trajectories and the interaction between inversion walls are unexplored. In chapter 3, the director patterns of Néel inversion walls (splay-bend and bend-splay inversion walls) of a nematic thermotropic liquid crystal polyether are examined by optical microscopy and imaged at higher resolution via a lamellar decoration technique using atomic force microscopy. Inversion walls that form irregularly shaped loops or terminate in disclinations of half integral strength are presented. The dynamics of the inversion walls is also studied from an energetic view. The analysis of chapter 4 concerning the influence of elastic anisotropy on inversion wall structure is used to evaluate the energy per unit area of Néel bend and Néel splay walls. We gain insight to the dynamics of inversion wall during magnetic reorientation.

Elastic constants are basic material constants of liquid crystals. Elastic constants are of importance in determining the response time and threshold field strength for switching (molecular reorientation) in the presence of an applied field, such as in liquid crystal display applications. It is of interest to investigate the influence of elastic anisotropy on structure of the inversion wall, a defect structure formed by an applied field, and on inversion wall dynamics. Chapter 4 shows how the structures of the inversion walls depend on elastic anisotropy, and gives a new approach to determine the elastic anisotropy and elastic constants in TLCPs.

Chapter 5 summarizes the results of the thesis and suggests some future directions of liquid crystal defect research.

1.1 Definition of the three types of liquid crystal phases and their associated director fields

Liquid crystals are usually classified into three types: nematics, cholesterics and smectics (figure 1.1), according to the molecular order. It is apparent that nematics have long range uniaxially orientational order. The direction of orientation is characterized by the director field. The director is a dimensionless, nonpolar vector **n** (here **n** and **-n** are equivalent), which represents the direction of local preferred orientation of the molecules in the neighborhood of any point. Its orientation can change continuously in the medium except at some singularities.

Nematics usually consist of rodlike molecules (rigid units), which may be small molecules or the rigid segments of polymer chains. These rigid molecules tend to align with their long axes parallel to each other, which leads to a preferred direction **n**. The amount of ordering, another important aspect of orientational order, may be characterized by a local order parameter S:

$$S = 3/2\langle(\mathbf{p}_i\cdot\mathbf{n})^2\rangle - 1/2 \ , \qquad (1.1)$$

where the orientation of each rigid unit, $\mathbf{p}_i$ ($\mathbf{p}_i$ is, for example, along the segment axis) with respect to the director, **n**, is averaged. The order parameter is one for perfect alignment and zero in the isotropic phase. The order parameter of a liquid crystal decreases as the temperature increases. For typical nematics, $S \sim 0.6 - 0.8$.

The nematic phase is thermodynamically stable, and the phase transition between the nematic state and the isotropic state is of first order. There are two basic types of liquid crystal polymers: main chain LCPs, whose rigid segments are connected head to tail or there may be some flexible segments inserted between rigid units, and side chain LCPs, whose pendant rigid segments are attached to the flexible polymer backbone. A number of polymers, made of alternating rigid and flexible segments, give liquid crystal phases. Such liquid crystal phases when achieved by purely thermal processes are termed thermotropic. The liquid crystal phase may be also induced by increasing the concentration of polymer

(removing solvent at constant temperature); such LCPs are called lyotropic. This thesis exclusively deals with thermotropic LCPs.

1.2 Elastic free energy

A liquid crystal acts like an elastic medium under small deformation. There are three independent modes of distortions of a liquid crystal: splay, twist and bend (figure 1.2). The elastic constants, the so-called Frank constants, corresponding to these distortions are k_{11}, k_{22}, and k_{33}. If the director changes its direction only over large distances, i.e. there are only small gradients, the distortional free energy, g, may be expanded in powers of **n** from continuum theory as:[1]

$$g = \frac{1}{2} k_{11} (\nabla \cdot n)^2 + \frac{1}{2} k_{22} (n \cdot \nabla \times n)^2 + \frac{1}{2} k_{33} (n \times \nabla \times n)^2 \qquad (1.2)$$

When the orientation of director is uniform, the distortional free energy will be equal to zero, as the ground state of nematic phase. Since the uniaxial nematic phase is apolar and centrosymmetric, the free energy g is an even function of **n**, containing only $(\nabla \mathbf{n})^2$ terms.

For typical nematics, the Frank elastic constants are approximately 10^{-6} dynes.[2] The bend and splay constant are approximately equal, while the twist constant is significantly lower. The bend elastic constant in nematics increases with the persistence length, and the splay constant is proportional to the chain length.[3] It is expected that the splay constant is the largest in liquid crystal polymers. It should be also noted that the values of these elastic constants decrease rather strongly when temperature increases, since the order parameter decreases to zero in the high temperature isotropic state.

In the elastically isotropic case ($k_{11}=k_{22}=k_{33}$), the free energy density reduces to:

$$g_{el} = 1/2\, k\, (\nabla \mathbf{n})^2. \qquad (1.3)$$

Consider the two dimensional case, taking $n_x = \cos \phi$, $n_y = \sin \phi$ and $n_z = 0$. The Euler-Lagrange equation which minimizes the total free energy is then the Laplacian of ϕ:

$$\nabla^2 \phi = 0\,. \qquad (1.4)$$

Since the free energy expression depends only on the gradients of the director field and not on the specific orientation of the director, the distortions tend to disperse over the entire space of the director field.

1.3 Disclinations in nematics

In continuum theory the orientation of director field is assumed to be smooth. In fact, however, there are some line and point singularities in the orientational field, and the discontinuities in these fields are called disclinations. They are a type of rotational defect in liquid crystals, similar to dislocations in solids. The difference is that disclinations change both relative position and relative inclination, while dislocations change relative position only.[4,5]

1.3.1 The Volterra process

The Volterra process describes the creation of a line singularity in a perfectly ordered medium. The perfect medium is cut along a surface S, forming a cut bounded by a line L (figure 1.3[5]). Two lips S_1 and S_2 of the cut are displaced relative to each other by a translation, or a rotation, or a combination of both. Material is added to fill the void or material is removed so that the medium is smoothly connected along the two lips and allowed to relax.

When the disclination line, **L**, is along the axis of rotation, Ω, the disclination is called a wedge disclination. If **L** and Ω are perpendicular, the disclination is called a twist disclination (figure 1.4[6]). Disclinations may be characterized by a topological strength. The strength of a disclination, *s*, is defined by the number of times the director rotates by an angle 2π about the axis of the singularity. A positive value of *s* corresponds to the case in which the circulational direction of the Frank-Nabarro circuit is the same as the rotational direction of director.

S is a sheet of discontinuity after cutting and displacement. However, if the rotational angle Ω is such that two cut lips can match continuously, the resulting conformation is everywhere continuous, except on the line L. In nematics the condition for this is that Ω is a multiple of π, which is allowed by the orientational symmetry of medium.

Figure 1.5 demonstrates the Volterra process in the xy projection to create a -1/2 wedge disclination singularity line[5]. The medium is cut along S in (a), then two lips are separated by an angle π (b); perfect medium is inserted the void along S_1 and S_2. The medium is allowed to relax and produce the -1/2 disclination with its characteristic 3-fold rotational symmetry.

1.3.2 Disclination Structure

As mentioned above, the director is distorted around the disclination, especially in the vicinity of the central core, since the distortion grows as the director approaches the disclination core. In the two-dimensional case, as in a thin film which the director may be parallel to the film plane (xy-plane), there are only splay and bend distortions, and the disclination lines are normal to the surfaces. When the medium is elastically isotropic, i.e. $k_{11} = k_{33}$, the Euler-Lagrange equation becomes

$$\left(\frac{\partial^2 \phi}{\partial \theta^2}\right) = 0 \qquad (1.5)$$

as has already been solved by Frank.[1] The director field is simply

$$\phi = s\theta + c \quad , \qquad (1.6)$$

where θ = arctan (y/x), c is a constant, and s is the strength of the disclination. The value of s is chosen to make the solution single valued. This means that changing θ by 2π must retain the same director field. Since **n** and -**n** are indistinguishable, the angle ϕ must be equal to $m\pi$ when θ turns by 2π. m is any integer except zero, and m=0 means a uniform director field without a disclination (monodomain). The director fields of disclinations with various strength for a material with $k_{11}=k_{33}$ are shown in figure 1.6.[5]

To find the two dimensional director fields for a disclination with elastic anisotropy ($k_{11} \neq k_{33}$), the free energy density may be written in polar coordinates (figure 1.7) as:[7]

$$g(r, \phi(\theta)) = \frac{k}{2r^2} \left(\frac{\partial \phi}{\partial \theta}\right)^2 (1+\varepsilon \cos 2(\phi-\theta)) \tag{1.7}$$

where r is the radial distance from the disclination center (core), ϕ is the angle between director and reference axis (ϕ is only a function of θ). θ is the angle of rotation from the reference axis. ε is the elastic anisotropy given as:

$$\varepsilon = \frac{k_{11} - k_{33}}{k_{11} + k_{33}} \tag{1.8}$$

and $k=(k_{11}+k_{33})/2$ is the mean elastic constant. The corresponding equation of equilibrium is

$$0 = \left(\frac{\partial^2 \phi}{\partial \theta^2}\right) (1 + \varepsilon \cos 2(\phi-\theta)) + \left[2\left(\frac{\partial \phi}{\partial \theta}\right) - \left(\frac{\partial \phi}{\partial \theta}\right)^2 \right] \varepsilon \sin 2(\phi-\theta) \tag{1.9}$$

The energy of an isolated disclination in a circular layer of radius R and unit thickness can be calculated as:

$$E = \iint g(r)\, r\, dr\, d\theta = E_c + \pi k s^2 \ln (R / r_c) \ , \tag{1.10}$$

where E_c is the unknown disclination core energy with a core radius r_c. Note that as $R \rightarrow \infty$, $E \rightarrow \infty$, i.e. an isolated disclination in an infinite medium would have infinite energy, but such a situation does not arise in practice due to the presence of pairs of disclinations with opposite signs to compensate the overall molecular distortions.

The energy of single defect is proportional to s^2; therefore, defects of strength $|s|>1/2$ should be unstable and dissociate into $|s|=1/2$ defects. Disclinations of integral strength, however, may escape into the third dimension leaving the core nonsingular.[8] The line singularity is relieved by a favorable splay-bend distortion and leave a point singularity at the end. Point disclinations may be observed at the interface between a nematic and an isotropic liquid, and they may be visualized as originating on integral lines at the encounter of two opposite escapes.

Experimentally, most of the defects in TLCPs which have been found are indeed half integer disclination, which is consistent with the theoretical prediction.[4,9] However, a schlieren texture comprised of only integer strength ($s=\pm1$) point defects was created by special boundary conditions and thermal quenching from the isotropic state to the nematic state. The structures of point integer disclinations and their dynamics will be described more fully in chapter 2.

1.3.3 Interaction between disclinations

Since in the equiconstant case, the differential equation for the director field is linear, the director field of a material containing an array of disclinations is simply described by superposition of the individual director fields $\phi(x,y)$:

$$\phi(x,y) = \sum_i s_i \tan^{-1}\left(\frac{y-y_i}{x-x_i}\right) \quad , \tag{1.11}$$

where disclination i of strength s_i is located at coordinates (x_i,y_i).

The interaction between disclination lines is analogous to electrostatics, unlike sign pairs of defects attract each other while like sign pairs repel. The energy of a pair of disclinations separated by a distance r_{12} is given as:

$$E = \pi k (s_1+s_2)^2 \ln (R / r_c) - 2\pi k\, s_1\, s_2 \ln (r_{12}/ 2r_c) \, , \tag{1.12}$$

with the assumption of $r_c << r_{12} << R$. The force on each disclination, $F_{12}=dE/dr_{12}$, due to the another is:

$$F = - \frac{2\pi k\, s_1\, s_2}{r_{12}} \quad , \tag{1.13}$$

which is inversely proportional to their separation and acts along the line of their separation.

As mentioned, disclinations of opposite sign, which act as a long range dipole, tend to attract each other to lower the distortional energy. Eventually they can annihilate leaving behind undisturbed material. In chapter 2, we find the relation between pair separation, D,

and annihilation time, t_0, scales as $D \sim (t_0-t)^{0.5}$ which is in good agreement with scaling solution prediction by Pargellis et al.[10]

A cluster of four disclinations (two of each sign) with a special diamond type arrangement, called the Lehmann configuration, are commonly observed in either magnetically or extensionally flow-aligned samples.[9] Figure 1.8 shows the calculated director patterns of Lehmann clusters without an external field. Note that the distortion of a Lehmann cluster is quite localized. Hudson and Thomas have found that the Lehmann clusters are stabilized at intermediate field strengths, but a second-order symmetry-breaking transition occurs at high fields, where the two pairs of opposite signed disclinations selectively interact and annihilate.[9]

1.4 Inversion walls: defect structures in the presence of an external field

In addition to point or line singularities (disclinations) in nematic liquid crystals, there are also possible nonsingular surface defects, such as Helfrich inversion walls in uniformly nematic liquid crystals under an external field.[11] The director distribution across these walls is continuous. Walls may form loops or terminate at sample boundaries or terminate in disclinations.

1.4.1 Helfrich inversion walls

When a liquid crystal is placed in a magnetic field, the free energy density can be written as:[2]

$$g = g_{el} - \frac{1}{2}\mu_0 H^2 (\chi_\perp + \chi_a \cos^2\psi) \qquad (1.14)$$

where g_{el} is given by equation 1.1; H is the strength of the applied magnetic field; ψ is an arbitrary angle between magnetic field and the director field; $\chi_a = (\chi_{||} - \chi_\perp)$, where $\chi_{||}$ and $\chi_\perp$ are the principal diamagnetic susceptibilities per unit volume along and perpendicular to the director field. The macroscopic diamagnetic susceptibility anisotropy, χ_a, is equal to $N \cdot S \cdot (\zeta_{||} - \zeta_\perp)$, where N is the number of rigid units per unit volume, S is the orientational

order parameter, and $\zeta_{\parallel}(\zeta_{\perp})$ is the diamagnetic susceptibility of a single rigid unit parallel (perpendicular) to its long axis.[12] Note that the orientational order parameter, S, relates the macroscopic anisotropy to the microscopic order, and the molecular susceptibility contains both parallel and perpendicular induced magnetic dipoles within a rigid unit. For a positive χ_a, the director therefore favors a parallel or antiparallel orientation to the field for minimum energy.

A region separating the parallel and antiparallel alignment along an applied field is called an inversion wall since the director passing through it turns by π. An inversion wall can be a twist wall or a bend-rich wall or a splay-rich wall, similar to the Bloch or Néel walls in spin systems[4,11] (figure 1.9). For the equiconstant case, the width of the wall can be characterized by twice the magnetic coherence length, $\xi = (k/\chi_a H^2)^{1/2}$, which describes the size of the distorted region in the magnetic field. The stronger the field, the smaller is the distorted region. By measuring ξ from TEM images of samples containing walls thermally quenched in a magnetic field of known strength, the elastic constants can be determined if χ_a is known for the material.[13,14]

A flow field can orient the director field as well as magnetic or electric fields. Since the nematic is an anisotropic liquid, the viscosity is expected to depend on the orientation of the director with respect to the velocity gradient. From Leslie-Ericksen (LE) theory of nematic continuum, the viscous stress σ_{LE} is:[15,16]

$$\sigma_{LE} = \alpha_1 n_\alpha n_\beta n_\mu n_\rho A_{\mu\rho} + \alpha_2 n_\alpha N_\beta + \alpha_3 n_\beta N_\alpha + \alpha_4 A_{\alpha\beta} + \alpha_5 n_\alpha n_\mu A_{\mu\beta} + \alpha_6 n_\beta n_\mu A_{\mu\alpha}, \quad (1.15)$$

where A is the rate of deformation tensor, N_i is the angular velocity of the director relative to that of the fluid and the Greek indices denote x, y or z. n_α represents the local director along the α-direction. The constitutive parameters α_i (i=1...6) possess dimensions of viscosity, so-called Leslie coefficients. α_2 and α_3 play a special role since α_2 and α_3 are the coefficients relating to the viscous torque when the director is parallel to the velocity gradient or to the flow direction, respectively.

If the director field is planar, the differential equation derived for the director field subjected to flow and magnetic fields is:[17]

$$0 = [(\alpha_3 - \alpha_2)\frac{\partial}{\partial t} - k(\frac{\partial^2}{\partial x^2} + \frac{\partial^2}{\partial y^2})]\phi + \chi_a H^2 \sin(\phi - \phi_H)\cos(\phi - \phi_H)$$
$$- 2(\alpha_3 + \alpha_2)\dot{e}\sin\phi\cos\phi - 2\dot{\gamma}(\alpha_3\cos^2\phi - \alpha_2\sin^2\phi) \qquad (1.16)$$

where α_i are Leslie coefficients, k is the Frank elastic constant, χ_a is the magnetic susceptibility, $\dot{e}$ and $\dot{\gamma}$ are the rate of strain for elongational and shear flow respectively, ϕ is the angle between director field and x-axis, and ϕ_H is the angle between magnetic field and x-axis. Each of these terms represents a torque in the director. As can be seen from equation 1.16, the effect of elongational flow on the director is expected to be analogous to that of an applied magnetic field. Hudson and Thomas [9] have exploited this correspondence to observe texturing of defects in nematic liquid crystalline polymers. They found many inversion walls and characteristic disclination clusters in both types of fields.

1.4.2 Interaction of disclinations and inversion walls

Inversion walls may be formed during magnetic reorientation. Such walls are a higher energy state since they contain localized molecular distortions. Since the lowest energy state of a liquid crystal in the presence of an external field is full alignment along the field, the inversion walls are metastable and tend to decay to the uniform equilibrium state. They may shrink or interact with each other to annihilate. A wall segment may also collapse by the production of disclinations. All these mechanisms lead towards the uniform equilibrium texture.

Rey calculated the velocity of a disclination line attached to π inversion wall in a magnetic field using an entropy balance approach and obtained:[18]

$$v \sim (2H/\pi\gamma_1 s^2 \ln(\xi/r_c))(\chi_a k)^{1/2} \sim (2k/(\pi\gamma_1 \xi s^2 \ln(\xi/r_c))) . \qquad (1.17)$$

The velocity thus scales with the inverse of the wall thickness and the ratio of elastic to viscous effects k/γ_1. Rey[19] also showed that a splay-bend inversion wall segment may collapse by the production of disclinations (figure 1.9).

The interaction between disclinations and inversion walls or between inversion walls and themselves has been seldom investigated. The interactive potential energy between two opposite inversion walls (one is the inverted image of the other) in the equal elastic case can be described as:[20]

$$U = U_0 + 4\chi_a H^2 \exp(-2d/\xi) \tag{1.18}$$

where 2d is the distance between the walls. The force that one inversion wall feels from the other is

$$f = \frac{\partial U}{\partial d} = 4k/\xi \exp(-2d/\xi) \tag{1.19}$$

In the more general case, the interaction between two inversion walls with elastic anisotropy possesses similar physics but a different energy of interaction. A detailed description of the interaction of inversion walls is yet incomplete. We traced the formation of these walls and followed the evolution of their interaction to gain insight into the mechanism of molecular reorientation during magnetic field alignment.

1.5 Introduction to the thesis

The purpose of this dissertation is to obtain a better understanding of the behavior of defects in thermotropic liquid crystal polymers (TLCPs), and the mutual interaction of defects in a sample with or without an externally applied field. The definitions and basics of nematic liquid crystal textures have been introduced in the first chapter. The experimental work for observing the textural features mainly employs optical microscopy (OM), scanning electron microscopy (SEM), transmission electron microscopy (TEM), and atomic force microscopy (AFM). Since LCPs are birefringent, polarized light provides an excellent tool to study LCP textures. For planar samples, orientations of the director

parallel to either the polarizer or the analyzer produce an extinction of the light intensity. This characteristic makes OM suitable to identify disclinations and inversion walls. Details are given in the following chapters. However, a major limitation of the light microscope is the relatively low resolution, just under a micron.

The superior resolution of SEM, TEM, and AFM has been used to image director textures of TLCPs.[13,14,21] The information on the director fields of disclinations, of inversion walls, and on interacting inversion walls can be obtained. A combination of OM and AFM techniques permits time evolution of structures at various length scales since both these observational techniques are nondestructive.

Structures of point disclinations and their annihilation behavior in TLCPs is investigated in chapter 2. Point disclinations are created by special boundary conditions and thermal quenching from the isotropic state into the nematic state. The director patterns around the point disclinations are revealed by scanning electron microscopy (SEM) using lamellar decoration and an amine etch technique.[22]

In chapter 3, we study the response of the director to a magnetic field. A transient texture develops first and eventually evolves into Néel inversion walls. Since the lowest energy state, uniform orientation along the field, is still available, Néel inversion walls are metastable. We investigate the transient textures, the formation mechanism of Néel inversion walls, and the interaction dynamics of inversion walls.

As previously mentioned, the elastic anisotropy of liquid crystals plays a crucial role in their response to an applied field, for example, the application of an electric field in a liquid crystal display. In chapter 4, we numerically solve the differential equation describing the director orientation across Néel inversion walls under an applied magnetic field, and plot the structures of Néel inversion walls at different values of the elastic anisotropy. The values of the elastic anisotropy for a specific liquid crystal material were obtained from the images through the direct measurement of the director field.

Chapter 5 summarizes the principal findings of this dissertation and suggests new directions of research on defects in TLCPs. In this dissertation, we are able to gain insight into the structure and dynamic behavior of disclinations and inversion wall through direct microscopied observation of the director field and numerical solution to the director orientation across Néel inversion walls and the corresponding Néel wall energy. The findings of this dissertation provide study of defects in LCPs with a direct method to investigate the interactive behavior among disclinations and Néel inversion walls.

References

(1) Frank, F. C. *Disc. Faraday Soc.* **1958**, 25, 19.

(2) de Gennes, P. G. *The Physics of Liquid Crystals*; Clarendon Press: Oxford, 1974;

(3) Meyer, R. B. *Polymer Liquid Crystals*; A. Ciferri; W. R. Drigbaum; R. B. Meyer, Eds; Academic Press: New York, 1982; 133.

(4) Kléman, M. *Points, Lines, and Walls*; Wiley: Chichester, 1983;

(5) Demus, D.; Richter, L. *Textures in Liquid Crystals*; Verlag Chemie: New York, 1978;

(6) Harris, W. F. *Scientific American* **1977**, 237, 130.

(7) Chandrasekhar, S.; Ranganath, G. S. *Advances in Physics* **1986**, 35, 507.

(8) Kléman, M. *Liquid Crystallinity in Polymers*; A. Ciferri, Eds; VCH: New York, 1991; 365.

(9) Hudson, S. D.; Thomas, E. L. *Physical Review A* **1991**, 44, 8128.

(10) Pargellis, A.; Turok, N.; Yurke, B. *Physical Review Letters* **1991**, 67, 1570.

(11) Helfrich, W. *Phys. Rev. Lett.* **1968**, 21, 1518.

(12) Priestley *Introduction to Liquid Crystals*; E. B. Priestley; P. J. Wojtowicz; P. Sheng, Eds; Plenum Press: New York, 1975; p 71.

(13) Hudson, S. D., *Polymer Nematic Liquid Crystals: Disclination Structure and Interaction*; University of Massachusetts at Amherst: 1990;

(14) Ding, D.-K.; Thomas, E. L. *Macromolecules* **1993**, 26, 6531.

(15) Ericksen, J. L. *Trans. Soc. Rheol.* **1961**, 5, 23.

(16) Leslie, F. M. *Archs Ration. Mech. Anal.* **1968**, 28, 265.

(17) Stephen, M. J.; Straley, J. P. *Rev. Mod. Phys.* **1974**, 46, 617.

(18) Rey, A. D. *Liquid Crystals* **1990**, 7, 315.

(19) Rey, A. D. *Liquid Crystals* **1989**, 4, 409.

(20) de Gennes, P. G. *J. de Phys.* **1971**, 32, 789.

(21) Hudson, S. D.; Thomas, E. L. *Physical Review Letters* **1989**, 62, 1993.

(22) Hudson, S. D.; Vezie, D. L.; Thomas, E. L. *Makromol. Chem., Rapid Commun.* **1990**, 11, 657.

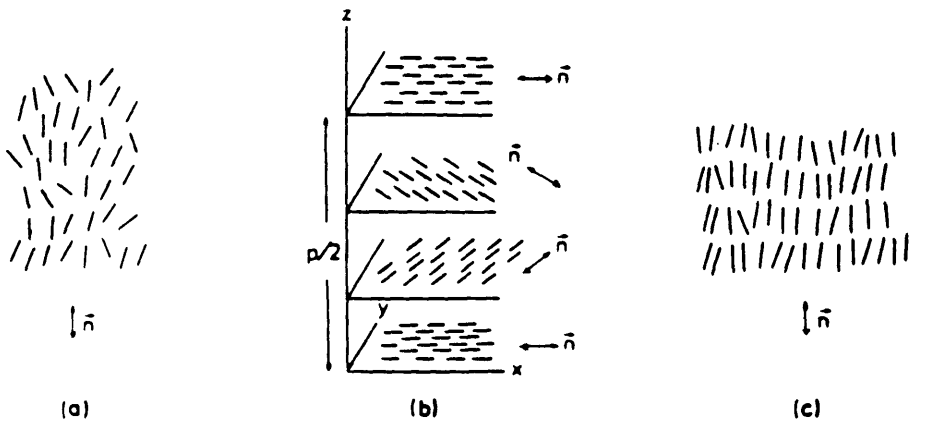

Figure 1.1: nematic, cholesteric or chiral nematic, and smectic.

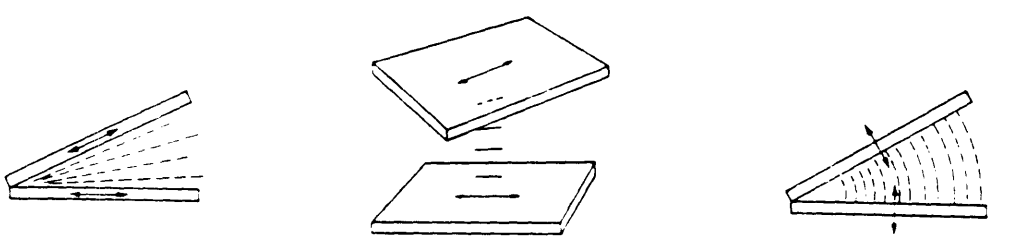

Figure 1.2: Three types of distortion in a nematic liquid crystal.

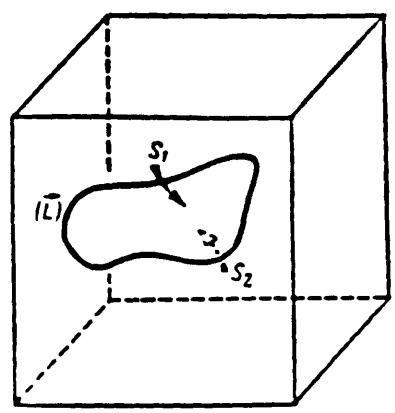

Figure 1.3: A singularity line $\vec{L}$ generated by a Volterra process.[5]

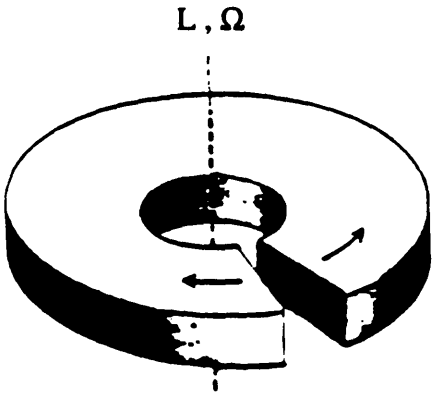

Wedge disclination

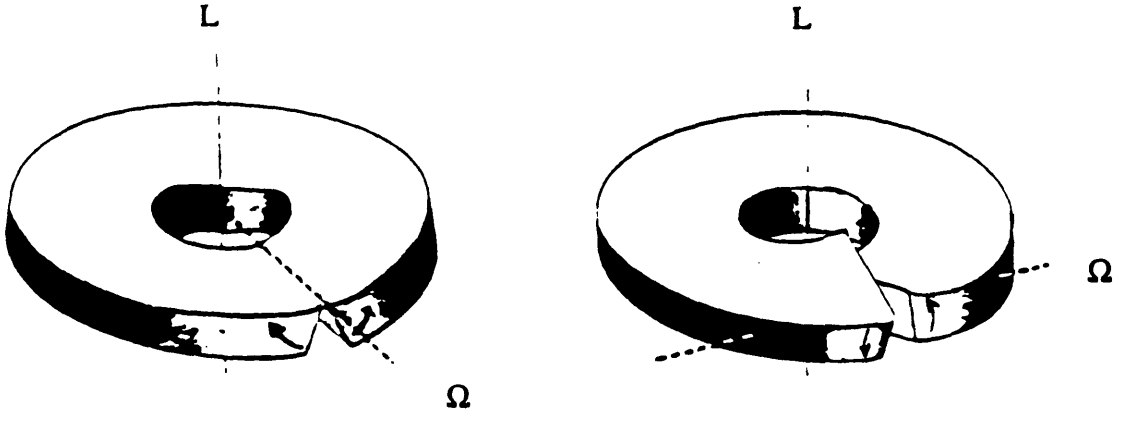

Twist disclinations

Figure 1.4: Wedge disclination (disclination line, L, parallel to rotational axis, Ω) and twist disclinations (disclination line, L, perpendicular to rotational axis, Ω).

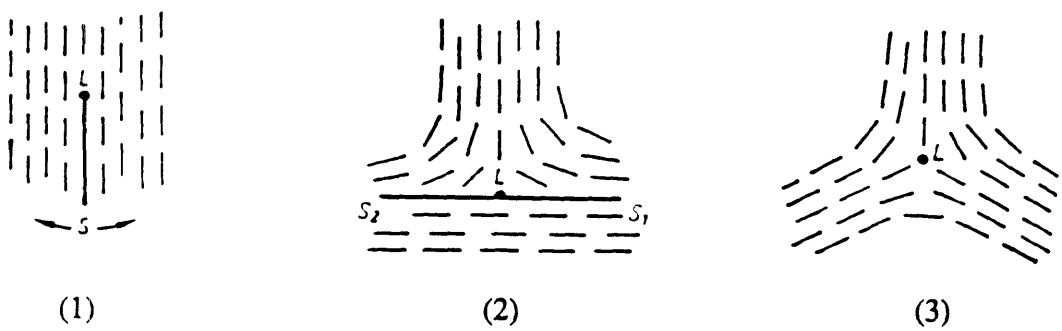

Figure 1.5: A Volterra process of creating a -1/2 disclination.

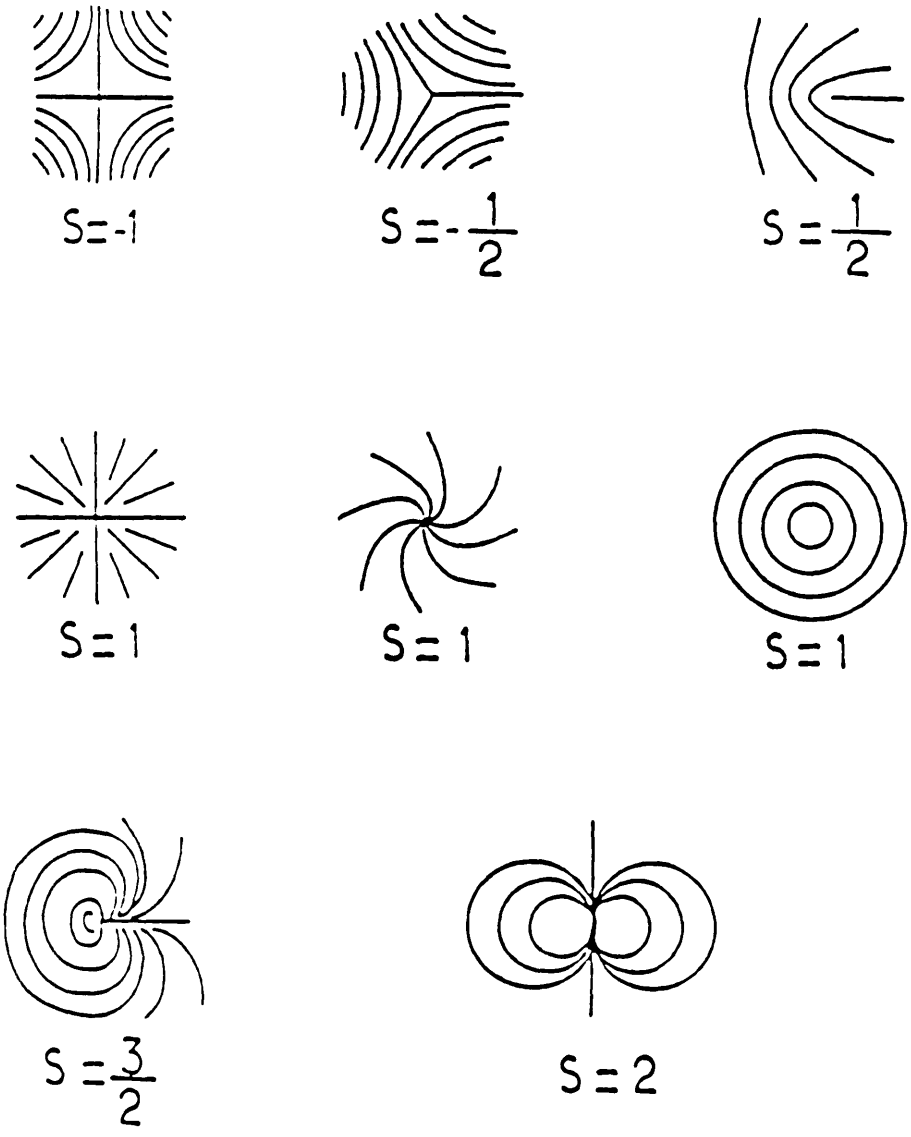

Figure 1.6: Director patterns of disclinations with different strength.[1]

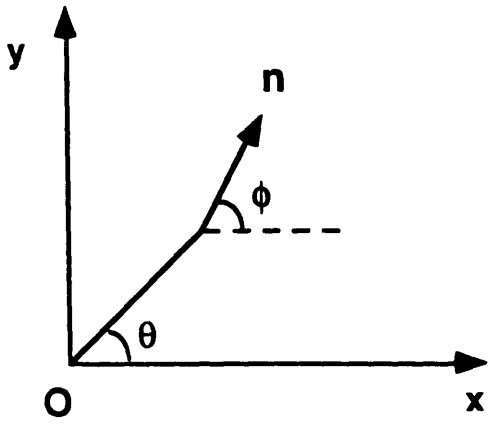

Figure 1.7: Schematic of polar coordinate

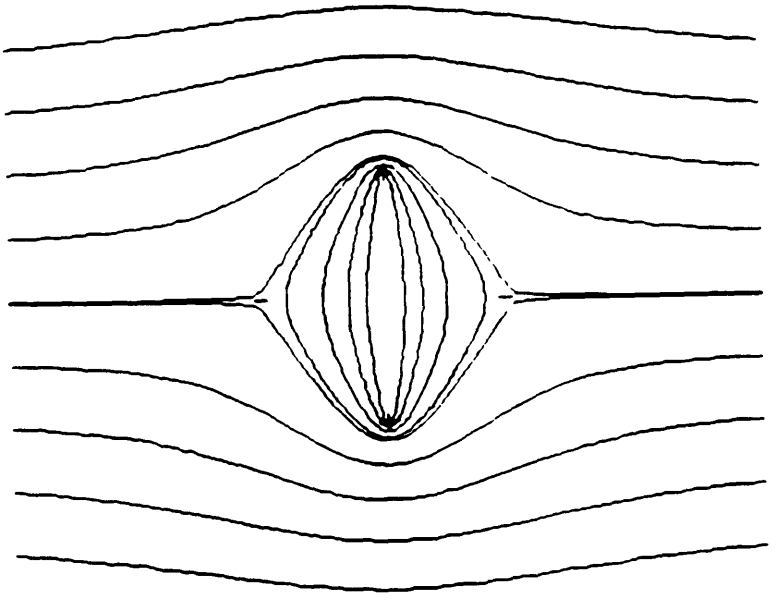

Figure 1.8: Director patterns of a Lehmann cluster comprised of two pairs of ±1/2 dislcinations.

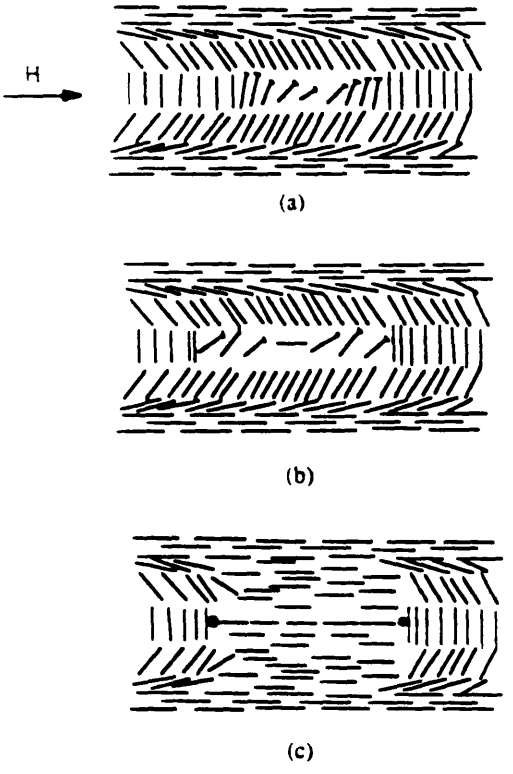

Figure 1.9: Schematic of a splay-bend wall dissolution.[19] (a) The wall is unstable to two dimensional perturbations. (b) The non-linear evolution results in the nucleation of a ±1/2 disclination pair. (c) The wall pulls the disclination lines apart.

CHAPTER 2

STRUCTURES OF POINT INTEGER DISCLINATIONS AND THEIR ANNIHILATION BEHAVIOR IN THREMOTROPIC LIQUID CRYSTAL POLYESTERS

Abstract

A schlieren texture composed of integer strength point disclinations has been observed in a thermotropic liquid crystal polymer. The director patterns about positive and negative disclinations are studied by optical microscopy and scanning electron microscopy. Defects are located at the specimen-air interface and occur due to the different boundary conditions of the liquid crystal at the air and glass interfaces. The annihilation behavior of these integer defects, created by a temperature-drop procedure from an initial isotropic state into the nematic state, was also investigated. It was found the relation between pair separation, D, and annihilation time, t_0, was $D \propto (t_0-t)^{0.5}$, which was in good agreement with the recent scaling solution prediction by Pargellis et al.[1]

2.1 Introduction

In recent years scientists and engineers have become interested in thermotropic liquid crystal polymers because of their attractive properties, combining virtues from polymers and from liquid crystals. Their unusual physical properties have made them exciting materials for fundamental research. The schlieren textures of liquid crystals are easily visible under optical microscope. These textures essentially originate from rotational defects in the orientationally ordered liquid. Defects and textures are well described in the monographs by Demus and Richter[2] and by Kléman.[3] In nematic phases there are two main kinds of rotational defects: line and point disclinations. Defects are characterized by their strength, s, defined by the total change of the orientation of the director in a circuit

around the singularity divided by 2π. A positive (negative) value of strength corresponds to the case which the circulational direction and the rotational direction of director are the same (opposite). The director distortions involved in point disclinations are three dimensional, whereas line disclinations in thin films produce a two dimensional distortion. Most line disclinations found in liquid crystals are half-integer defects due to their more favorable energetic state. However, integer defects with nonsingular cores due to director escape in the third dimension may be found in thin capillaries.[4]

A typical procedure to create defects in a liquid crystal is to use symmetry breaking via the phase transition from the disordered isotropic phase to the ordered phase by varying the temperature or pressure.[5] DeGennes[6] has also described a way to create point defects by applying a magnetic field normal to the liquid crystal free surface or to the interface between the nematic and isotropic phase with a homogeneous or conical boundary condition. Meyer [7] has studied point disclinations at the upper air surface in a nematic small molecule liquid crystal (SMLC). A regular network of point disclinations in a SMLC without a magnetic field has been observed[8], in which the homeotropic boundary condition at the glass-specimen interface played the role of the magnetic field in deGennes' description. Point defects may also be found along the central axis of a glass tube.[1,4,9] The orientation at the glass boundary is approximately homeotropic while it is approximately homogeneous in the center of the tube.

Integer strength disclinations in thermotropic liquid crystal polymers have seldom been reported or commented upon, although several published images reveal their presence.[10,11] In this paper, we describe the nature of integer point defects in a thermotropic liquid crystal polyester produced simply by changing temperature through the isotropic-nematic phase transition. The sign of the integer defects is determined using a first order red plate or a quarterwave plate under polarized light. Their detailed director structures are revealed via the lamellar decoration technique[12] with optical microscopy and scanning electron microscopy. In addition to the structure of defects, we also study the

defect dynamics. Defect dynamics in liquid crystals has recently become an important issue since the defect strings provide a laboratory system to test the "one-scale" model for cosmic string evolution.[5] Only a few investigations have reported the dynamic behavior of defects in polymeric or in small molecule liquid crystals.[1,13-15] Recently, a small molecule liquid crystal, 4-cyano-4'-*n*-pentylbiphenyl, was used to study the dynamic behavior of integer point defects, created by an order-disorder phase transition.[1] The pair annihilation and coarsening behaviors of the schlieren texture of our polymeric liquid crystal samples were similar to the SMLC scaling-solution prediction.

2.2 Experimental

The material used in this study is a main chain semi-flexible thermotropic liquid crystal polyester based on 1,10-decane bisterephthaloyl chloride with methyl hydroquinone (MHDT). This polymer was synthesized at Cornell University with the help of Prof. C. Ober, and its synthesis and characterization are described in more detail in reference 16. The transition temperatures are T_{cn}=145°C and T_{ni}=170°C. Repeated DSC traces demonstrate that MHDT is relatively chemically stable under thermal cycling up to approximately 200°C. This stability makes it possible to conduct nematic-isotropic transitions by thermal cycling, whereas most liquid crystal polymers become unstable when they approach their isotropic (clearing) temperature.

A thin polymer film about 10 μm thick was prepared in the melt state by blade shearing on a glass slide. The glass slide is first cleaned with chloroform in an ultrasonic bath, followed by immersion in a stirred solution of hydrogen peroxide/ammonia/water (1:1:5 mixture) at 70°C. The glass slide is then washed by water and dried by nitrogen gas. After blade shearing, the polymer film sample, whose top surface is free, is placed in a Linkam hot stage and heated into the isotropic state (180°C). The temperature was then quickly dropped to 160°C which is just below the isotropic-nematic transition temperature[7] to create a large number of defects. The sample was then kept at constant temperature to

allow some defect annihilation for easier examination. These defect textures could be captured by slow cooling or by quenching the sample into room temperature water. To directly visualize the defect structures, the samples were then annealed for a short time at a temperature 25°C below melting temperature. During annealing, the quenched glassy nematic polymer partially crystallizes into a lamellar morphology, where the director of the remaining glassy liquid crystal is normal to the lamellae. The lamellar serve to decorate the underlying molecular arrangement of the frozen nematic.[12] Finally, for good contrast in SEM, the sample was etched within 40 wt% methylamine in water[17] and coated with Au and viewed in secondary electron imaging mode (SEI) with a Cambridge Instruments SEM at 5 KeV. To study the defect annihilation behavior, the whole process, including the defect creation and the coarsening of schlieren textures at constant temperature (160°C), was recorded in situ using a Zeiss optical microscope (OM) equipped with Javelin video camera.

2.3 Results and Discussion

2.3.1 Defect Structures

Defects in liquid crystals cause abrupt changes of the director field resulting in elastic distortion of the director configuration near them. Defects prefer to form in pairs of opposite sign to compensate long range elastic distortion, known as splay cancellation. A defect pair (dipole pair) will tend to approach one another until they annihilate to minimize the total energy. A stable dipole pair may be formed by an air bubble (which acts as a positive integer defect) compensating a negative integer point defect.[7]

A typical schlieren texture of integer strength defects is shown in figure 2.1, which is very similar to the defect textures in SMLCs. The schlieren textures produced by the temperature-drop defect creation procedure are different each time, that is, the defects are randomly created. The sign of each defect can be determined by rotating the crossed polars.

The defects do indeed form in negative-positive pairs, which can be confirmed by tracing the connecting brushes.

From continuum theory[18], assuming the director is confined to the xy-plane, the energy of an individual defect is proportional to s^2. Defects of strength $|s| > 1/2$ should be unstable and dissociate into $|s| = 1/2$ defects. Dzyaloshinskii[19] has shown that a s=1 concentric line defect is stable only if $k_{22}>2k_{33}$ and $k_{11}>k_{33}$. It is expected that the s=1 line defect occurs only rarely in typical nematics because of the usual small value of the twist elastic constant k_{22}.

Disclinations of integer strength are always formed in our experiments. We believe this kind of schlieren texture of *only* integer defects in a main chain thermotropic liquid crystal polymer has not been previously reported. These integer defects are point defects which arise in the present case due to the particular boundary conditions at the air interface (homogeneous) and at the glass interface (homeotropic) (see schematic figure 2.2). Whether or not a singular line integer defect is stable or "escapes" to a point defect for this thermotropic polyester material is unknown at present. Attempts at producing a radial s=+1 line defect in a glass capillary with homeotropic conditions were unsuccessful due to sample handling difficulties.

To prove an approximate homeotropic condition with the glass surface, a thin film was made between two glass slides. If homeotropic conditions occur at both glass-specimen boundaries, then the sample will not show any birefringence through crossed polars since in this arrangement the molecular axes are along the optical axis (uniaxial). Apparent zero birefringence is indeed observed for samples between two glass slides and this oriented nematic state can be distinguished from the isotropic state by simply pressing on the cover glass causing some nonaxial orientation, which causes the dark nematic region to brighten immediately. The approximately homogeneous condition at upper free surface can be shown by the edge-on lamellar orientation described next.

To directly visualize the director pattern at the upper (air) sample surface at high resolution, the lamellar decoration and etch technique is used.[12,17,20] The director field (molecular axes) is revealed in SEM images by the pattern of crystalline lamellae (~15nm thick), which are formed by crystallization during the quench or upon sample annealing. TEM and electron diffraction prove that the molecular axes are normal to the lamellae so the director pattern is the set of trajectories orthogonal to the pattern of lamellae, which means the molecular axes are in the plane of the film at the upper free surface. To enhance SEI contrast an amine etch is used. The ester linkages in MHDT are cleaved by the amine and the etching rate of noncrystalline glassy nematic regions between the lamellae is faster than that of the crystalline lamellae. Therefore, the edge-on lamellae protrude from the polymer surface such that the director fields can be imaged by SEI in the SEM (or by TEM of surface replicas[21]).

Optical microscopy may be used to determine the sign of the integer defects. Figure 2.3 is a crossed-polars OM image of radial (s=+1) and hyperbolic (s=-1) defects. Stripes result from sample crystallization into bundles of parallel oriented lamellae during the cooling process, and the different interference colors arise from regions of different sample thickness. A low magnification OM of the schlieren texture fields is shown in figure 2.4a. Figure 2.4b is an SEM micrograph showing better detail of director patterns around integer defects. The individual integer defect structures of s=+1 and s=-1 are clearly evident in the pattern of the lamellae. Since the molecular axes are normal to the lamellae, the schematic inserts show the actual director patterns.

When either a quarterwave plate or a first order red (Red I) plate is employed with the differential interference contrast mode, image contrast increases and yellow and blue regimes will be present, depending on the local orientation and film thickness. Such color images are useful to determine the approximate orientation of the molecular axis from birefringent interference figures, which correspond to the fast and slow directions of the transmitted light. For a quarterwave plate, if the fast component in the sample and

quarterwave plate are parallel, the total path difference is increased, and the interference color goes up scale, perhaps to yellow. If the fast component of the sample is parallel to the slow component of the plate, the interference color goes down to blue. The reverse occurs for insertion of a Red I plate, i.e. the color shows blue if the fast components in the sample and the plate are parallel, while showing yellow if the slow component of the sample is parallel to the fast component of the plate.

Usually the fast component of transmitted light (smaller index of refraction) is along the main chain molecular axis, thus it is easy to identify the approximate orientation of the molecules. Figure 2.5 shows the interference image of the schlieren texture using a Red I (figure 2.5a, 2.5b) or a quarterwave (figure 2.5c) plate. For the s=+1 defect, since the director field is symmetrical around the defect, when the sample is rotated 45°, the interference color does not change, while the interference color of the s=-1 rotates around the defect (figure 2.5a and 2.5b). One way to identify s=-1 defects is to find points whose blue color crosses two quadrants, which indicates the asymptotic axes of the defect are in between the polarizer and analyzer directions. Once one defect is identified, it is easy to determine the sign of an adjacent defect by tracing the brushes connecting the opposite sign defect. In our samples, if a Red I plate is inserted, the interference color of s=+1 defects is blue for the second and fourth quadrants, which means the molecular axes are approximately tangential about the defect center. This is consistent with SEM which shows radial lamellae near the disclination core corresponding to a concentric molecular director pattern about the defect. The s=+1 defects are thus approximately pure bend, suggesting $k_{11}>k_{33}$ for this TLCP. Hudson and Thomas[21] previously measured the elastic anisotropy ε, $\varepsilon=(k_{11}-k_{33})/(k_{11}+k_{33})$ of this same polyester and found $k_{11}=1.5k_{33}$ in agreement with the concentric (easy bend) s=+1 defect director pattern in figure 2.4b. Points with blue color in the first quadrant can be identified as s=-1 defects.

2.3.2 Annihilation Behavior

Defects of opposite sign tend to attract each other until they annihilate to minimize the distortional energy. Figure 2.6 shows a typical pair annihilation sequence which occurs during isothermal coarsening of the schlieren texture . In this case the positive defect seems to move faster than the negative one, but the reverse effect were also found with other defect pairs. Figure 2.7 shows a sequence of schlieren textures between crossed polarizers during the isothermal coarsening process. A square quad-defect was formed (lower-center region of micrograph) and the shape is maintained during annihilation. This implies the velocity of both positive and negative integer defects is similar. Such a symmetric arrangement of four disclinations (two positive, two negative) was depicted in Lehmann's 1918 monograph.[22] A similar zero net dipole arrangement of four half integer defects has been identified in both flow and magnetic field oriented TLCPs.[23]

The variation of defect mobility may be due to some impurities, or the presence of lower or higher molecular weight polymer around the core area of the defects impeding the movement of defects. Mazelet and Kléman[24] have noted the movement of s=-1/2 defects is faster than the movement of s=+1/2 defects, which they suggest may be due to an excess concentration of chain ends at the disclination core for the +1/2 defects.

Recently, experimental and theoretical investigations have concerned the time evolution of both the number density of defects, $\rho(t)$, and the separation distance between opposite signed defects, D(t). By assuming that the approach velocity depends inversely on the defect separation distance, Pargellis et al.[1] predicted D(t) is given $(t_0-t)^{0.5}$, where t_0 is the time to annihilation. Considering the number density of the defects and the average separation distance of a pair-defect, these two quantities can be related by $D \propto \rho^{-1/d}$, where d is the spatial dimensionality. In the two dimensional case, defects move within the plane, therefore, the number density is scaled by the annihilation time as $\rho(t) \sim t^{-1}$. An earlier model by Dreizin and Dykhne [25] also produces a $D(t) \propto (t_0-t)^{0.5}$ behavior by assuming that the attractive interaction between defects is balanced by the retarding viscous force.

Pargellis et al.[1] found $D(t) \propto (t_0-t)^{0.5}$ behavior at large times for point defects induced in a SMLC via pressure jumps or thermal quenches. A similar result for the defect pair separation was observed in films for which the thickness exceeds the typical separation distance[26]. However, other experimental results yielded $D(t) \propto (t_0-t)$ behavior for samples which the thickness was much less than pair separation distance.[1,27] A different experimental power law, $D \propto t^{0.35}$ was determined by Shiwaku et al.[28] in a liquid crystal polymer system containing predominantly half-integer defects with the average defect separation distances larger than polymer film thickness (1μm).

Three data sets of separation distance D against time before annihilation (one from figure 2.6) are plotted in figure 2.8. The scaling relation between separation distance and annihilation time is approximately $D \propto (t_0-t)^{0.5}$, where separation distances are from 1-30 μm and the film thickness is around 10 μm. It is straightforward but somewhat tedious to count the total number of defects in our system, especially at the beginning of the annihilation process. Figure 2.9 shows as the number of defects decreases with time, the average distance between neighboring defects increases. The data fit the anticipated t^{-1} power law for times between 30 seconds and 500 seconds. At longer times, we find a tail effect. This tail effect results from pinned defects due to impurities or lower molecular weight material still in the isotropic state at the temperature of observation (160°C). These motionless defects are always accompanied by a defect of opposite sign, as noted by Meyer.[7]

2.4 Summary

We have described a simple way to create integer point defects and to study the annihilation behavior of these defects in a thermotropic liquid crystal polyester. The schlieren texture comprised of only integer strength ($s=\pm1$) defects was created by thermal quenching from the isotropic state to the nematic state. The detailed director patterns around defect nuclei were observed by scanning electron microscopy using the lamellar decoration

technique. The defects are identified as point disclinations arising due to the different boundary conditions, one (homogeneous) at the free surface and one (homeotropic) at the glass-polymer interface. The schlieren textures are statistically reproducible with thermal cycling. In addition to the method of rotation of cross polars to determine the sign of the disclinations, the first order red plate and quarterwave plate methods were also used to determine the sign of integer point disclinations. The dynamic behavior of defects in liquid crystals, which is related to topological defects in the universal view, was also investigated. The annihilation behavior of defect pairs in our sample is similar to that for point defects in small molecule liquid crystals.[1,26] The pair separation distance decreases with annihilation time t_0 as $D \propto (t_0-t)^{0.5}$. The coarsening behavior of schlieren textures from experimental results are in good agreement with the scaling prediction[5] of asymptotic behavior of disclination density $\rho(t) \propto t^{-1}$.

References

1. A. Pargellis, N. Turok, and B. Yurke, *Physical Review Letters* **67**, 1570 (1991).
2. D. Demus and L. Richter, *Textures in Liquid Crystals* (Verlag Chemie, New York, 1978).
3. M. Kléman, *Points, Lines, and Walls* (Wiley, Chichester, 1983).
4. P. E. Cladis and M. Kléman, *J. Phys., Paris* **33**, 591 (1972).
5. I. Chuang, R. Durrer, N. Turok, and B. Yurke, *Science* **251**, 1336 (1991).
6. P. G. DeGennes, *The Physics of Liquid Crystals* (Clarendon Press, Oxford, 1974).
7. R. B. Meyer, *Mol. Cryst. Liq. Cryst.* **16**, 355 (1972).
8. N.V. Madhusudana and K.R. Sumathy, *Mol. Cryst. Liq. Cryst.* **129**, 137 (1985).
9. A. Saupe, *Mol. Cryst. Liq. Cryst.* **7**, 59 (1973).
10. G. Galli, M. Laus, A.S. Angeloni, P. Ferneti, and E. Chiellini, *Eur. Polym. J.* **21**, 727 (1985).
11. P. LeBarny, J.C. Dubois, C. Friedrich, and C. Noel, *Polym. Bull.* **15**, 341 (1986).
12. E.L. Thomas and B.A. Wood, *Faraday Discuss. Chem. Soc.* **79**, 229 (1985).
13. T. Shiwaku, A. Nakai, H. Hasegawa, and T. Hashimoto, *Polymer Communications* **28**, 174 (1987).
14. P.E. Cladis, W. van Saarloos, P.L. Pinn, and A.R. Kortan, *Phys. Rev. Lett.* **58**, 222 (1987).
15. S. Rojstaczer and R.S. Stein, *Mol. Cryst. Liq. Cryst.* **157**, 293 (1988).
16. S. Antoun, R.W. Lenz, and J.I. Jin, *J. Polymer Sci. Polym. Chem. Ed.* **19**, 1901 (1981).
17. S.J. Organ and P.J. Barham, *Polymer Preprints* **29**, 602 (1988).
18. F.C. Frank, *Disc. Faraday Soc.*, **25**, 19 (1958).

19. I.E. Dzyaloshinskii. *Sov. Phys. JETP* **31**, 773 (1970).

20. S.D. Hudson, D.L.Vezie, and E.L. Thomas, *Makromol. Chem., Rapid Commun.* **11**, 657 (1990).

21. S.D. Hudson and E.L. Thomas, *Physical Review Letters* **62**, 1993 (1989).

22. O. Lehmann, *Die Lehre von den flussigen Krystallen* (Wiesbaden, Bergman, 1918).

23. S.D. Hudson and E.L. Thomas, *Physical Review A* **44**, 8128 (1991).

24. G. Mazelet and M. Kléman, *Polymer* **27**, 714 (1986).

25. Y.A. Dreizen and A.M. Dykhne, *Sov. Phys. JETP* **34**, 1140 (1972).

26. A.S. Sonin, A.N. Dhuvyrov, A.A. Sobachkin, and V.L. Ovchinnikov, *Sov. Phys. Solid State* **18**, 1805 (1976).

27. O.D. Lavrentovich and S.S. Rozhkov, *JETP Letter* **47**, 254 (1988).

28. T. Shiwaku, A. Nakai, H. Hasegawa, and T. Hashimoto, *Macromolecules* **23**, 1590 (1990).

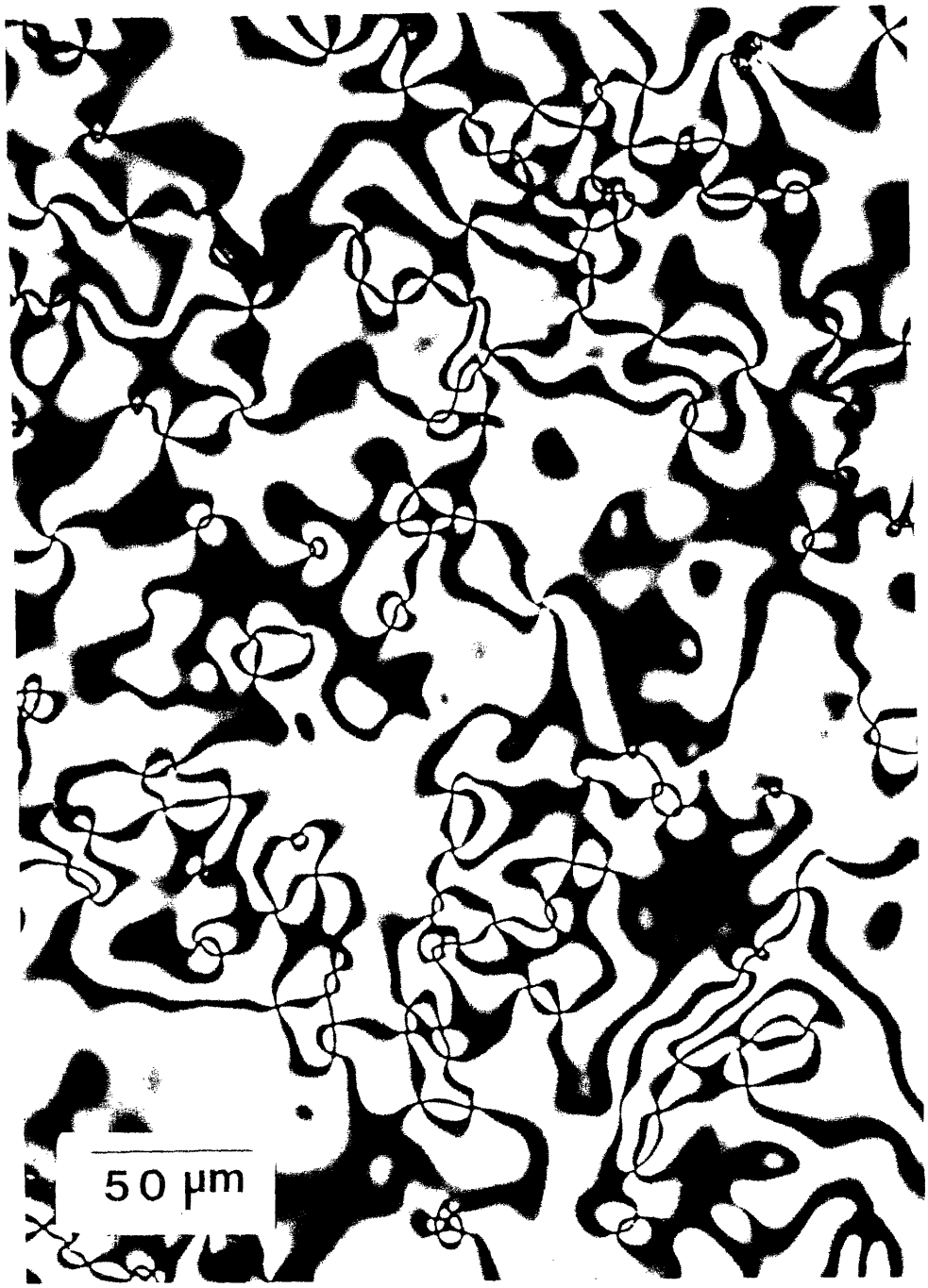

Figure 2.1: OM of schlieren texture of MHDT film created by quenching the sample from the isotropic (180°C) state to the nematic (160°C) state. The points with four brushes indicate the presence of integer defects of s=±1.

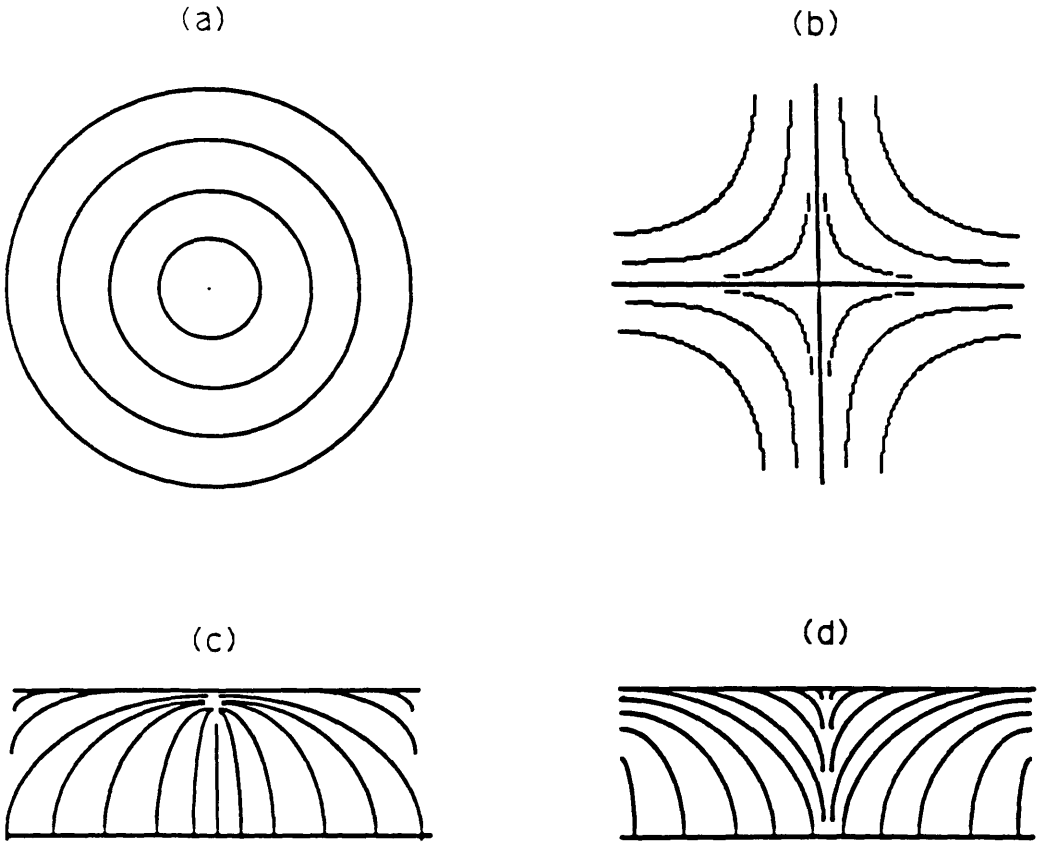

Figure 2.2: Schematic of the integer defects structure[7]. (a) and (b) show the top view. (c) and (d) show the side view.

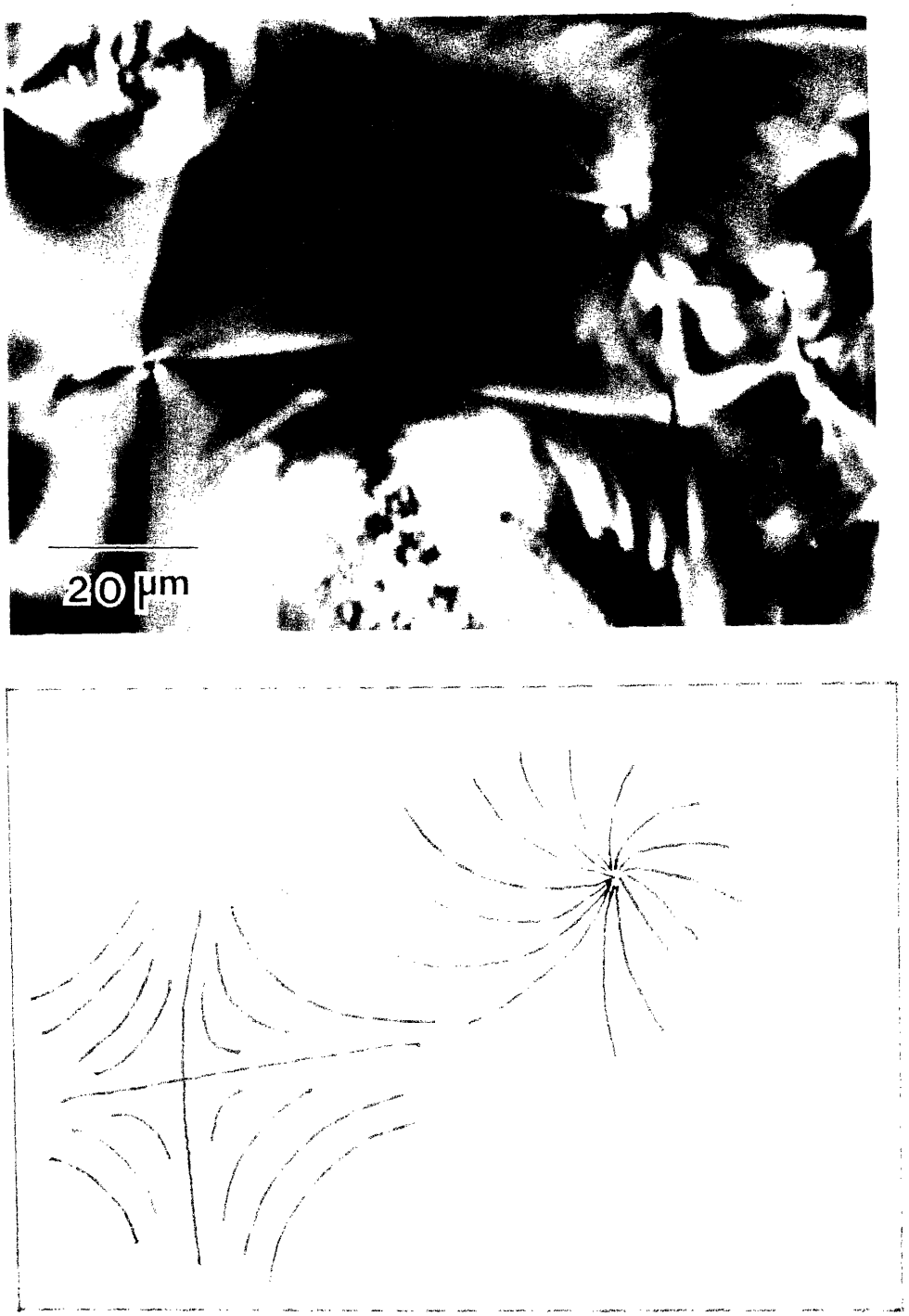

Figure 2.3: OM of integer defects of MHDT quenched from the nematic state into room temperature water. The stripes resulted from sample crystallization during the cooling process.

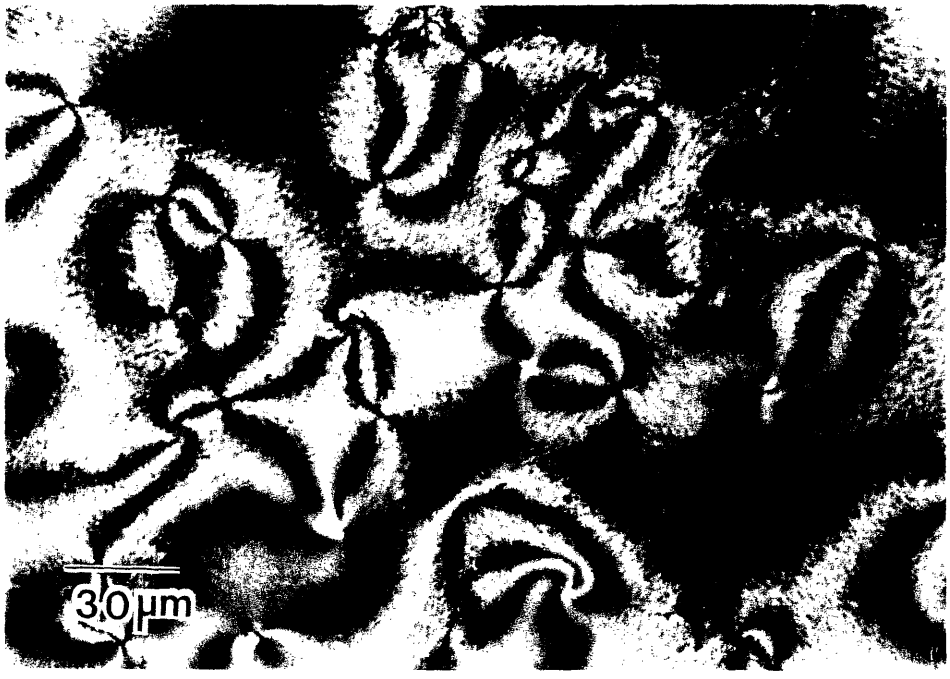

Figure 2.4(a): OM of MHDT quenched to room temperature, and annealed at 120°C for 15 minutes, and etched in 40 wt% methylamine/water solution for 20 minutes.

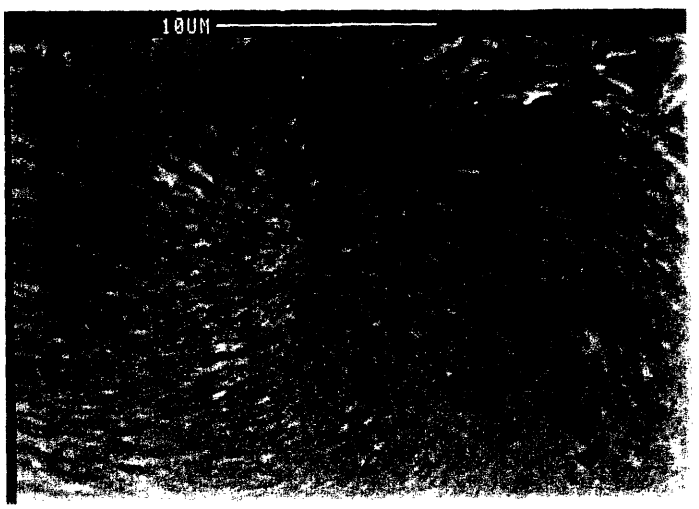

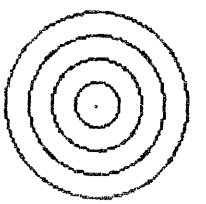

S = +1

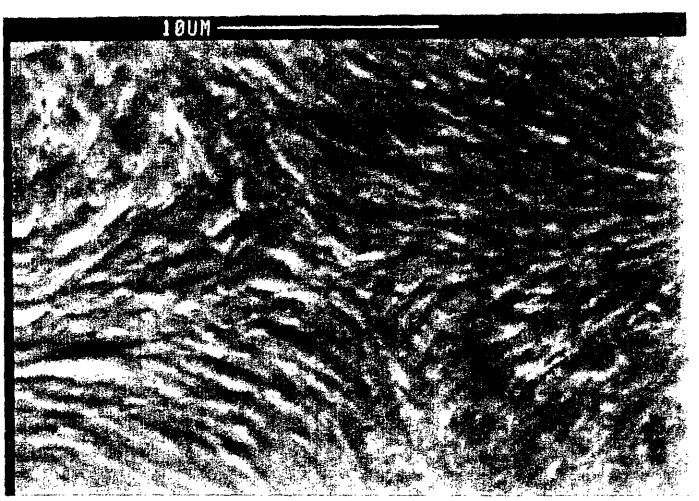

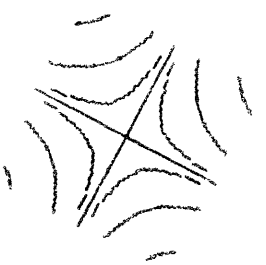

S = -1

Figure 2.4(b): SEM of the etched sample in figure 4(a) showing the detailed director fields of a positive integer defect and negative integer defect. The director fields of the schlieren texture are directly seen due to lamellar decoration.

Figure 2.5(a): The schlieren texture under cross polars.

Figure 2.5(b): The schlieren texture with first order red plate.

Figure 2.5(c): Sample stage rotated 45° from (b).

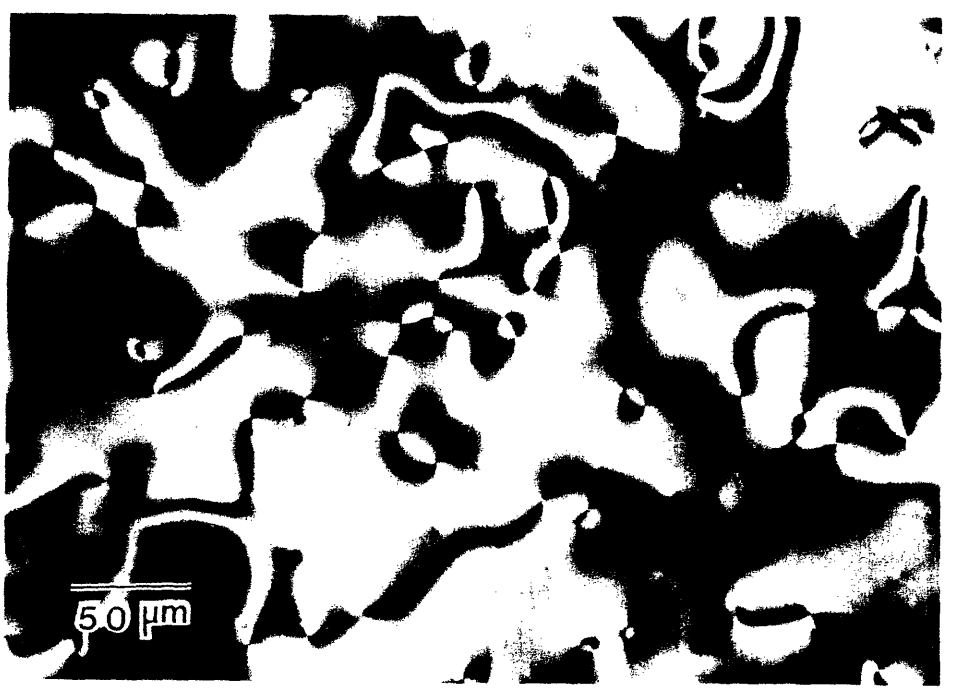

Figure 2.5(d): The schlieren texture with quarterwave plate.

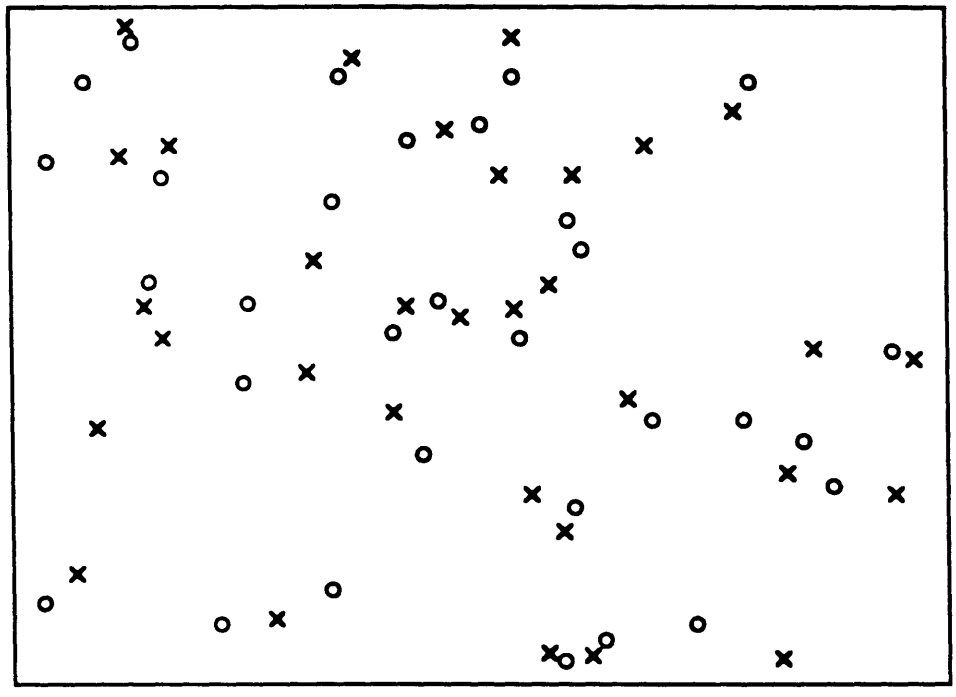

Figure 2.5(e): Defects are identified by positive (open circle) and negative (cross) sign.

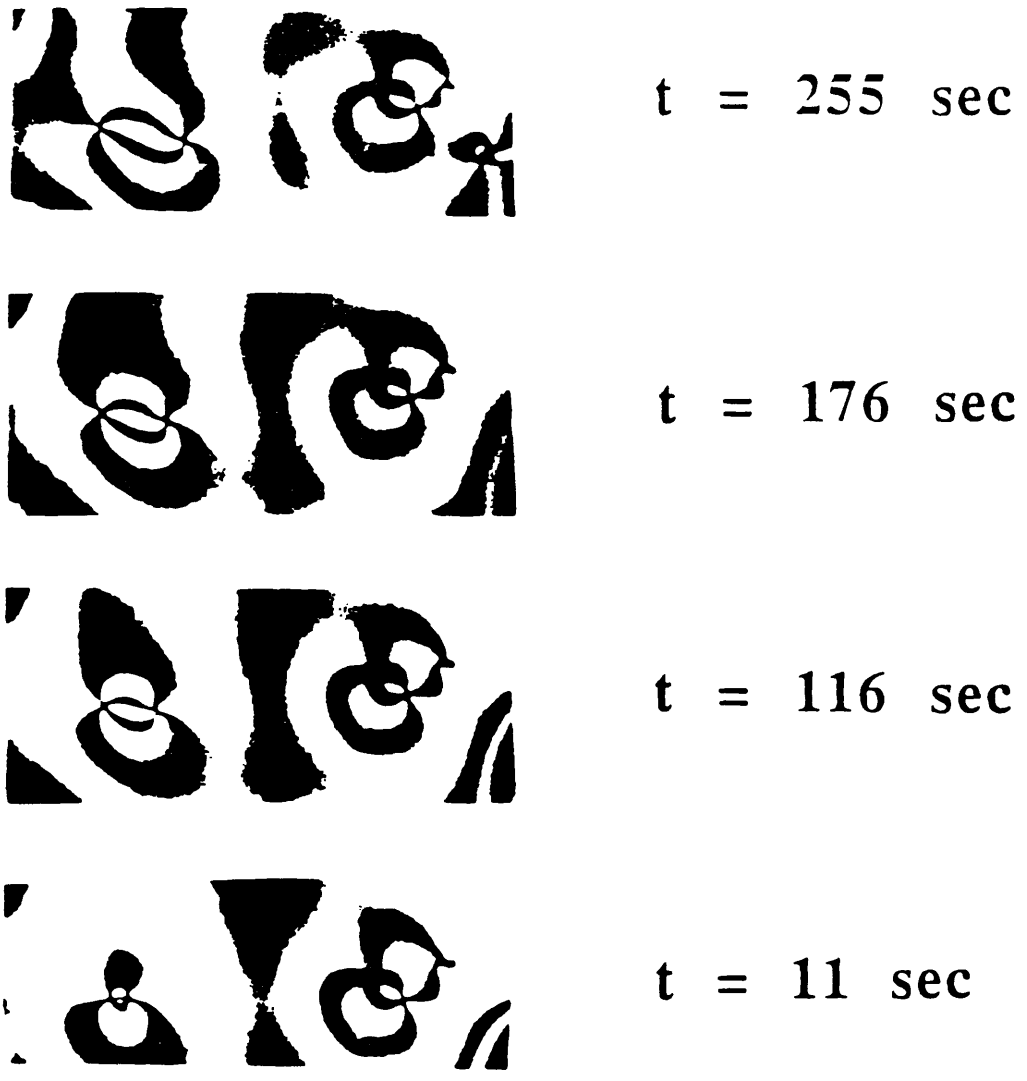

Figure 2.6: A typical pair annihilation sequence with experimental time shown on the left side. A pair of defects are pinned at the right side.

(a)

t = 1 s

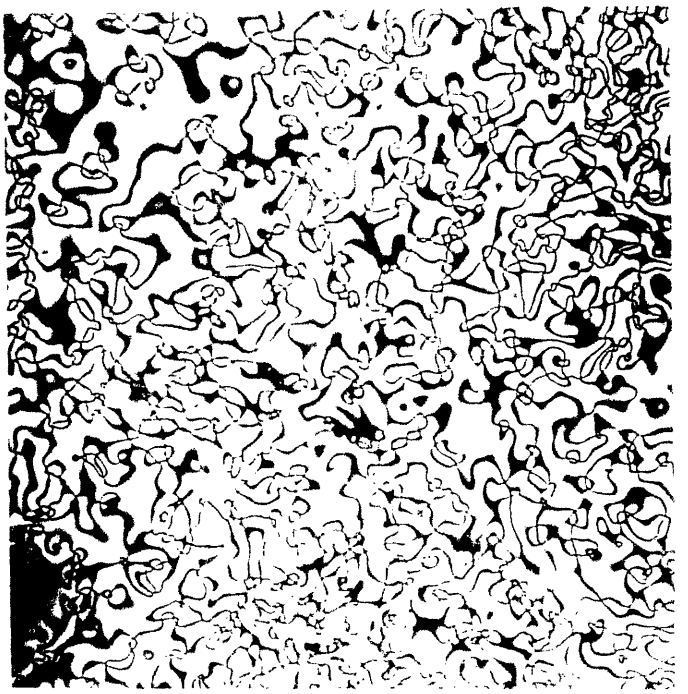

50 μm

(b)

t = 40 s

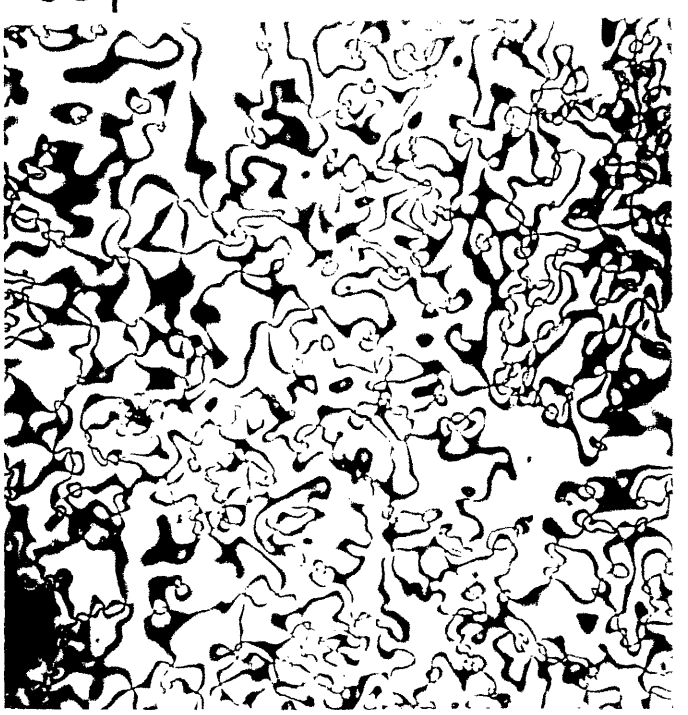

Figure 2.7(a)&(b): OM between crossed polars of overall isothermal coarsening sequences of schlieren textures, created by a thermal quench.

(c)

t = 95 s

(d)

t = 189 s

Figure 2.7(c)&(d): OM between crossed polars of overall isothermal coarsening sequences of schlieren textures, created by a thermal quench.

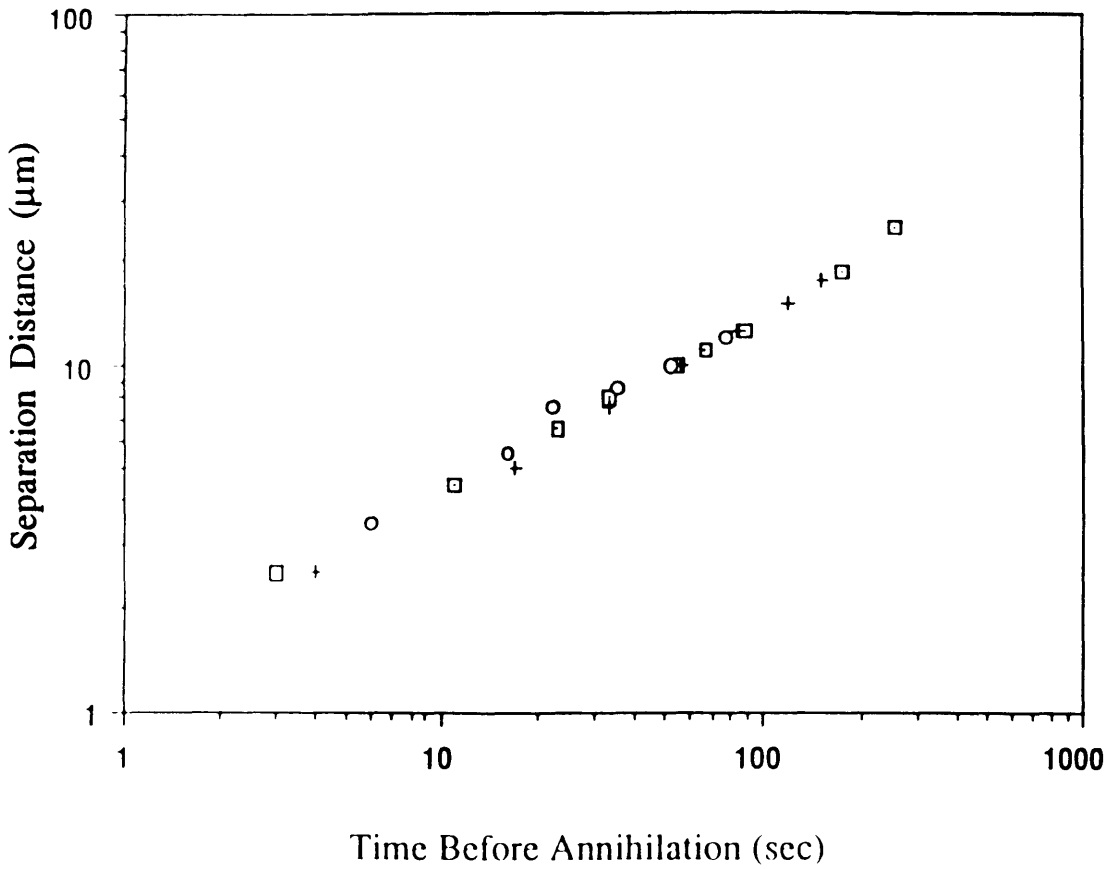

Figure 2.8: The pair distance D vs time before annihilation for three sets of data. The slope fits the scaling prediction by Pargellis et al [1].

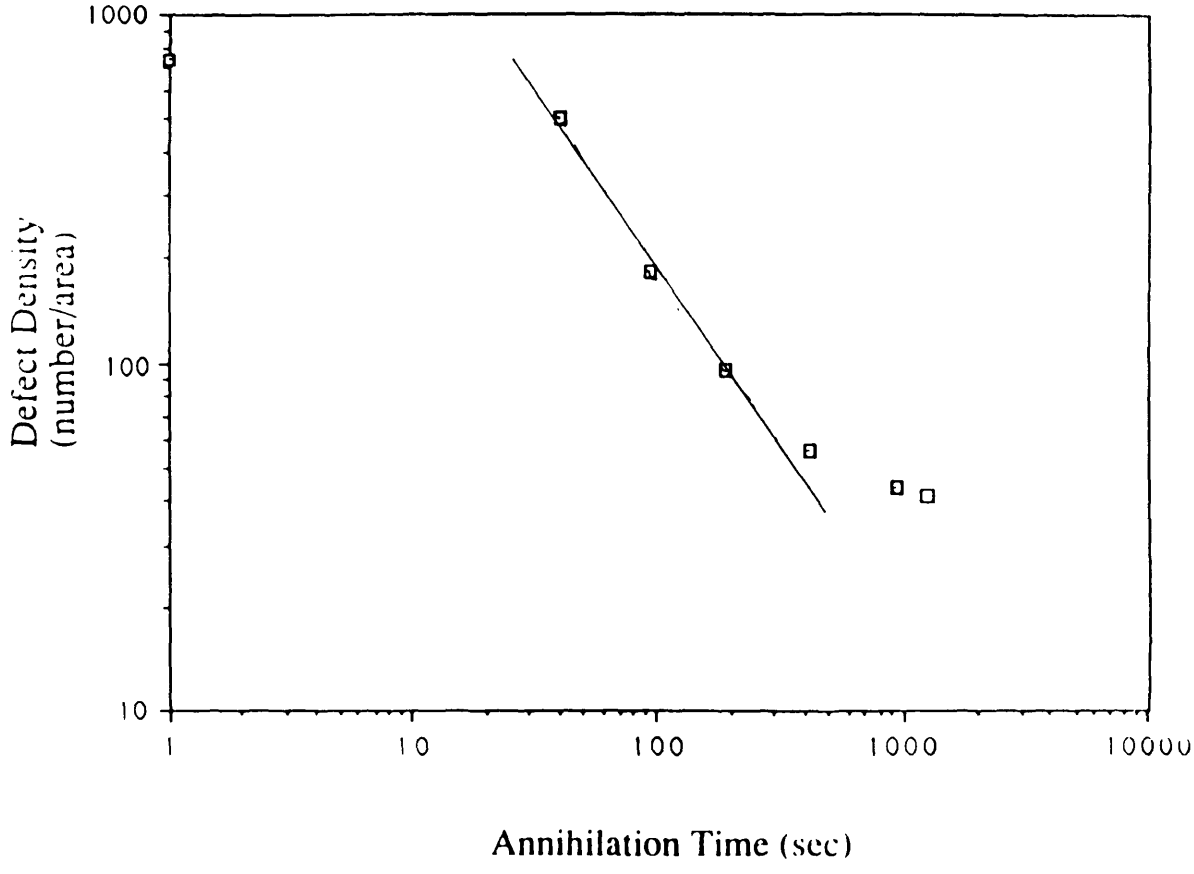

Figure 2.9 : Defect density vs annealing time at 160°C using data as in figure 7.

CHAPTER 3

STRUCTURE AND DYNAMICS OF INVERSION WALLS IN A THERMOTROPIC LIQUID CRYSTAL POLYETHER

Abstract

The director patterns of Néel (splay-bend) inversion walls, which are formed via magnetic field alignment of a nematic thermotropic liquid crystal polyether, are examined by optical microscopy and imaged at high resolution via a lamellar decoration technique using atomic force microscopy. A Néel inversion wall loop forming mechanism during magnetic reorientation is presented. The inversion walls form 'irregularly' shaped loops or terminate in disclinations of half integral strength. The formation of 'irregular' shaped inversion wall loops occurs through a coalescence process. The dynamic behavior of the inversion walls is also studied.

3.1 Introduction

In nematic liquid crystals, inversion walls may be formed via flow, electric, or magnetic fields during director reorientation.[1-5] The different types of director distortions in inversion walls were first calculated by Helfrich.[6] The molecular trajectories across inversion walls can be shown via the lamellar decoration technique in crystallizable thermotropic liquid crystal polymers.[3,7] This 'lamellar decoration' provides an extremely useful tool for direct visualization of the molecular trajectories. In this study, we utilize lamellar decoration to characterize two types of splay-bend walls, induced by realignment of a semiflexible main chain liquid crystal polyether in a magnetic field. In small molecule liquid crystals the two types of walls are difficult to distinguish by optical microscopy.

Nematic liquid crystals, in general, are characterized by a nonpolar vector called the director, **n**, (here **n** and -**n** are equivalent) which indicates the locally preferred orientation

of the molecules. There are three basic director distortions: splay, twist and bend, which give rise to the Frank elastic constants k_{11}, k_{22} and k_{33}, respectively. The lowest free energy configuration is uniform alignment of the director. When a nematic liquid crystal of positive diamagnetic anisotropy is placed in an external field, the director orients along the field direction to lower the system energy. The transient texture, the first response in the presence of a magnetic field, is a higher energy state than the final reoriented ordered state. The transient texture evolves into inversion walls, which eventually evolve into the reoriented monodomain state.

After application of the field, regions of uniform orientation along the field direction can be separated by an inversion wall, where the director orientation changes by an angle π on crossing the wall. These walls are analogous to the Bloch (pure twist) or the Néel (combination of splay-bend) walls in spin systems. Néel walls can be either bend-rich (Néel bend) or splay-rich (Néel splay).[8] The different types of inversion walls formed under the action of an applied field depend on the local direction of director reorientation which sets the wall orientation with respect to the applied field.[9] If the wall is formed parallel to the applied field, it can be a Néel-bend or Bloch twist wall. If the wall is formed perpendicular to the applied field, a Néel-splay wall is formed. Inversion walls are topologically constrained to end only at surfaces or disclinations of unlike strength, or loop upon themselves.[1,4,5,10,11]

For small molecule liquid crystals, Léger has observed twist-bend wall loops created via the Freedericks transition using a magnetic field.[4] During shrinkage the walls attain a fixed ellipticity. Figueiredo Neto et al.[12] have computed the director texture of a Néel-bend wall with twist deformation perturbation, and they argued the ellipticity of closed loop inversion walls in polymer nematics ($k_{11}>>k_{22}, k_{33}$) would be approximately two times greater than that earlier predicted for SMLCs ($k_{11}\equiv k_{33}=3k_{22}$) by Léger. Stieb et al. have studied the structure of twist walls of SMLCs in electric fields, and observed the shrinkage of closed loops and the splitting of closed loops into a loop segment terminated by pair of

sharp disclination lines[5]. Rey has proposed a detailed molecular model of the collapse of the Néel bend inversion wall segment with the production of a disclination line pair of strength ±1/2[13].

Although liquid crystalline polymer nematics exhibit the same topologically stable defects (point, line, or wall-like defects) as small molecule liquid crystals (SMLCs), defects in a polymer liquid crystal are different with respect to their energetic stability due to the long chain character of the polymer.[14] The bend elastic constant in liquid crystals increases with the persistence length, and the splay constant is proportional to the chain length.[15] However, the polydispersity in length and possible presence of hairpins in nematic main chain polymers may change both the effective bend elastic constant and the splay constant.[16,17]

Experiments on SMLCs usually employ a glass sandwich cell with a thickness on the order of 10-100 μm, so that the systems take advantage of the lower twist elastic constant and form twist walls. The structure of Néel-splay walls has been seldom reported in small molecule liquid crystals and liquid crystal polymers.[18] Hudson et al.[2,7] observed a Néel-bend inversion wall terminated in +1/2 and -1/2 disclinations in a liquid crystal polyester, however, Néel-splay walls terminated with disclinations have not yet been reported.

The free energy density for a nematic in a magnetic field is comprised of a linear gradient elastic term and a nonlinear magnetic term given as:

$$g(k_{ii},\chi_a,H,\mathbf{n}) = \frac{1}{2}(k_{11}(\nabla\cdot\mathbf{n})^2 + k_{22}(\mathbf{n}\cdot\nabla\times\mathbf{n})^2 + k_{33}(\mathbf{n}\times\nabla\times\mathbf{n})^2) - \frac{1}{2}\chi_a\,(\mathbf{n}\cdot H)^2 \quad (3.1)$$

where χ_a is the diamagnetic susceptibility anisotropy. The two terms in the free energy balance each other. The linear gradient elastic term tends to disperse distortions, while the nonlinear magnetic term globally orients the director and localizes the distortion, i.e. creates inversion walls. In a thin film the director may be confined to lie in the plane of the film, so the director has only one degree of freedom, ϕ, the angle with respect to some fixed axis contained in the plane. Assuming the director is confined to xy plane and the field is along the y-direction such that ϕ_H=0, the free energy density can be written as:

$$g = \frac{1}{2}\left((k_{11}\cos^2\phi + k_{33}\sin^2\phi)\left(\frac{\partial\phi}{\partial x}\right)^2 + (k_{11}\sin^2\phi + k_{33}\cos^2\phi)\left(\frac{\partial\phi}{\partial y}\right)^2 + 2(k_{33}-k_{11})\sin\phi\cos\phi\left(\frac{\partial\phi}{\partial x}\right)\left(\frac{\partial\phi}{\partial y}\right)\right) - \frac{1}{2}\chi_a (n\cdot H)^2 \quad . \tag{3.2}$$

The total free energy of the system is

$$G = \iiint g \, dxdydz \quad . \tag{3.3}$$

Helfrich minimized the total free energy, G, and found the structure of inversion walls in the equal elastic constant case.[6] We recently solved the special cases for Néel bend and Néel splay walls with elastic anisotropy assuming the director distortions depend only on distance from the wall.[18] Details are described in a later section. Since the molecular distortions in a Néel bend (bend-splay) wall and in a Néel splay (splay-bend) wall are different, the distortional energy for the Néel bend wall is expected to be different from that of the Néel splay wall for the nematics with elastic anisotropy. This should result in different wall dynamics for Néel bend and Néel splay walls in the presence a magnetic field.

The elastic anisotropy of liquid crystal polymers can be obtained directly from microscopic images (TEM, SEM, or AFM) of inversion walls by measuring the director orientation as a function of distance from straight sections of a π inversion wall oriented approximately parallel to or normal to the magnetic field. The measurement of wall width, provides the arithmetical average of the splay constant and bend constant. Combined with knowledge of the magnetic susceptibility anisotropy, this in turn yields the absolute value of elastic constants, k_{11} and k_{33}.

Defect dynamics in liquid crystals has recently become an important issue since the defect strings provide a laboratory system to test the "one-scale" model for cosmic string evolution.[19] Rey calculated the velocity of the disclination line due to the force between two opposite sign disclinations in a magnetic field using an entropy balance approach and obtained:[13]

$$v \sim (2H/\pi\gamma_1 s^2 \ln(\xi/r_c))(\chi_a k)^{1/2} \sim (2k/(\pi\gamma_1 \xi s^2 \ln(\xi/r_c))), \quad (3.4)$$

where H is the magnetic field strength, γ_1 is the rotational viscosity, s is the strength of disclination, k is the Frank elastic constant (equal elastic constant approximation), χ_a is the magnetic susceptibility anisotropy, and r_c is a molecular cut-off length to avoid infinite core energies. This relationship holds as long as distance between disclinations, r, is much larger than characteristic magnetic coherence length, ξ, which is defined as $\xi=[k/(\chi_a H^2)]^{1/2}$, and for $r>>\xi$. The force between disclination defects is independent of distance instead of the usual inverse of distance force law. Note that the velocity scales with the inverse of the wall thickness and the ratio of elastic to viscous effects k/γ_1. This provides a direct method to study the relationship among the movement of disclination, the elastic constant, and rotational viscosity.

The present work concerns the development of transient textures in liquid crystal polymers during magnetic reorientation, the formation mechanism of Néel inversion walls, and the interaction dynamics of Néel walls. Once the monodomain sample is placed in the field, the director tends to realign with the imposed field. The transient textures develop first in response to the field and eventually evolve into the Néel inversion walls. Néel inversion walls are metastable and can interact with each other, shrink and/or transform into twist walls. A wall may also collapse by the production of a pair of disclinations. All these mechanisms lead to a new uniform equilibrium state with the director parallel to the field direction.

3.2 Experimental

The polymer under examination is a semiflexible main chain liquid crystal polyether (TPP5) obtained by the phase transfer catalyzed polyetherification of 1-(4-hydroxy-4'-biphenyl)-2-(4-hydroxyphenyl)propane with 1,5-dibromopentane. Its chemical formula is:

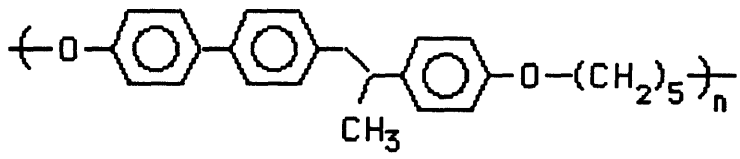

The number average molecular weight is equal to 11,200 with $\overline{M}w/\overline{M}n=2.5$ (THF-polystyrene standards); Phase behavior was determined by DSC (20°C/min) and wide and small angle X-ray scattering. On heating (20°C/min) the glass transition temperature is approximately 48°C, the crystals melt into a nematic phase at 149°C and the nematic to isotropic transition occurs at 183°C. Upon cooling (20°C/min), the isotropic to nematic transition occurs at 173°C the nematic to crystal transition at 108°C and the glass transition appears at 39°C. The crystal phase k is a distorted hexagonal one with tilted chains in which the repeat unit is almost fully extended. Detailed synthesis and characterization of TPP5 will be presented elsewhere.[20]

In order to follow the defect dynamics, the sample was repeatedly placed in the field. A 1-2μm thin film of TPP5 was first sheared with a razor blade on a glass slide in the liquid crystalline phase. A uniformly nematic domain specimen was obtained by further aligning in a 13.5T magnetic field parallel to the shearing direction at 160°C for 30 minutes. This uniform specimen was then quenched in the field to room temperature at a rate of ~10°C/sec with a flow of nitrogen gas, and then replaced in the magnet with the field normal to the initial orientation. The field was turned on at room temperature and the temperature was then jumped to 160°C (where the crystals rapidly melt and the liquid crystal phase reorients in the field), held for a 5 or 10 minute interval, and the sample again quenched to room temperature. Subsequently, the field was turned off and the sample was examined outside the magnet using optical or atomic force microscopes. After appropriate annealing, the quenched glassy nematic polymer partially crystallizes into a lamellar morphology. The variations in the director field are easily made visible by the lamellae, which are everywhere perpendicular to the local director.[7] After the images of the director

texture were taken, the sample was again placed back in the field, and the cycle of heating, field aligning, quenching and observation was repeated.

A Zeiss polarized light microscope (PLM) was used to observe the sample at room temperature. PLM can be used to identify the characteristic type of inversion walls, either Néel (splay-bend) walls or Bloch (twist) walls. High resolution details of the director field are obtained from AFM images using a Nanoscope III operated in a contacting repulsive mode. The same area of the PLM images of inversion walls can be scanned by AFM by location of a specific wall with the help of an auxiliary optical microscope.

The structures of inversion walls are preserved through a cold nitrogen gas quench before taking the sample out of the magnetic field. This liquid crystal polyether slowly crystallizes at room temperature due to the proximity of the glass transition. Since these crystalline lamellae which visualize the director texture adequately protrude out of polymer thin film surface, the film did not need any etching treatment before examination under AFM. Furthermore, AFM is free from the SEM requirement of a sufficiently high specimen surface conductivity, which necessitates a coating of metal which can sometimes obscure the surface morphology and would prohibit dynamical studies of a particular sample area.

3.3 Energy of the Néel Inversion Walls

It is expected that wall dynamics will be significantly affected by wall energy and that elastic anisotropy will influence the relative energy of the various types of inversion walls. In this section, we derive the general form of the wall energy for both the Néel bend and Néel splay walls in a nematic with elastic anisotropy by calculating their energy from the numerical solutions of the director trajectories across the walls.[18]

For a nematic with elastic anisotropy, the energy per unit area of the Néel bend wall along the field may be derived from equations (3.2) and (3.3) as

$$\frac{G}{l^2} = \int_{-\infty}^{\infty} \frac{1}{2}(k_{11}\cos^2\phi + k_{33}\sin^2\phi)(\frac{\partial\phi}{\partial x})^2\, dx - \int_{-\infty}^{\infty} \frac{1}{2}\chi_a\,(\mathbf{n}\cdot\mathbf{H})^2 dx \quad , \tag{3.5}$$

where ϕ is a function of x only. Similarly, the energy per unit area of the Néel splay wall normal to the field, where ϕ is a function of y only, is given as

$$\frac{G}{l^2} = \int_{-\infty}^{\infty} \frac{1}{2}(k_{11}\sin^2\phi + k_{33}\cos^2\phi)(\frac{\partial\phi}{\partial x})^2\, dy - \int_{-\infty}^{\infty} \frac{1}{2}\chi_a\,(\mathbf{n}\cdot\mathbf{H})^2 dy \quad . \tag{3.6}$$

Assuming a typical value of χ_a on the order of $1.0\cdot10^{-7}$ emucgs/g for a semiflexible main chain liquid crystal polymer,[21] the approximate values of the splay and bend constants for TPP5 are $k_{11} = 2.8\cdot10^{-6}$ dyn and $k_{33} = 0.9\cdot10^{-6}$ dyn at 160°C. The numerically calculated director distribution across the Néel bend wall and the Néel splay wall permits evaluation of equations (3.5) and (3.6) and yields values of the wall energy per unit area for Néel bend wall and Néel splay in TPP5, as $G/l^2 \sim 0.105$ erg/cm^2 and 0.123 erg/cm^2, respectively.[18] The elastic energy contribution in the Néel bend wall and Néel splay wall are calculated as, 0.053 erg/cm^2 and 0.062 erg/cm^2, respectively, so both the elastic and magnetic terms contribute approximately equally to the total wall energy per unit area in both Néel bend and Néel splay walls.

In the general case, the energy of the Néel bend wall can be rewritten as:

$$\frac{G}{l^2} = \frac{k}{2\zeta}\int_{-\infty}^{\infty} ((1+\varepsilon)\cos^2\phi + (1-\varepsilon)\sin^2\phi)(\frac{\partial\phi}{\partial x'})^2 dx' - \int_{-\infty}^{\infty} \frac{1}{2}\chi_a\,(\mathbf{n}\cdot\mathbf{H})^2 dx \quad , \tag{3.7}$$

and the energy of the Néel splay wall as:

$$\frac{G}{l^2} = \frac{k}{2\zeta}\int_{-\infty}^{\infty} ((1-\varepsilon)\cos^2\phi + (1+\varepsilon)\sin^2\phi)(\frac{\partial\phi}{\partial x'})^2 dx' - \int_{-\infty}^{\infty} \frac{1}{2}\chi_a\,(\mathbf{n}\cdot\mathbf{H})^2 dx \quad . \tag{3.8}$$

where $k = (k_{11}+k_{33})/2$ is the mean elastic constant, $\varepsilon = (k_{11}-k_{33})/(k_{11}+k_{33})$ is the elastic anisotropy, $\zeta = ((k_{11}+k_{33})/\chi_a)^{0.5}/H$ is the characteristic length for the Néel type inversion wall, and $x'=x/\zeta$ is the dimensionless distance.[18] Performing the numerical integral at different values of the elastic anisotropy gives the values of energy for the Néel bend and

splay walls with different values of elastic anisotropies (see table 3.1). Since the numerical solution of molecular distortions across the Néel bend and Néel splay walls are identical except the elastic anisotropies are switched, the energy per unit area of wall formula of a Néel bend wall is the same as that of a Néel splay wall when the elastic anisotropies are switched. The formula in table 3.1 are suitable for both thermotropic nematic polymers and SMLCs.

3.4 Results and Discussion

3.4.1 Early Stage Development

Before the director fully reorients along the imposed magnetic field, transient textures develop, followed by formation of inversion walls. The OM images of the evolution of the director field during magnetic reorientation in TPP5 are shown in figure 3.1. The OM images taken after short times in the applied field show transient textures before the Néel inversion walls become well developed. These transient textures appear as a periodic texture normal to the field direction. An aperiodic texture also develops along the field direction. Lonberg et al. [22] showed (λ_1 in figure 3.2) the wavelength of the periodic structure which forms normal to the field is that which can be formed fastest. The optimum wavelength decreases with magnetic field strength and viscosity anisotropy, and it increases with increasing elastic constant.

Periodic transient textures have been observed in magnetic field reorientation of a lyotropic liquid crystal polymer (poly-γ-benzyl-glutamate, PBLG, in a solvent mixture of methylene chloride and dioxane) by Srajer et al.[23] They referred to this transition as a periodic twist instability and presented schematics of the director response (figure 3.2(a)). Since the molecules can turn in either the clockwise or counterclockwise direction to align parallel to the applied field, a secondary periodicity may also exist as shown in figure 3.2(b). Both these periodic structures may be regarded as immature inversion walls. From

the statistical view of wall formation, the probability of forming the Néel bend wall and Néel splay wall is the same. However, since the inversion wall energy of the Néel splay wall is higher than that of Néel bend wall in polymers where $k_{11}>k_{33}$, the formation of the secondary periodicity may be hindered. This may explain the observed non-periodic transient textures we observed in TPP5 where $k_{11}=3k_{33}$.

A suggested mechanism for formation of a Néel inversion wall loop is drawn in figure 3.3. When a magnetic field is applied normal to the initial shearing direction or to the initial magnetic field direction ($\mathbf{n}_0$), the molecules tend to reorient parallel or antiparallel to the field direction. Since the thermal motion of the molecules comes fluctuations of the director, then for example, the molecules in region A reorient by clockwise rotation while the molecules in the neighboring regions such as B and C reorient by counterclockwise rotation (figure 3.3(b)). Thus a portion of Néel bend wall forms between regions A and B, and a portion of Néel splay wall between regions A and C (figure 3.3(c)). When the molecules outside region A reorient by counterclockwise rotation, a Néel wall loop containing both Néel bend and Néel splay wall is formed (figure 3.3(d)). Figure 3.4 shows the AFM image of transient texture with the developing Néel bend and Néel splay walls. These transient textures may be regarded as incomplete inversion walls.[24]

The planar director field of Néel inversion wall loops is shown in figure 3.5(a). Since the directors are globally well aligned and turn π degrees across the inversion wall, PLM can be used as a preliminary tool to identify Néel inversion walls within the sample. If the director fields of liquid crystals are parallel to the polarizer or to the analyzer, a dark extinction region of zero birefringence will be observed. Therefore, when the Néel inversion wall is examined under PLM with the field aligned at 45° to the polarizer and to the analyzer, the wall will show two parallel-like extinction lines along the inversion wall, which correspond to extinction regions of the structure differing in their orientation by $\pi/2$ (figure 3.5(b)). When the polarizer is parallel to the field, the directors on both sides of

inversion walls are parallel to the polarizer and 90° to the analyzer, then the wall appears as a bright region with a single central dark extinction line (figure 3.5(c)).

A twist inversion wall loop may be formed by either (i) tilting the molecules out of plane by π across the wall or (ii) by rotating by π degrees in layers. If the directions of polarizer or analyzer are oriented 45° to the direction of the magnetic field, then a twist wall will appear as a ring of bright intensity. When a wall loop is formed by a portion of Bloch wall and a portion of Néel splay wall, two parallel extinction lines appear in the middle section of Néel splay wall and taper to meet with one another as the wall character changes to twist.

PLM images of inversion wall loops in a thin area (0.5 to 1 μm) of the sample are shown in figure 3.6(a), where the directions of polarizer and analyzer were oriented 45° to the direction of the magnetic field. Not only elliptical shaped loops but 'irregular' inversion wall loops were formed. Two parallel-like dark extinction contours are clearly observed along each wall loop, which indicates the director field turns 180° across inversion wall. When the direction of polarizer or analyzer was rotated parallel to the field direction, a bright region with a single central extinction loop is apparent (figure 3.6(b)). Extinction regions are also obvious on both sides of the inversion walls, which demonstrates that the molecules are well aligned along the magnetic field. Figure 3.6(c) shows a AFM image of a small Néel wall loop. It is evident that inversion wall loops in the thinner areas of TPP5 dominantly possess the Néel wall (splay-bend) character.

Hudson et al. observed Néel bend inversion walls connecting pairs of oppositely signed 1/2 integer disclinations in a thermotropic polyester.[1,2] Such structures arise when walls form between nearby oppositely signed defects in an initial schlieren texture subjected to an applied field. This is not the case in the present situation since our initial film was a defect free monodomain. Figure 3.7 shows a Néel bend inversion wall terminated at a -1/2 disclination and a +1/2 disclination. This structure formed via production of a disclination line pair from an initial loop, which then proceed to move apart along the loop (also see

figure 3.8)[13]. Images of Néel-splay walls terminating at a -1/2 disclination are often observed. However, a Néel splay wall ending with a +1/2 disclination is *seldom* observed. Instead the wall takes on bend character before terminating in a +1/2 defect (figure 3.7). This suggests that the director for a +1/2 disclination at a wall 90° to the field direction is of higher energy.

3.4.2 Wall energy and dynamics

As mentioned earlier, not only elliptically shaped loops but 'irregularly' shaped inversion wall loops are formed throughout the sample (recall figure 3.6). Examining these loops carefully, we note there are some large and small irregularly shaped loops, such as those marked α and β; some elliptical loops with unusually long axes along the field, such as ς, and long axes normal to the field, such as δ. The irregularly shaped inversion wall loops have also been observed for a thermotropic liquid crystal polyester.[1]

In order to understand how these different shapes of inversion wall loops form, the interactions among inversion walls were followed by optical microscopy. Figures 8 and 9 show the evolution of various loops with time. It is clear that the interaction among wall loops is quite complicated. Loops can shrink, smooth out their curvature, coalesce, as well as split into a wall terminated by two opposite sign disclinations. Figure 3.8 shows the coalescence of two inversion wall loops into a single loop which then splits into a wall terminating in two opposite signed disclinations. Initially, two nearby portions of Néel bend walls of each wall loop annihilate into a well aligned region and leave zig-zag shaped curvatures in the upper and lower part of the new coalesced wall loop. From the statistical view of wall loop formation and wall annihilation, it is understandable that the 'irregularly' shaped regions of inversion wall loops, such as α and β, are formed through the process of coalescence. Prolate and oblate loops such as ς and δ may also form by coalescing several Néel splay walls or Néel bend walls at the same time.

It is clear that the coalescence between the Néel inversion walls is an important mechanism which leads to the homogeneous oriented equilibrium state. Figure 3.10(a) shows the AFM image of two coalescing Néel bend walls. It is easy to trace the director trajectories as the orthogonal directions to the lamellae. Based on these figures, we suggest a coalescence mechanism between two adjacent Néel bends wall is as shown in figure 3.10(b). In this process, as the inversion wall travels and shrinks, the director distortion is replaced by parallel alignment.

The Néel inversion wall energy per unit area G/l^2 of the wall for the equal elastic constant condition, $k_{11}=k_{33}=k$, is given as[6]

$$\frac{G}{l^2} = 2H(\chi_a k)^{1/2} . \tag{3.9}$$

This wall energy expression indicates that the change of the total wall energy is simply proportional to the change of total wall length. The force causing the inversion wall to shrink is independent of wall length. This means the rate of wall shrinkage, resulting from the movement of the disclination along the wall or from the shrinkage of the wall loop itself, is constant at a specified condition, such as at the same field strength and temperature (which controls the elastic constants). Therefore, the shrinkage of an isolated wall should be with a self-similar shape for equal elastic constants.

The bend elastic constant increases with the persistence length, and the splay constant is proportional to the chain length.[15] These two elastic constants are usually not the same, especially for liquid crystal polymers, where the splay constant is expected to be largest due to the long polymer chain.[25] The molecular distortions in Néel bend (bend-splay) wall and Néel splay (splay-bend) wall are different, hence the distortional energy for the Néel bend wall is different than that from the Néel splay wall for the nematics with elastic anisotropy.[18] Therefore, Néel bend and Néel splay walls should exhibit different shrinkage rates. The numerical calculation in the previous section showed that the energy of the Néel splay wall is 23 percent more than that of the Néel bend wall for this specific polyether, for

which $k_{11}=3k_{33}$ at T=160°C. From the calculation, it is also found that the magnitude of energy contribution from the gradient elastic term and the magnetic term is approximately the same. A typical wall loop shrinkage sequence is shown in the upper part of figure 3.8. It is obvious that the loop shrinkage is anisotropic (different shrinkage parallel and perpendicular to the field) and that the shrinkage rate of the Néel splay wall is larger than that of Néel bend wall, which can be understood as due to the different energy contributions of the elastic splay and bend constants. This is also consistent with the Néel inversion wall loops appearing as small ellipses with long axes along the field in the final stage before they disappear (see figure 3.6).

The smoothing of curvature of the inversion wall is also evident during the wall loop shrinkage process. Figure 3.9 shows the effect of wall smoothing during wall shrinkage, especially for a portion of zig-zag shaped wall previously formed by coalescence (regions ϑ). Sometimes a portion of the inversion wall loop becomes pinned by impurities (small loop Λ in the lower right part of figure 3.9), while the remainder of the wall still undergoes shrinkage and smoothing. The processes of coalesce and anisotropic shrinkage of Néel wall loops with various ellipticities is sketched in figure 3.11. Isolated loops may attain an equilibrium elliptical shape and shrink in a self-similar process (constant ellipticity) with the ellipticity dependent on the elastic anisotropy.

The wall smoothing mechanism can be easily explained by the conception of *line tension*. The higher energy state of the inversion wall arises from the director distortion across the inversion wall, as defined in equation (3.9) or table (3.1) for Néel walls. For a curved inversion wall, containing both the Néel bend and Néel splay character, the line tension will produce forces tending to straighten the inversion wall and thus reduce the total energy. The direction of force is along the local normal to the inversion wall and concavely towards to the center of curvature. As shown in the figure 3.9, curved walls straighten through the wall smoothing mechanism, regardless of the field direction.

The interactive potential energy between two parallel inversion walls (one is the inverted image from the other) in the equal elastic constant case can be described as:[26]

$$U = U_0+4\chi_a H^2 \exp(-2d/\xi) \qquad (3.10)$$

where 2d is the distance between the walls. The force that one inversion wall feels from the other is

$$f = 4k/\xi \exp(-2d/\xi) \ . \qquad (3.11)$$

The more exact description of interaction of inversion walls with elastic anisotropy still needs to be explored.

The inversion wall loops both coalesce and shrink to lower their energy. The temporal evolution of the inversion walls is primarily by coalescence initially because the decrease of inversion wall length is much faster than for shrinkage. These processes may have some considerable effect on the ordering dynamics.

As mentioned before, another possible mechanism to lower the wall energy is that a wall segment may collapse with production of a pair of line disclinations, which will then proceed to move apart. Disclination movement at the end of a wall is also an energetically favorable process and initially appears as though the pair of opposite disclinations repel one other since the disclinations move away from one another. This is because the interaction between disclinations under an applied field is no longer as same as in the case without a field. It is understandable that disclinations move along the inversion wall and leave well aligned regions behind, which is energetically favorable. The rotational viscosity may be obtained by measuring the disclination movement through the relationship between velocity of disclinations and rotational viscosity (equation 3.5), which is valid for static inversion walls and moving disclination lines.

Let us consider qualitatively the interaction between two disclinations terminating a circular Néel inversion wall loop as shown in figure 3.12(a). Here θ is the angle with respect to wall breaking point, r is the radius of the circular loop. If both disclinations have the same mobility, the disclinations will annihilate at $\theta=\pi$. Following Rey's treatment

which assumes that the moving disclination experiences both the force from the decrease in inversion wall energy, F_w, and the attractive force from the other opposite signed disclination (as a dipole force), F_d, the total force, F_{net}, on each disclination along the wall is:

$$F_{net} = F_w + F_d \cdot \cos\theta \quad . \tag{3.12}$$

Using the equal elastic constant approximation such that $F_w = 2k/\xi$ and $F_d = 2\pi ks/L$, where $L \sim r \cdot \sin\theta$, is the disclination line separation, gives

$$F_{net} = \frac{2k}{\xi} + \frac{2\pi ks^2}{r}\cot\theta \quad . \tag{3.13}$$

The magnitude of each component of the force along the inversion wall loop is shown in figure 3.12(b). The pulling force from the inversion wall is a constant until $\theta=\pi$ (disclinations annihilate) whereas the disclination dipole force is an increasing attractive force. Therefore, it is expected that the movement of disclination along the wall accelerates. However, the magnitude of F_w is on the order of one dyne while F_d depends on k/L. Most of time $L>>\xi$, so the attractive dipole force is so small that the interaction between the two disclinations acts essentially distance independent. The acceleration from the dipole force is only significant when $L \sim \xi$.

In the general case, the movement of disclinations along the Néel inversion wall is quite complicated, which involves the different energies of the Néel bend and Néel splay wall, the different velocities of +1/2 and -1/2 disclination, and the wall dynamics itself.[16]

3.5 Summary

In this paper we have examined the transient textures of a liquid crystal polymer during Helfrich magnetic reorientation, the formation mechanism of inversion wall loops, and their interaction dynamics. The director patterns of Néel bend and Néel splay inversion walls, which were not well distinguished before, were identified and imaged at high resolution via a lamellar decoration technique using atomic force microscopy. The Néel bend and Néel

splay walls are metastable structures, which evolve from the transient textures produced from the initial monodomain state during magnetic reorientation. These Néel inversion wall loops may shrink, smooth, coalesce, and split into a wall terminated by two opposite sign disclinations to reach the new uniform equilibrium state parallel to the applied magnetic field. The energy of the Néel bend and Néel splay wall of a nematic with elastic anisotropy under magnetic field effect is also derived and calculated. For the particular TLCP investigated here, the energy of the Néel splay wall is larger than that of the Néel bend wall since $k_{11}=3k_{33}$, which results in faster shrinkage rate of the Néel splay wall. The formation of 'irregular' shaped inversion wall loops and elliptical loops with various ellipticities is mainly through the effect of shrinkage and coalescence recombination process of the inversion wall loops.

References

(1) Hudson, S. D.; Thomas, E. L. *Physical Review A* **1991**, 44, 8128.

(2) Hudson, S. D.; Vezie, D. L.; Thomas, E. L. *Makromol. Chem., Rapid Commun.* **1990**, 11, 657.

(3) Ford, J. R.; Bassett, D. C.; Mitchell, G. R.; Ryan, T. G. *Mol. Cryst. Liq. Cryst.* **1990**, 180B, 233.

(4) Léger, L. *Mol. Cryst. Liq. Cryst.* **1973**, 24, 33.

(5) Stieb, A.; Baur, G.; Meier, G. *J. Physique* **1975**, 36, C1-185.

(6) Helfrich, W. *Phys. Rev. Lett.* **1968**, 21, 1518.

(7) Thomas, E. L.; Wood, B. A. *Faraday Discuss. Chem. Soc.* **1985**, 79, 229.

(8) Kléman, M. *Points, Lines, and Walls*; Wiley: Chichester, 1983; p244.

(9) Stephen, M. J.; Straley, J. P. *Rev. Mod. Phys.* **1974**, 46, 617.

(10) Nehring, J.; Saupe, A. *J. Chem. Soc. Faraday Trans. II* **1972**, 68, 1.

(11) Mineev, V. P.; Volovik, G. E. *Phys. Rev.* **1978**, B13, 3197.

(12) Figueiredo Neto, A. M.; Martinot-Lagarde, P.; Durand, D. *J. Physique Lett.* **1984**, 45, L-793.

(13) Rey, A. D. *Liquid Crystals* **1990**, 7, 315.

(14) Kléman, M. *Liquid Crystallinity in Polymers*; A. Ciferri, Eds; VCH: New York, 1991; p365.

(15) Meyer, R. B. *Polymer Liquid Crystals*; A. Ciferri; W. R. Drigbaum; R. B. Meyer, Eds; Academic Press: New York, 1982; 133.

(16) Mazelet, G.; Kleman, M. *Polymer* **1986**, 27, 714.

(17) Li, M. H.; Brulet, A.; Davidson, P.; Keller, P.; Cotton, J. P. *Phys. Rev. Lett.* **1993**, 70, 2297.

(18) Ding, D.-K.; Thomas, E. L. *Macromolecules* **1993**, 26, 6531.

(19) Chuang, I.; Durrer, R.; Turok, N.; Yurke, B. *Science* **1991**, 251, 1336.

(20) Percec, V.; Chu, P.; Ungar, G.; Cheng, S. Z. D.; Yoon, Y. *Submitted to J. Mater. Chem.* **1993,**

(21) Hardouin, F.; Achard, M. F.; Gasparoux, H.; Liebert, L.; Strzelecki, L. *J. Polym. Sci., Polym. Phys. Ed.* **1982,** 20, 975.

(22) Lonberg, F.; Fraden, S.; Hurd, A. J.; Meyer, R. E. *Phys. Rew. Lett.* **1984,** 52, 1903.

(23) Srajer, G.; Fraden, S.; Meyer, R. B. *Physical Review A* **1989,** 39, 4828.

(24) Hudson, S. D., *Polymer Nematic Liquid Crystals: Disclination Structure and Interaction*; University of Massachusetts at Amherst: 1990;

(25) Sun, Z.; Kléman, M. *Mol. Cryst. Liq. Cryst.* **1984,** 111, 321.

(26) De Gennes, P. G. *J. de Phys.* **1971,** 32, 789.

Elastic Anisotropy (ε)	Néel Bend Wall Energy (erg/cm^2)
1	$1.00\ H(k_{11}+k_{33})\chi_a)^{0.5}$
0.5	$1.24\ H(k_{11}+k_{33})\chi_a)^{0.5}$
0	$1.42\ H(k_{11}+k_{33})\chi_a)^{0.5}$
-0.5	$1.52\ H(k_{11}+k_{33})\chi_a)^{0.5}$
-1	$1.58\ H(k_{11}+k_{33})\chi_a)^{0.5}$

Elastic Anisotropy (ε)	Néel Splay Wall Energy (erg/cm^2)
1	$1.58\ H(k_{11}+k_{33})\chi_a)^{0.5}$
0.5	$1.52\ H(k_{11}+k_{33})\chi_a)^{0.5}$
0	$1.42\ H(k_{11}+k_{33})\chi_a)^{0.5}$
-0.5	$1.24\ H(k_{11}+k_{33})\chi_a)^{0.5}$
-1	$1.00\ H(k_{11}+k_{33})\chi_a)^{0.5}$

Table 3.1: Calculated energies of the Néel bend walls and the Néel splay walls at different values of elastic anisotropy.

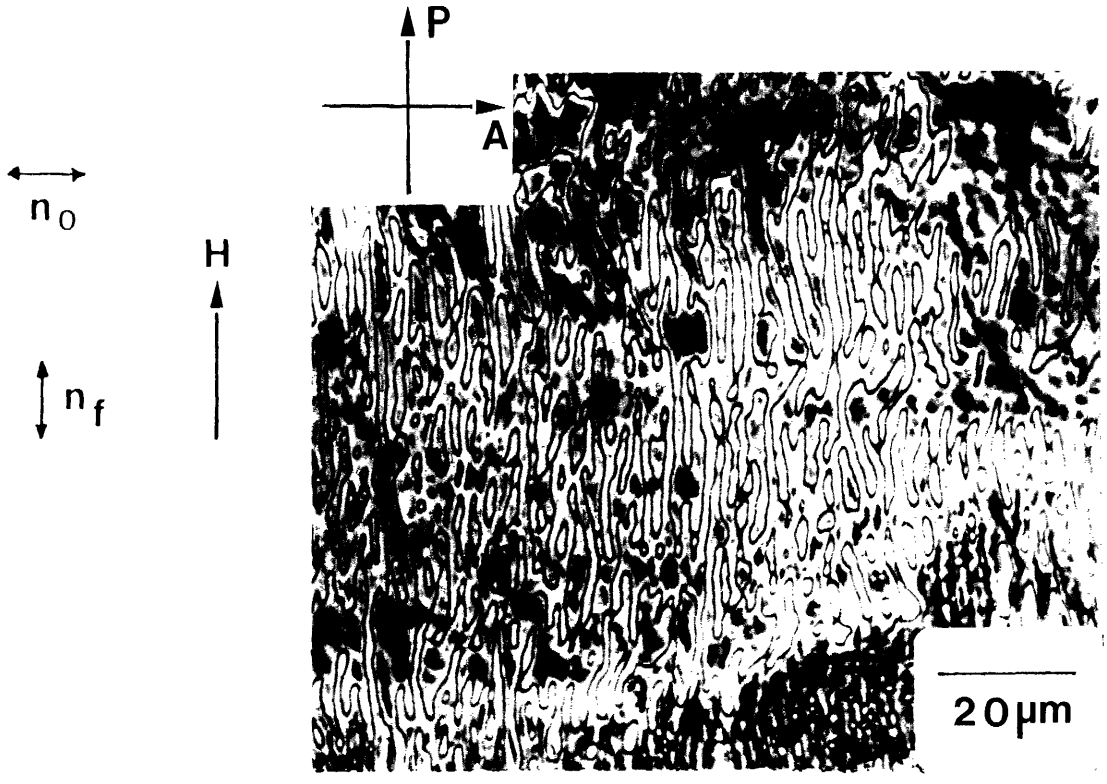

Figure 3.1: Polarized light microscope image of transient textures in TPP5 at short time response during magnetic reorientation before the Néel walls are well developed.

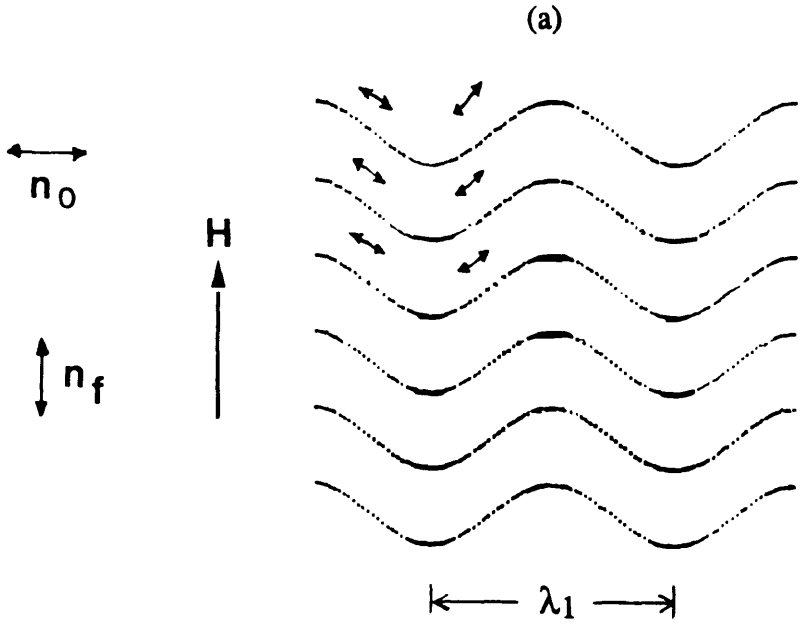

Figure 3.2: Two possible responses upon magnetic reorientation: (a) a wall developing along the field, λ_1 is wavelength of an immature Néel bend periodic texture, and (b) a wall developing normal to the field, λ_2 is wavelength of an immature Néel splay periodic texture.

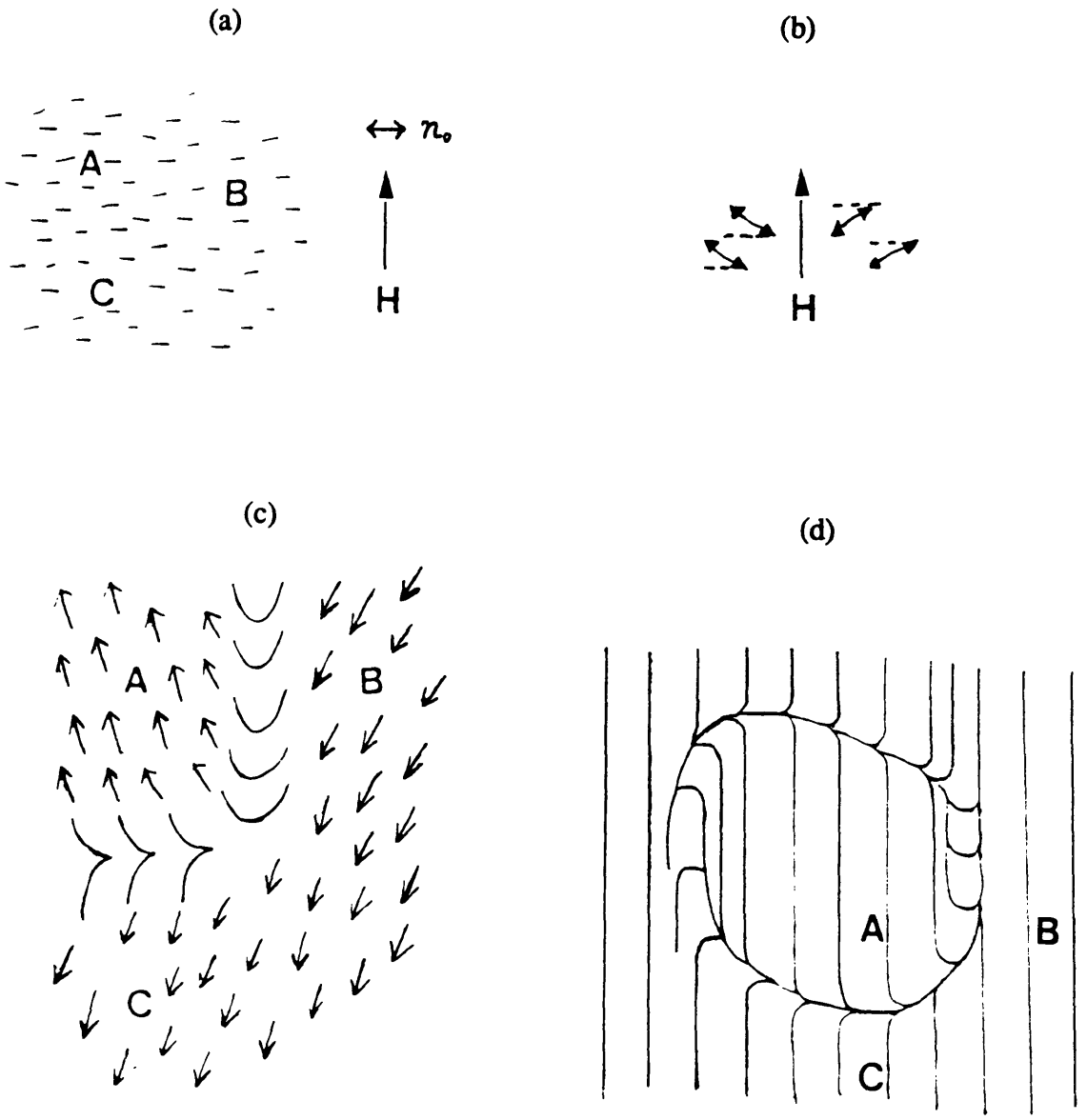

Figure 3.3: Schematic mechanism for formation of a Néel inversion wall loop. (a) A magnetic field is applied normal to the initial direction of molecules, n_0. (b) The molecules tend to reorient parallel or antiparallel to the field. (c) The molecules in region A reorient by clockwise rotation and the molecules in regions B and C reorient by counterclockwise rotation, forming a Néel bend wall parallel to the field and a Néel splay wall normal to the field. (d) Wall segments connect and a Néel inversion loop is formed.

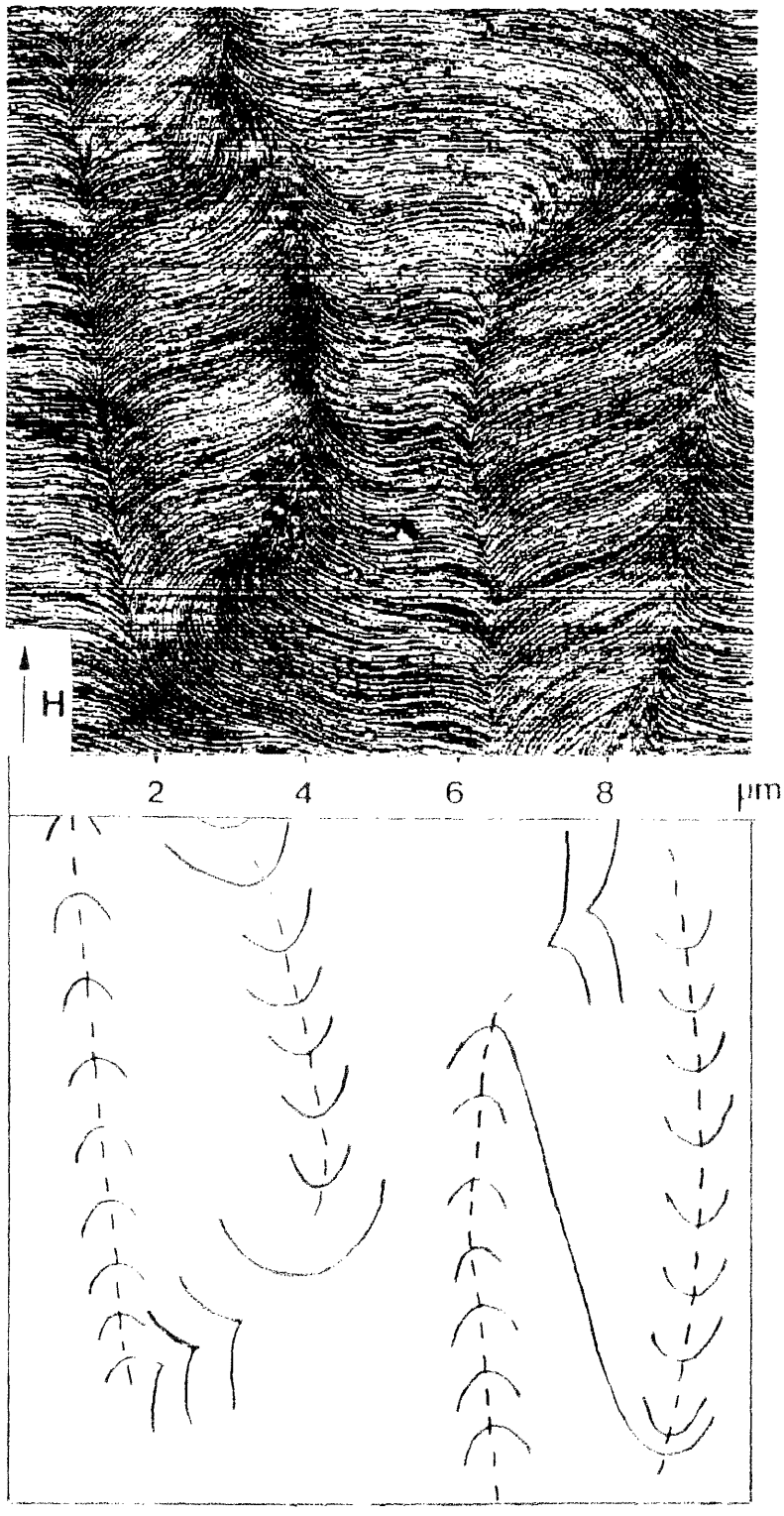

Figure 3.4: Atomic force microscope image of transient texture in TPP5 with the developing Néel bend and Néel splay walls. Contrast results from lamellar decoration of the underlying director field. A wall which appears as bend-rich in the lamellae is a splay-rich wall due to the orthogonal relation between the long axis of the crystalline lamellae and the molecular director.

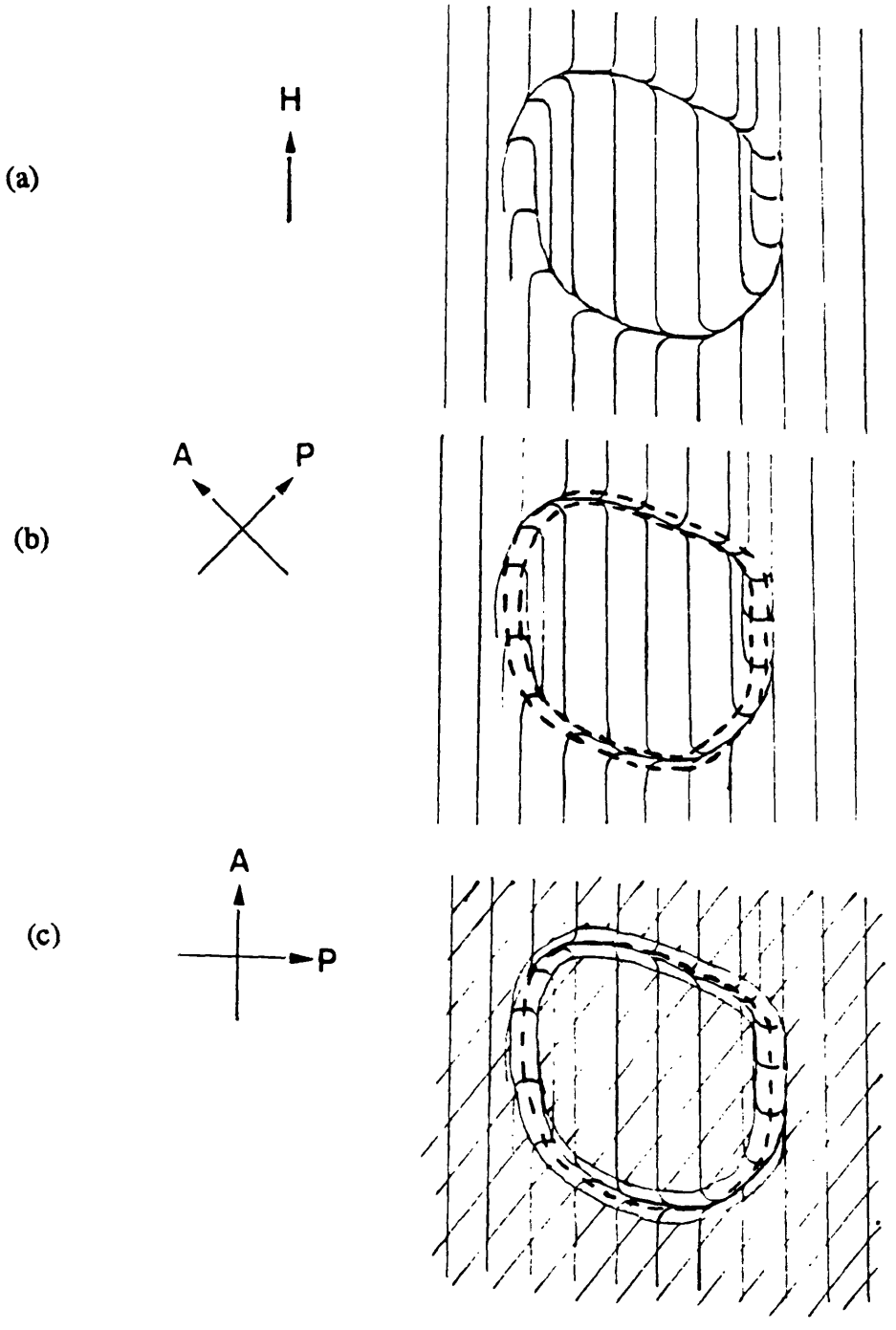

Figure 3.5: The planar director field of a Néel inversion wall loop and the extinction patterns under cross polars. There are two parallel extinction lines along the inversion wall when the polarizer is oriented 45° to the direction of the magnetic field. The wall appears as a bright region with a single central dark extinction line when the polarizer is parallel to the field.

(a)

(b)

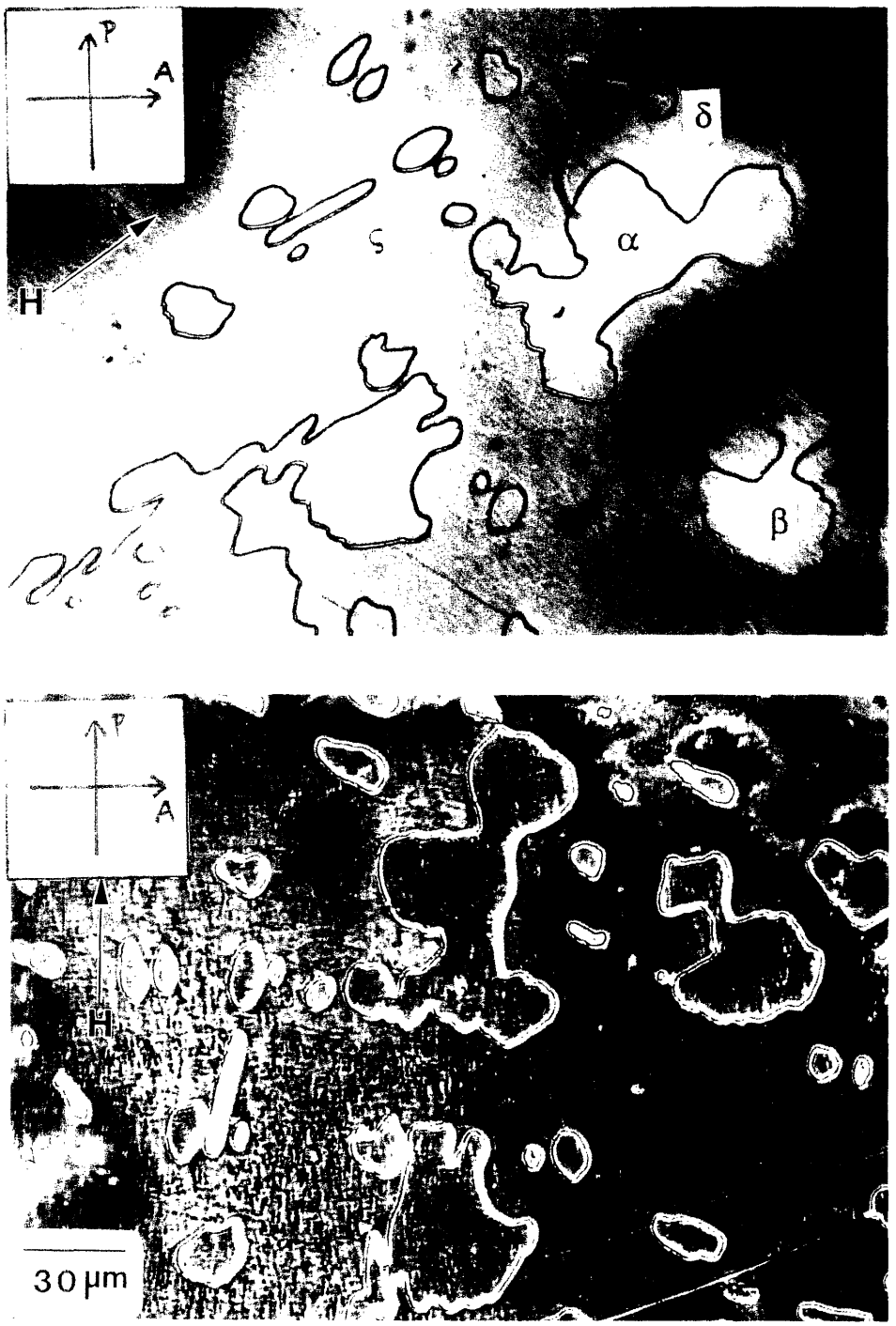

Figure 3.6: PLM images of inversion wall loops in TPP5 indicating Néel type inversion walls. Both elliptically shaped and irregular inversion wall loops have formed. (a) The polarizer is oriented 45° to the direction of the magnetic field, and the wall contrast displays two parallel extinction lines. (b) The polarizer is parallel to the field and a single extinction line occurs.

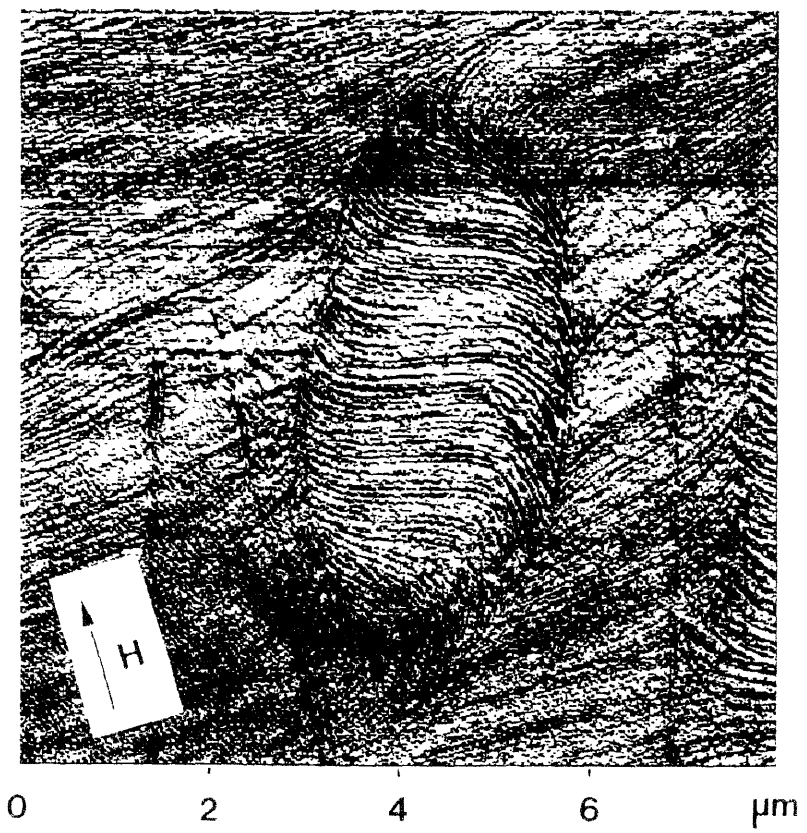

Figure 3.6(c) AFM micrograph of a small Néel inversion wall loop in TPP5.

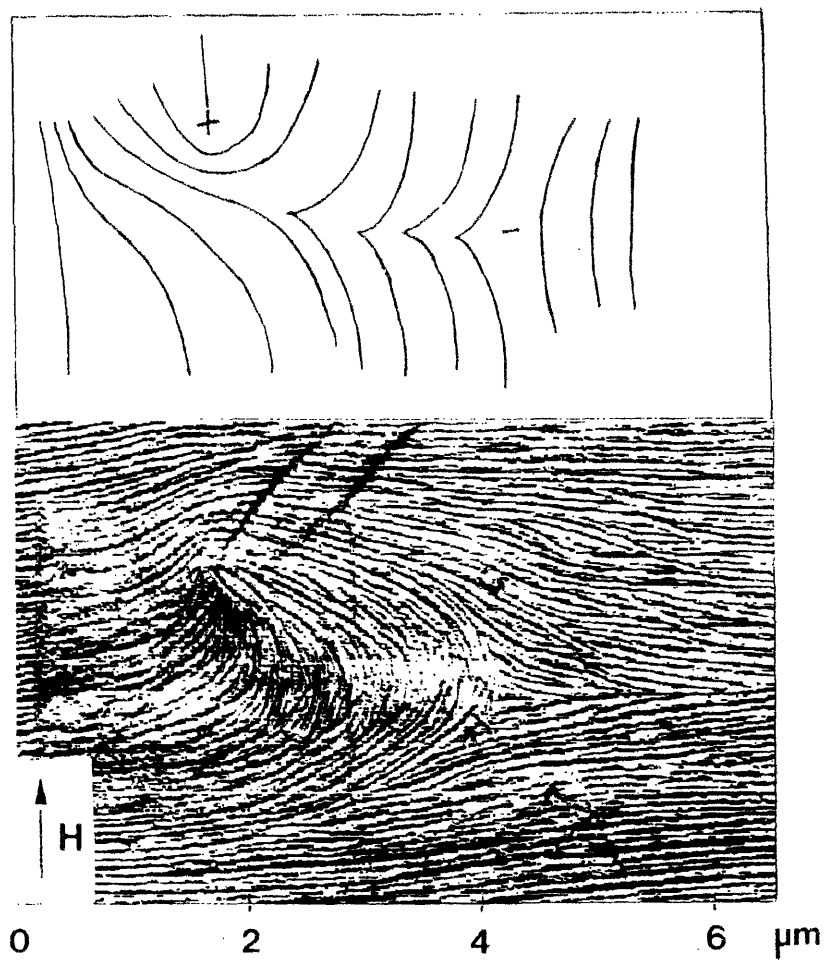

Figure 3.7: AFM micrograph (and schematic inset of director pattern) of a Néel splay wall terminated at a -1/2 disclination and a distorted +1/2 disclination.

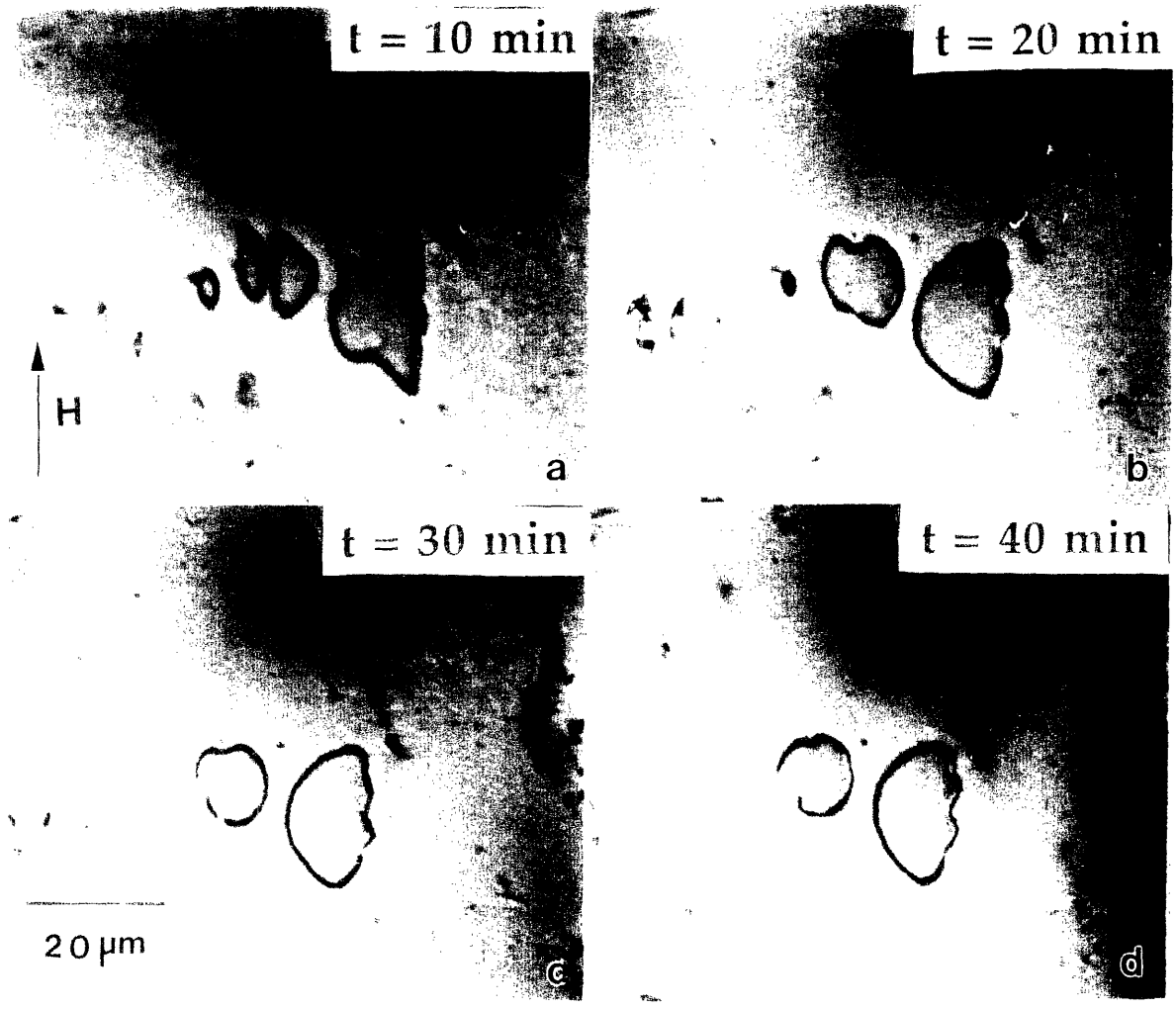

Figure 3.8: PLM of inversion wall dynamics in TPP5 under a 13.5 T magnetic field at 160°C. The coalescence of two inversion wall loops into one inversion wall and the collapse of the inversion wall with production of a disclination line pair is evident.

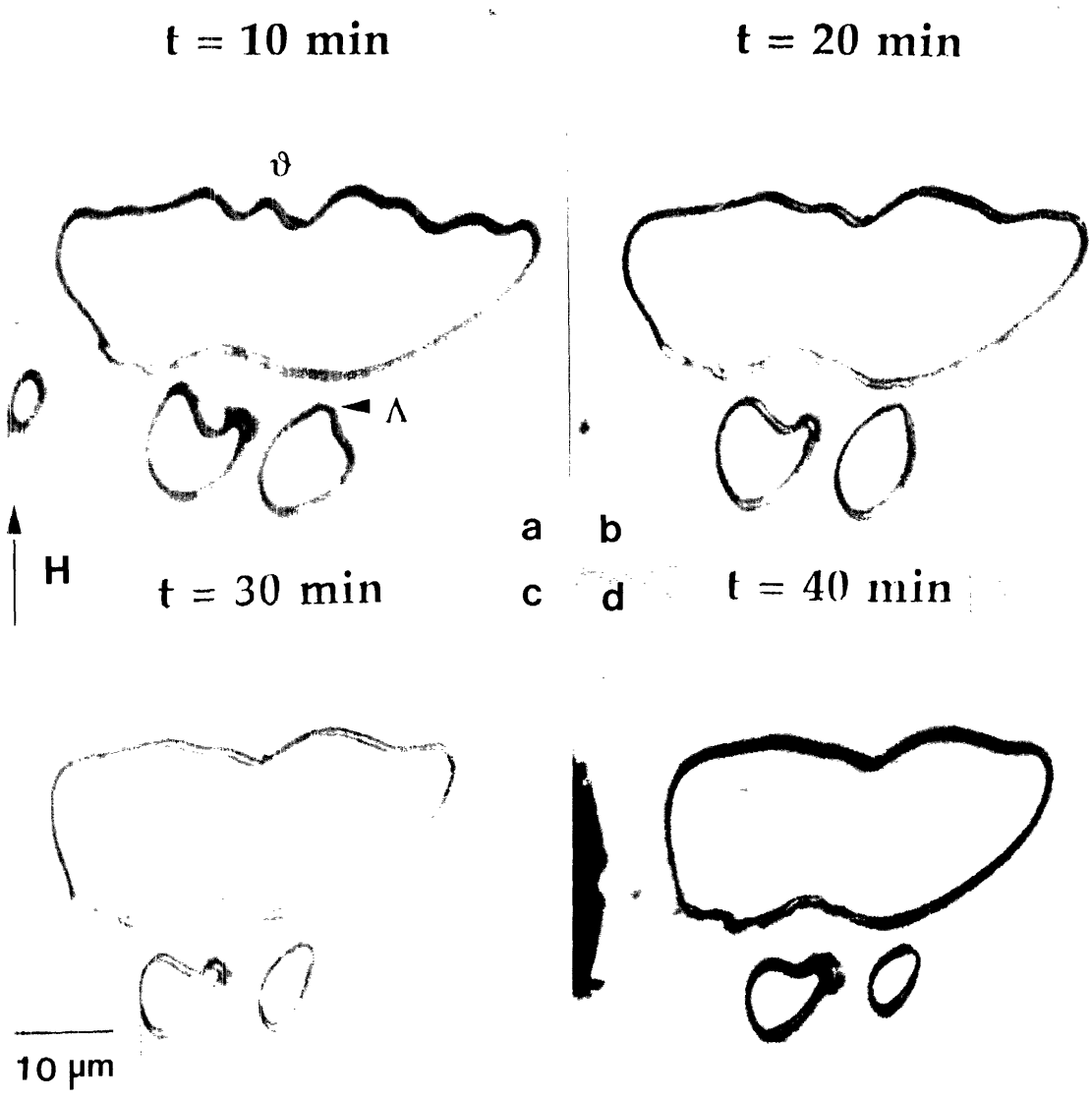

Figure 3.9: PLM of inversion wall dynamics in TPP5 under a 13.5 T magnetic field at 160°C. Shrinkage and smoothing of the Néel inversion walls.

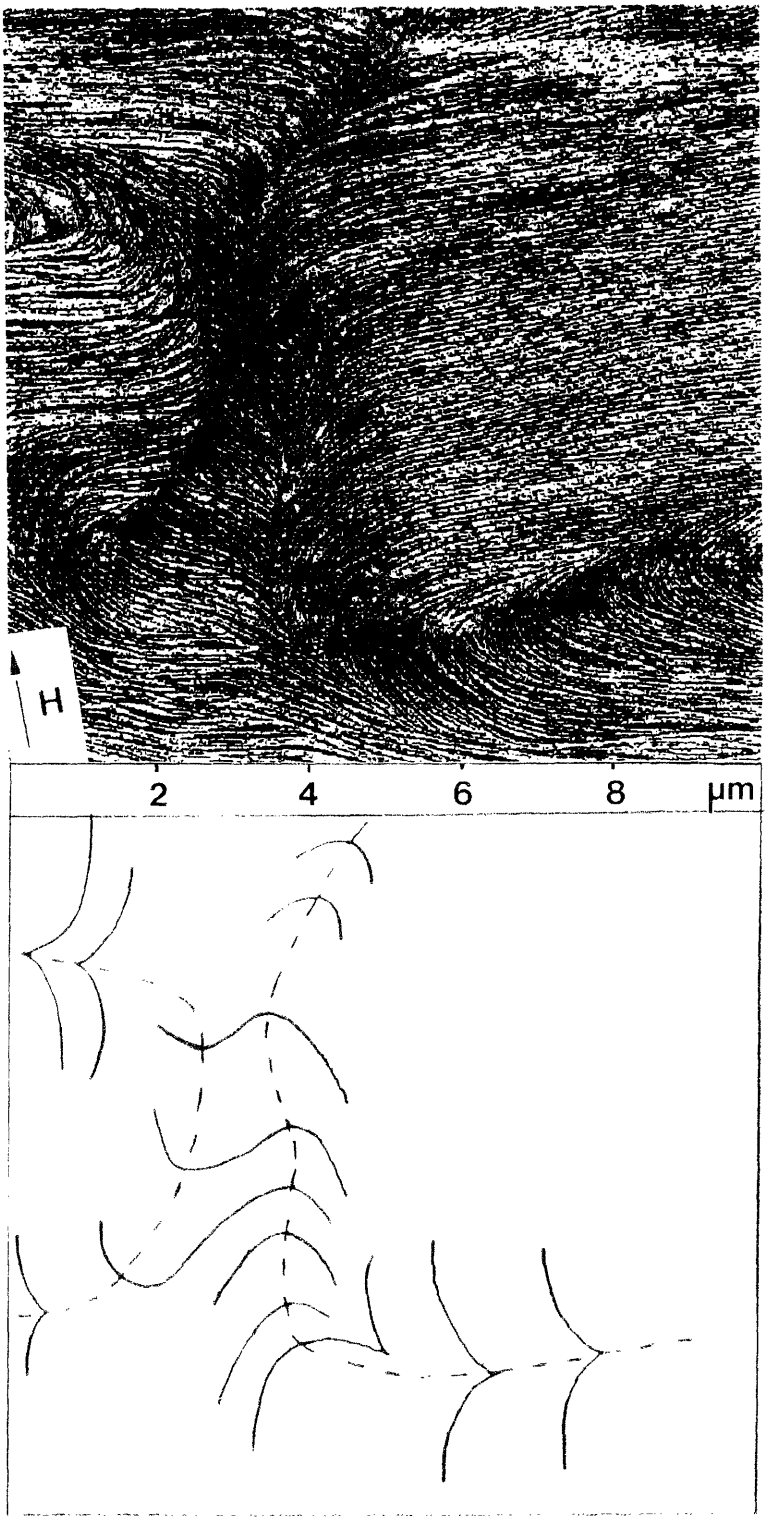

Figure 3.10(a): AFM image of a region where two Néel bend walls are undergoing coalescence.

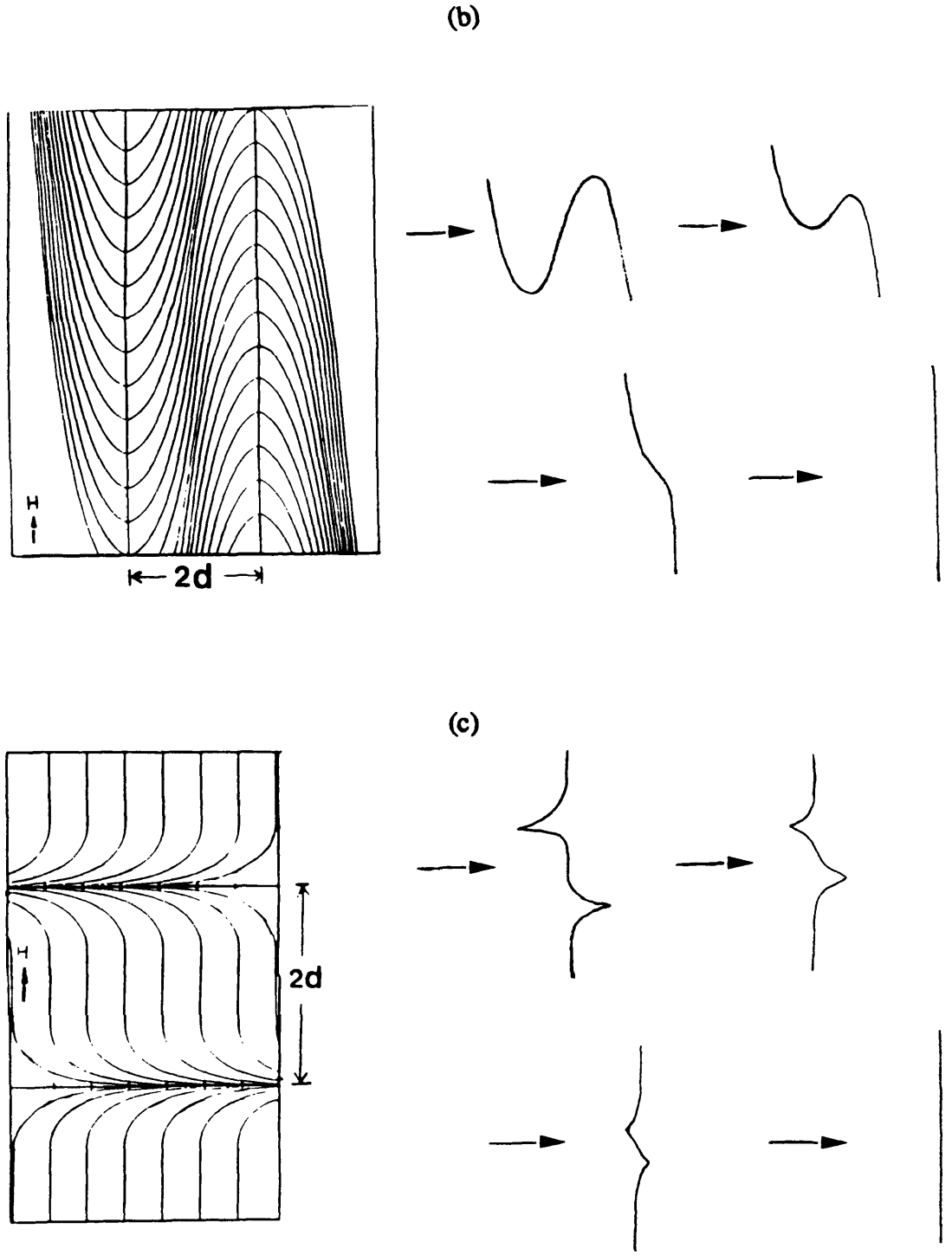

Figure 3.10: (b) Suggested coalescence mechanism of molecular trajectories between two bend-rich walls. (c) Suggested coalescence mechanism of molecular trajectories between two splay-rich walls.

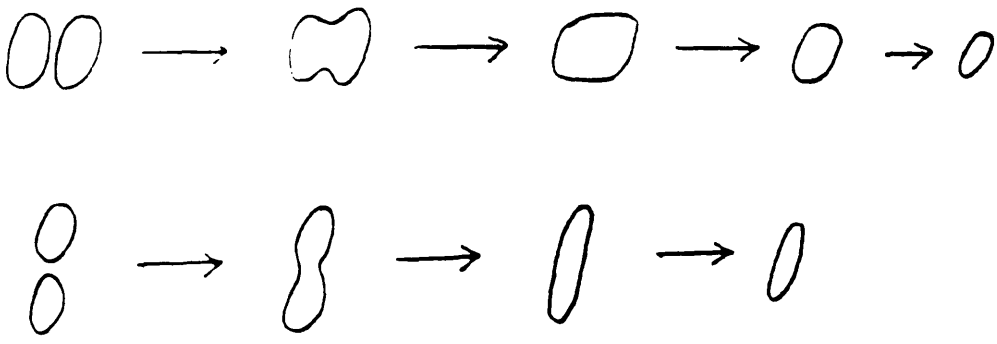

Figure 3.11: Schematics illustrating the processes of coalescence and anisotropic shrinkage of Néel wall loops. Such interactions can result in walls with various ellipticity. Eventually loops may attain an equilibrium shape and shrink with constant ellipticity.

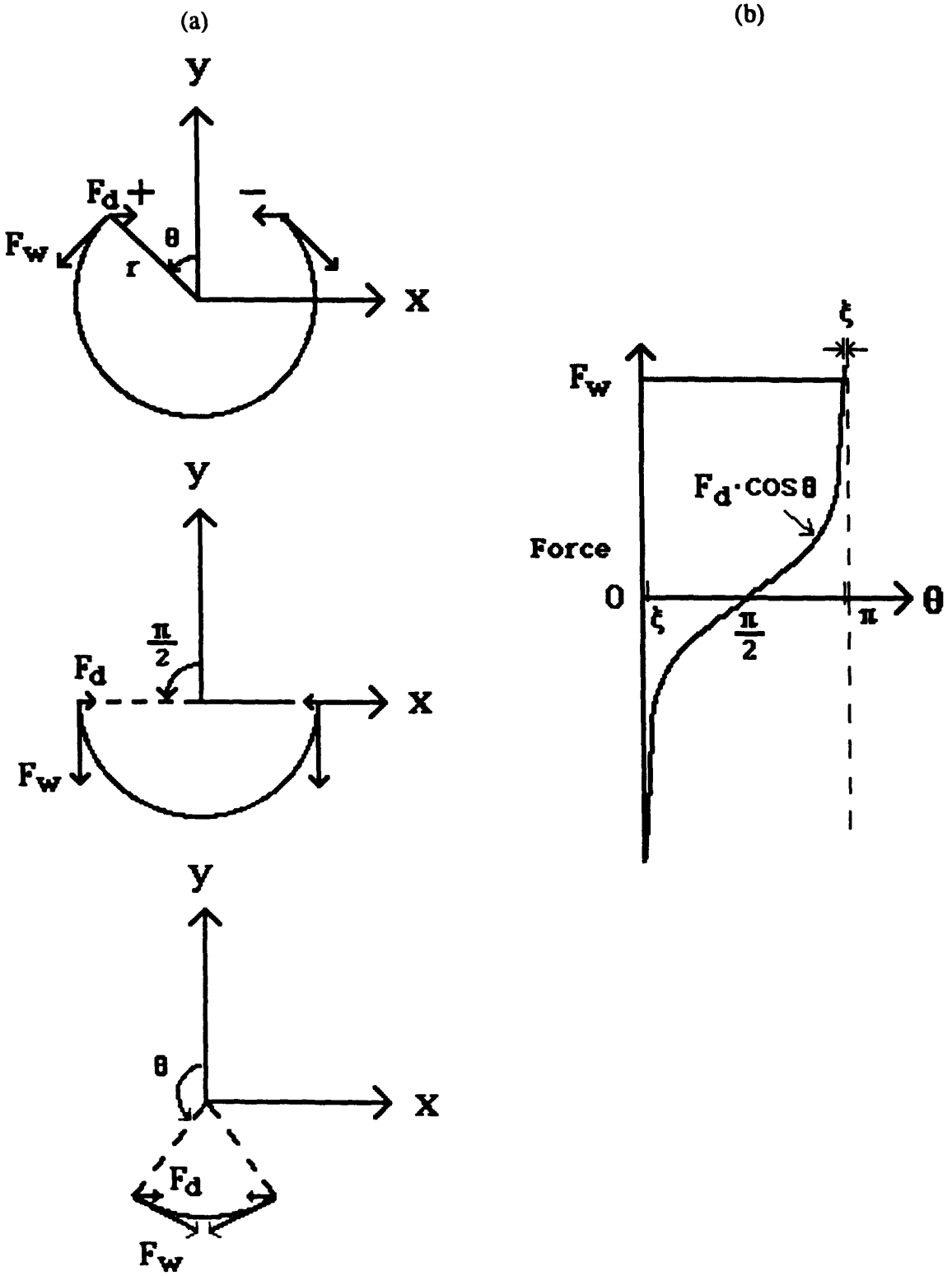

Figure 3.12: (a) Schematic of the movement of two opposite sign disclinations along a circular Néel inversion wall loop. (b) The magnitude of forces between two defects with respect to the azithumal angle θ depends on the force between disclinations F_d and the wall shrinkage force F_w.

CHAPTER 4

INFLUENCE OF ELASTIC ANISOTROPY ON THE STRUCTURE OF NÉEL INVERSION WALLS IN LIQUID CRYSTAL POLYMERS

Abstract

A solution of the director orientation across Néel inversion walls in a liquid crystal placed in a magnetic field for different values of the elastic anisotropy is presented. The appropriate characteristic length, containing the bend, k33, and splay, k11, elastic constants, for Néel type inversion walls is redefined as $\frac{1}{H}\sqrt{\frac{k_{11}+k_{33}}{\chi_a}}$ *. The qualitative, and in favorable cases, quantitative, values of the elastic anisotropy of a liquid crystal polymer can be obtained from the images through the direct measurement of the director field via a lamellar decoration technique.*

4.1 Introduction

Liquid crystals are typically aligned via flow or electric or magnetic fields. Different types of inversion walls may be formed during field alignment.[1] Liquid crystal polymers also form inversion walls under an applied field.[2-4] The structure of inversion walls should be different for rigid rod molecules as compared to flexible molecules. The bend elastic constant increases with the persistence length, and the splay constant is proportional to the chain length.[5] These two elastic constants are usually not the same, especially for liquid crystal polymers, where the splay constant is expected to be largest due to the long polymer chain.[6] Defect structures in liquid crystals depend dramatically on the values of elastic anisotropy, which is defined as, $\varepsilon = (k_{11}-k_{33})/(k_{11}+k_{33})$. However, the effect of elastic

anisotropy on the structure of inversion walls has seldom addressed in the literature[7,8] and up to now not reported for thermotropic liquid crystal polymers.

Liquid crystals, in general, are characterized by an nonpolar vector called the director, **n**, (here **n** and -**n** are equivalent) which indicates the locally preferred orientation of molecules. When a nematic liquid crystal of positive diamagnetic anisotropy is placed in a magnetic field, the director orients parallel to the field direction. Regions of uniform orientation along the field direction can be separated by a inversion wall, where the director orientation changes by an angle π on crossing the wall. These walls are analogous to the Bloch (twist) or the Néel (splay-bend) walls in spin systems[9]. They can terminate in disclinations of half integral strength or form loops[2,10]. The differential equation describing the director orientation across the inversion wall based on continuum theory[11] in the two dimensional case has been derived by Helfrich[1] and solved for the equal elastic constant approximation. The thickness of the inversion wall is defined by a characteristic length, $\xi=\frac{1}{H}(\frac{k}{\chi_a})^{0.5}$, where H is the magnetic field strength, k is the Frank elastic constant, and χ_a is the magnetic susceptibility anisotropy. Although optical microscopy has been used to measure elastic anisotropy via the ellipiticity of a closed wall in small molecule liquid crystals (SMLCs), because of low spatial resolution, this method offers little information about the detailed molecular orientation across the inversion walls[7]. The lamellar decoration technique permits high resolution imaging of the director field via TEM[12], SEM or AFM. Through the measurement of director field around a disclination, the value of elastic anisotropy may be obtained[13]. Some 'average' elastic constants of main chain thermotropic liquid crystal polymers were recently obtained from TEM and SEM utilizing lamellar decoration of the wall structure with the assumption of equal splay and bend constants.[2,4]

The present work concerns the influence of elastic anisotropy on the structure of Néel inversion walls. We present the numerical solutions for the director field across Néel inversion walls with elastic anisotropy. These solutions combined with the lamellar decoration technique of Thomas and Wood[12] permit quantitative measurement of the bend-

to-splay elastic anisotropy. Knowledge of the magnetic susceptibility anisotropy allows and the determination of absolute value of the elastic constants.

4.2 Director distribution equations of inversion walls

4.2.1 Equi-constant Inversion Wall

In a thin film, the director may be confined to lie in the plane of the film. In this case, the director has only one degree of freedom, ϕ, the angle with respect to some fixed axis contained in the plane. Assuming the field* is along the z-direction and the director is confined to the zx plane, a bend-splay (Néel bend) wall parallel to field and a splay-bend (Néel splay) wall normal to field may be formed (see figure 4.1). If the director, ϕ, is a function of x only, the equilibrium nonlinear differential equation of Néel bend (bend-splay) wall is given by[1]

$$\chi_a H^2 \sin\phi\cos\phi - k_{11}\cos\phi\frac{d}{dx}(\cos\phi\frac{d\phi}{dx}) - k_{33}\sin\phi\frac{d}{dx}(\sin\phi\frac{d\phi}{dx}) = 0 \quad . \tag{4.1}$$

For the equal elastic constant approximation, $k_{11}=k_{33}=k$, the equation simplifies to

$$\chi_a H^2 \sin\phi\cos\phi - k_{11}\frac{d^2\phi}{dx^2} = 0 \quad , \tag{4.2}$$

which can be solved subject to the boundary conditions,

---

* Either a magnetic field or an elongational flow field. The differential equation governing for the director field under magnetic and flow fields is:[14]

$0 = [(\alpha_3-\alpha_2)\frac{\partial}{\partial t} - k(\frac{\partial^2}{\partial x^2} + \frac{\partial^2}{\partial y^2})]\phi + \chi_a H^2 \sin(\phi - \phi_H)\cos(\phi - \phi_H) - 2(\alpha_3+\alpha_2)\,\dot{e}\sin\phi\cos\phi$

$- 2\gamma(\alpha_3\cos^2\phi - \alpha_2\sin^2\phi)$. The effect of elongational flow on the director fields is expected to be analogous to that of an applied magnetic field. Hudson and Thomas[2] exploited this correspondence to observe texturing of defects in nematic liquid crystal polymer. They found many inversion walls and characteristic disclination clusters in both types of fields.

$$\phi(x=-\infty)=0,\ \phi(x=+\infty)=\pm\pi,\quad \frac{d\phi}{dx}(x=-\infty)=\frac{d\phi}{dx}(x=+\infty)=0. \tag{4.3}$$

The solution first obtained by Helfrich is $\phi=2\tan^{-1}(\exp(\pm\frac{x}{\xi})$, where ξ is the characteristic length and equal to $\frac{1}{H}(\frac{k_{11}}{\chi_a})^{0.5}$ and 2ξ is a measure of the wall thickness. In the general case, the quantitative director orientation across the inversion wall with different values of the bend and splay constants has not been reported yet.

4.2.2 Néel inversion wall with elastic anisotropy

We introduce the elastic anisotropy, $\varepsilon=\frac{k_{11}-k_{33}}{k_{11}+k_{33}}$, a new characteristic length $\zeta=\frac{1}{H}(\frac{k_{11}+k_{33}}{\chi_a})^{0.5}$, and the dimensionless distance $x'=x/\zeta$, such that the differential equation of the Néel bend wall (more bend character in the bend-splay wall) can be rewritten as

$$\sin\phi\cos\phi+\varepsilon\sin\phi\cos\phi\,(\frac{d\phi}{dx'})^2+(\varepsilon\sin^2\phi-\frac{1+\varepsilon}{2})\frac{d^2\phi}{dx'^2}=0 \tag{4.4}$$

The differential equation (4.4) can be solved using the Runge-Kutta method for different values of the elastic anisotropy, ε. Since the director field across the wall should be symmetric, the director orientation only needs to be calculated from a sufficiently distant location x'_f, such that $\phi(x'_f)\approx 0$, up to the center of the inversion wall where $\phi(0)=\pi/2$. In practice, the differential equation is solved from $x'=-5$ (where the initial director orientation is guessed) to $x'=0$. If $\phi(x'=0)\neq\pi/2$, a new initial value of director orientation is chosen and the director orientation is calculated until the director angle is equal to $\pi/2$ at $x'=0$ (within .05% error). Solutions of $\phi(x')$ are shown in figure 4.2(a). As expected, the solutions show that the director field across the inversion wall depends significantly on the elastic anisotropy. The change of director orientation is almost constant for easy splay ($\varepsilon=-1$) from the center of the inversion wall until $x'\approx 1.5$, whereas the change of the director is rather continuous until $x'\approx 2.5$ for the easy bend case ($\varepsilon=1$). The director trajectories of Néel bend wall are plotted in figure 4.2(b). Because equation (4.4) cannot be solved for $\varepsilon=-1$, we used the approximation $\varepsilon=-0.99$ for the numerical calculation.

For the Néel splay wall, the differential equation of the inversion wall is identical to equation (4.1) except k_{11} and k_{33} are switched. Solutions of $\phi(x')$ are thus the same, except the elastic anisotropies are switched. That means the change of director orientation is almost constant for easy bend from the center of the inversion wall until $x' \approx 1.5$, whereas the change of the director is rather continuous until $x' \approx 2.5$ for the easy splay case (see figure 4.2(a)). The director trajectories of a Néel splay wall are precisely orthogonal to the director trajectories of a Néel bend wall and the magnetic field direction is rotated by 90 degrees with respect to the wall direction. It is evident from figure 4.2(b) of a Néel bend wall, that for $\varepsilon \approx -1$ (easy splay), the molecules align with the field more slowly than for the $\varepsilon \approx +1$ (easy bend) case, whereas from figure 4.2(c), in a Néel splay wall, the opposite is true.

4.3 Experiment and analysis

Inversion wall structures of two nematic main chain thermotropic liquid crystalline polymers are analyzed. A semiflexible main chain polyether (TPP5) has been supplied by Prof. Percec:

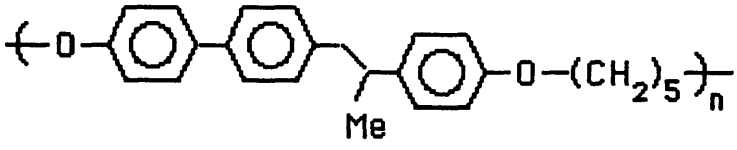

The crystal to nematic transition temperature is 148°C and the nematic to isotropic transition occurs at 180°C.

The specimen previously examined in Hudson et al.[2] was a random terpolymer of equal molar amounts of hydroxybenzoic acid, hydroquinone, and pimelic acid (HBA/HQ/DA):

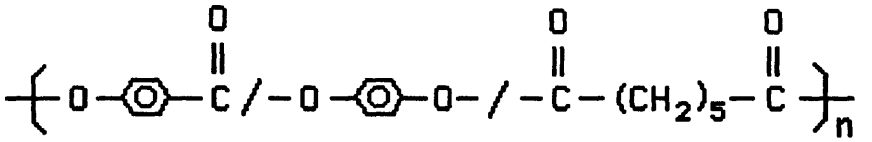

Its number average molecular weight is 3,000, and the crystal to nematic transition is 180°C and the nematic to isotropic transition is 250°C.

A 1-2μm thin film of each polymer was first sheared with a razor blade on a glass slide in the liquid crystalline state. In order to create inversion walls, the specimen was aligned in a 13.5 T magnetic field which was oriented in the plane of the specimen and perpendicular to the initial shearing direction. The sample was placed in the field for 30 minutes at 160°C for the TPP5 polymer and for 30 minutes at 230°C for the HBA/HQ/DA polymer and then quenched to room temperature at a rate of ~10°C/sec with a flow of nitrogen gas. After appropriate annealing, the quenched glassy nematic polymer partially crystallizes into a lamellar morphology. The variations in the director field are easily rendered visible by the lamellae, which are perpendicular to the local director.[12]

A Néel splay inversion wall which is normal to the field appears as a Néel bend wall in the AFM (or SEM[2]) image due to the orthogonal relation between the long axis of the lamellae and the director. Conversely, a wall parallel to the field is a Néel bend wall, which appears as a splay wall in the image of the lamellae. A different curvature of the lamellae in the two types of Néel walls would directly indicate different value of elastic anisotropy as shown in figure 4.1.

Detailed measurements of $\phi(x')$ were made as a function of distance from straight sections of π inversion walls oriented approximately parallel to and normal to the magnetic field. It is straightforward to qualitatively estimate the sign of ε, i.e., easy bend or easy splay, from the curvature of the director with respect to position. The width of the inversion walls was fit by trial and error to determine the value of elastic anisotropy. Note the orthogonal relationship between molecular trajectories and lamellae, and the reversed sign of elastic anisotropy of the Néel bend and Néel splay wall from the differential

equation. For example, the curvature of the lamellae imaged of a portion of Néel splay wall of the TPP5 polymer in figure 4.3(a) appears to be similar to the director trajectories within the range of $-1<\varepsilon<0$ in figure 4.1(a) of the Néel bend wall. This means that for TPP5 $k_{33}<k_{11}$. Open circles in figure 4.2(a) show the values of director orientation with respect to the dimensionless distance, $\phi(x')$. The measured elastic anisotropy is therefore approximately 0.5, i.e. $k_{11} = 3k_{33}$. The (new) characteristic length, ζ, was found to be 450 nm. Using a typical value of χ_a, which is on the order of $1.0 \cdot 10^{-7}$ emucgs/g for semiflexible main chain liquid crystal polymers,[15] and assuming a density of 1.0 g/cm^3, gives approximate values of $k_{11} = 2.8 \cdot 10^{-6}$ dyne and $k_{33} = 0.9 \cdot 10^{-6}$ dyne, respectively. These values are typical of small molecule and semi-flexible polymer nematics.

The $\phi(x')$ data from Hudson et al.[2] indicate the elastic anisotropy of HBA/HQ/PA is approximately zero (figure 4.2(a)), which is quite compatible with the result from previous measurements on the director field distribution around a disclination in this polymer.[13] The estimated average elastic constant for HBA/HQ/PA was determined as $2.3 \cdot 10^{-6}$ dyne.

4.4 Discussion

From our analysis, the width of both Néel bend and Néel splay walls is expected to be the same in a given specimen since both the splay and bend elastic constants enter into the characteristic width of the wall. Comparing the new characteristic length, which we call $\zeta = \frac{1}{H}\left(\frac{k_{11}+k_{33}}{\chi_a}\right)^{0.5}$, which combines both the splay and bend constants, with the characteristic length of the equal elastic constant case, $\xi = \frac{1}{H}\left(\frac{k_{11}}{\chi_a}\right)^{0.5}$ shows that $\zeta = \sqrt{2}\,\xi$ when the elastic constants are equal. Thus, the average elastic constant obtained from measurement of the characteristic length is the arithmetically average instead of a geometric average or some other average.

Although the Néel inversion (splay/bend) walls have been theoretically recognized by Helfrich, details on the molecular trajectory of Néel inversion walls have been seldom

reported[2-4] or distinguished, especially for the Néel splay wall. The Néel bend and Néel splay wall are quite distinct and they are easily identified via AFM (figure 4.3(a)/(b)) or SEM images for samples which exhibit lamellar decoration.

The AFM image in figure 4.3(a) also shows the height profile of the upper (free) surface of the sample containing a portion of Néel splay wall in a thin region of the TPP5 sample. The width of the inversion wall is around 1.5 μm and the maximum height variation across wall is 0.015 μm. It is evident that the deformation of director across the inversion wall is approximately two dimensional.

Since the twist elastic constant is usually the smallest in liquid crystals, twist deformation of the molecules should be considered. The equilibrium shape of closed inversion twist wall loops created by Freedericks transition is predicted to be elliptical.[16] Figueiredo Neto et al.[8] have calculated that twist deformation would lower the Néel bend wall energy during the Freedericks transition. However, the three dimensional solution for Helfrich inversion walls has not yet been solved. A greater difference ($1.5x10^1$ nm) in height is observed across a Néel bend wall in the thicker area of the TPP5 specimen (see figure 4.3(b)). This suggests that out of plane twist deformation may take place in thicker regions. Understanding such three dimensional director patterns provides a new challenge for liquid crystal physics.

4.5 Summary

We numerically solved the differential equation for Néel inversion walls with elastic anisotropy in the thin film (2D) approximation and calculated the director orientation across both Néel bend and Néel splay walls for different values of elastic anisotropy. The elastic anisotropy of liquid crystal polymers may be obtained directly from microscopic images (TEM, SEM, or AFM) of inversion walls by measuring the director orientation with the lamellar decoration technique.[2,4,12] Combined with the measurement of the wall width, which provides the information of the arithmetical average of the splay constant and bend

constant, the absolute value of elastic constants, k_{11} and k_{33}, can be obtained with knowledge of the magnetic susceptibility anisotropy.

References

(1) Helfrich, W. *Phys. Rev. Lett.* **1968**, 21, 1518.

(2) Hudson, S. D.; Vezie, D. L.; Thomas, E. L. *Makromol. Chem., Rapid Commun.* **1990**, 11, 657.

(3) Hudson, S. D.; Thomas, E. L. *Physical Review A* **1991**, 44, 8128.

(4) Ford, J. R.; Bassett, D. C.; Mitchell, G. R.; Ryan, T. G. *Mol. Cryst. Liq. Cryst.* **1990**, 180B, 233.

(5) Meyer, R. B. *Polymer Liquid Crystals*; A. Ciferri; W. R. Drigbaum; R. B. Meyer, Eds; Academic Press: New York, 1982; pp 133.

(6) Sun, Z.; Kléman, M. *Mol. Cryst. Liq. Cryst.* **1984**, 111, 321.

(7) Léger, L. *Mol. Cryst. Liq. Cryst.* **1973**, 24, 33.

(8) Figueiredo Neto, A. M.; Martinot-Lagarde, P.; Durand, D. *J. Physique Lett.* **1984**, 45, L-793.

(9) Kléman, M. *Points, Lines, and Walls*; Wiley: Chichester, 1983;

(10) Mineev, V. P.; Volovik, G. E. *Phys. Rev.* **1978**, B13, 3197.

(11) Frank, F. C. *Disc. Faraday Soc.*, **1958**, 25, 19.

(12) Thomas, E. L.; Wood, B. A. *Faraday Discuss. Chem. Soc.* **1985**, 79, 229.

(13) Hudson, S. D.; Thomas, E. L. *Physical Review Letters* **1989**, 62, 1993.

(14) Stephen, M. J.; Straley, J. P. *Rev. Mod. Phys.* **1974**, 46, 617.

(15) Hardouin, F.; Achard, M. F.; Gasparoux, H.; Liebert, L.; Strzelecki, L. *J. Polym. Sci., Polym. Phys. Ed.* **1982**, 20, 975.

(16) Brochard, F. *J. de Phys.* **1972**, 33, 607.

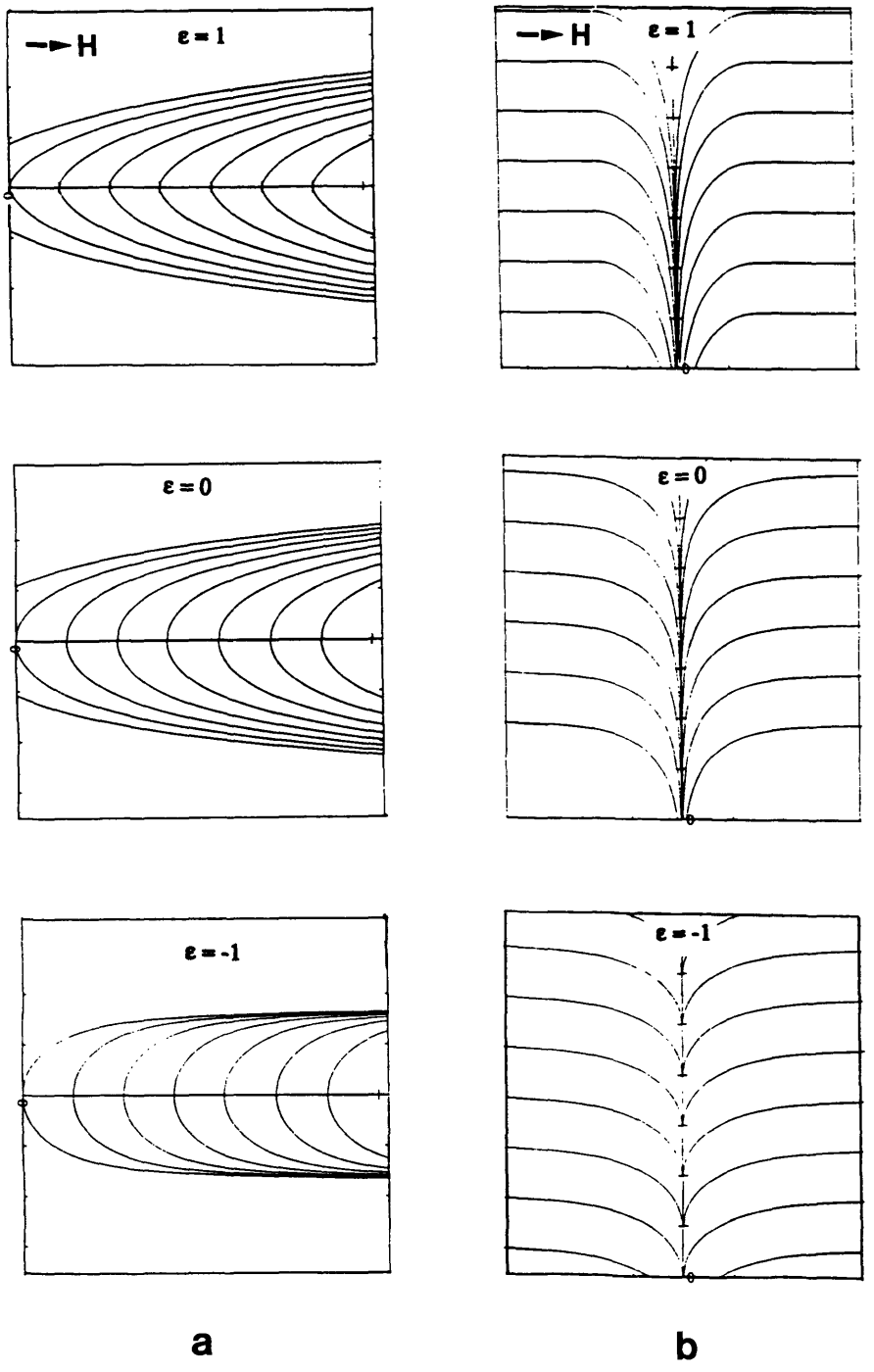

Figure 4.1: Schematics of the molecular director across π inversion walls. (a) Néel bend-splay walls parallel to the field ar different values of elastic anisotropy and (b) Néel splay-bend walls normal to the field at different values of elastic anisotropy. These figures are based on the numerical solutions in figure 4.2.

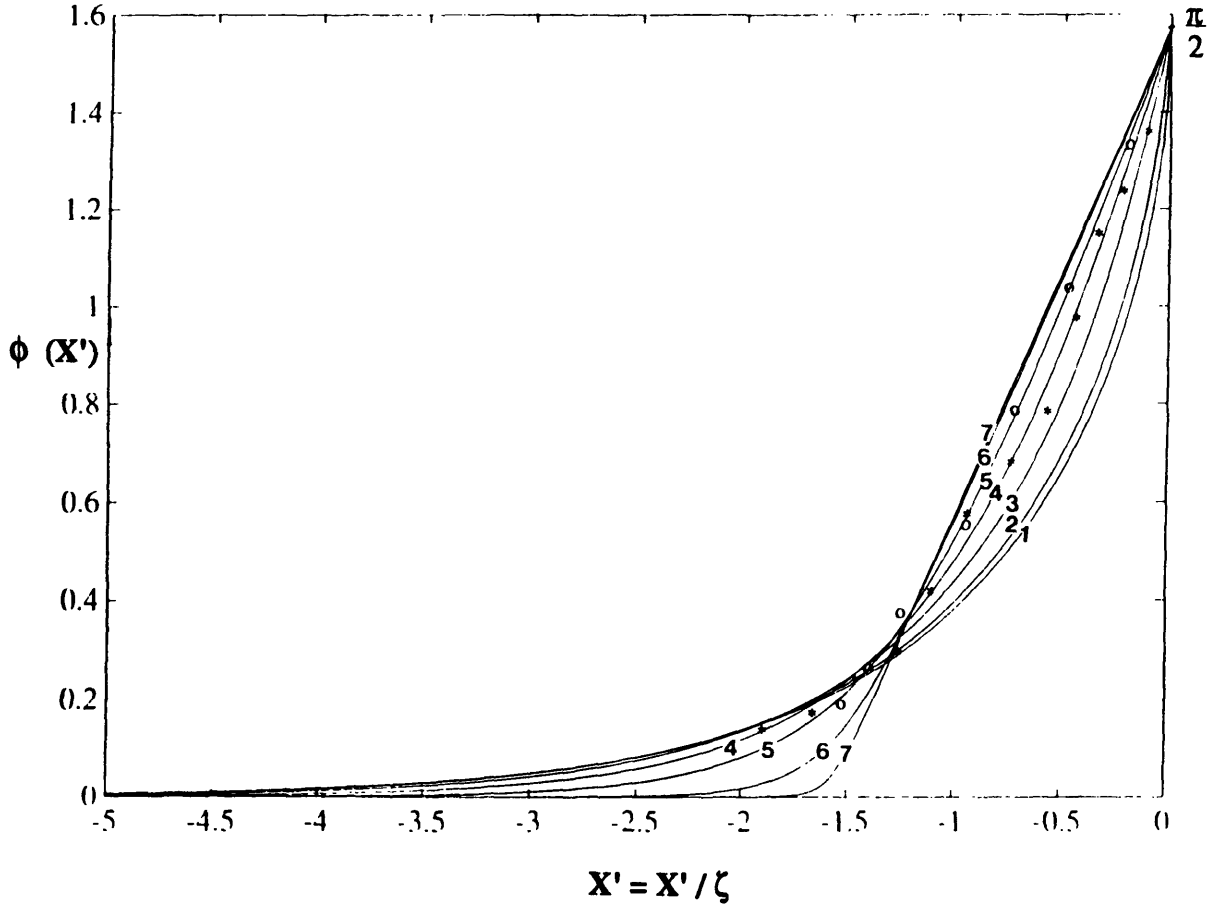

Figure 4.2 (a) Numerical solutions of director fields across Néel bend and Néel splay walls at different values of elastic anisotropy. Curves 1-7 are the solutions of ε = 1, 0.9, 0.5, 0, -0.5, -0.9, and -1 for Néel bend walls, while curves 1-7 correspond to ε = -1, -0.9, -0.5, 0, 0.5, 0.9, and 1, respectively, for Néel splay walls. Open circles and asterisks represent the measured values utilizing the lamellar decoration method for a AFM (see figure 4.3) and HRSEM[2] image. The best fit of the experimental data for TPP5 (open circles) is $\varepsilon \sim 0.5$ and for HBA/HQ/PA (asterisk) is $\varepsilon \sim 0$.

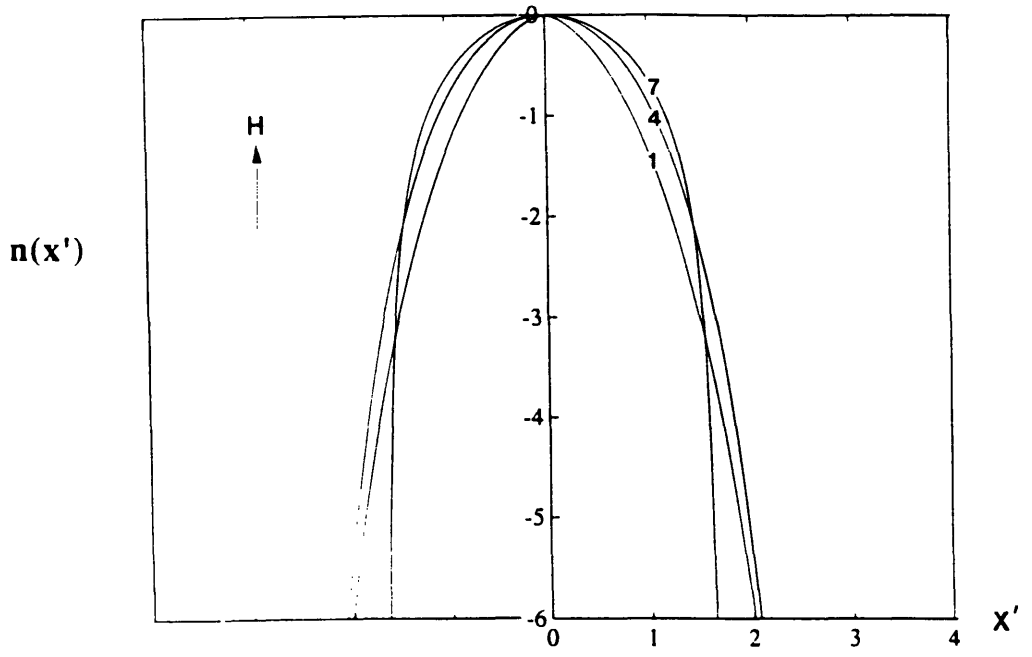

Figure 4.2 (b) Calculated director orientation across Néel bend walls.

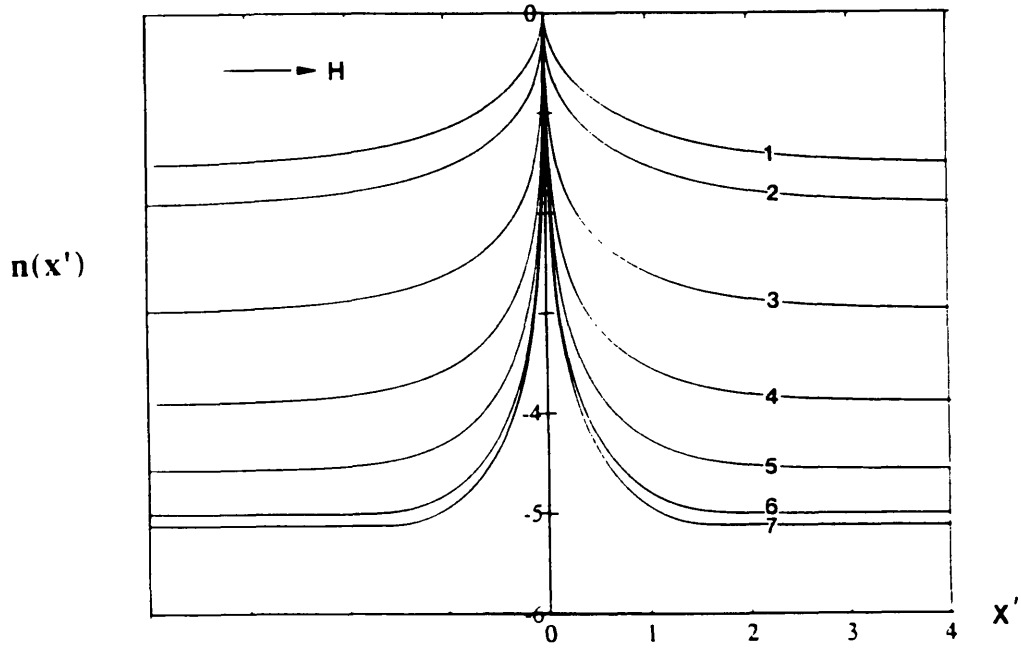

Figure 4.2 (c) Calculated director orientation across Néel splay walls. Curve 1 is the molecular trace for the easy splay case in Néel splay walls. Curve 1 also represents the lamellar image of a Néel bend wall for the easy bend case.

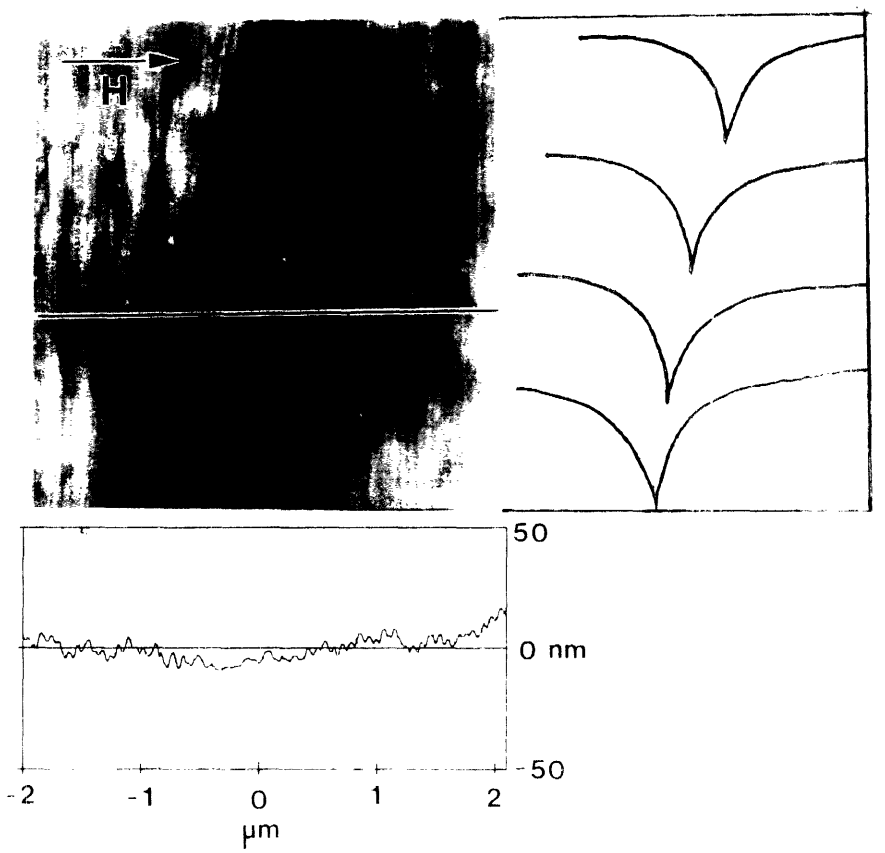

Figure 4.3 (a) AFM micrograph of a portion of the Néel splay inversion wall in TPP5. The observed lamellae are perpendicular to the local molecular director, and the deformation is approximately two dimensional.

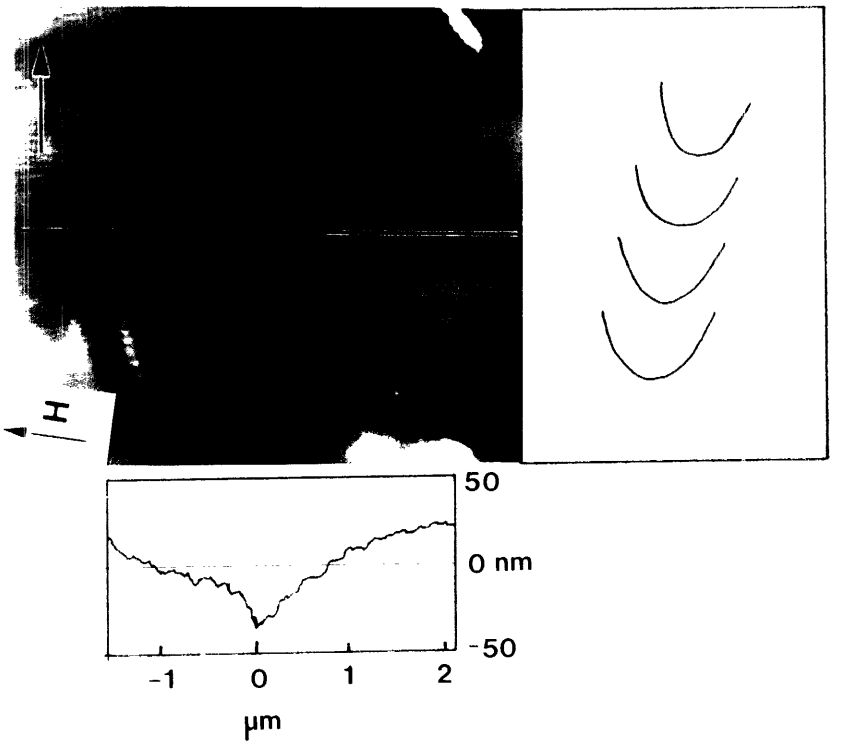

Figure 4.3 (b) Height variation across the Néel bend inversion wall indicating a small amount of out-of-plane (twist) deformation.

CHAPTER 5

CONCLUSIONS AND FUTURE WORK

5.1 Conclusions

This thesis addressed the structures and dynamics of defects, both singular type (disclinations) and non-singular type (inversion walls), in nematic thermotropic liquid crystal polymers. The results provide advancement in the understanding of defects in nematic liquid crystals with or without the presence of an external field. The liquid crystal state of crystallizable liquid crystal polymers can be revealed by SEM and AFM using the lamellar decoration technique, which preserves the nature of the liquid crystal state. This technique has been used to image the director fields of disclinations and inversion walls, which offers detailed information that light microscopy studies with small molecule liquid crystals can not provide.

A schlieren texture composed of only integer strength point disclinations was created by thermal quenching from the isotropic state to the nematic state in a thermotropic liquid crystal polyester. Integer point disclinations are located at the specimen-air interface and arise due to the different boundary conditions, one (homogeneous) at the free surface and one (homeotropic) at the glass-polymer interface. We were able to use the first order red plate and quarterwave plate to determine the sign and structure of the integer point disclinations. The annihilation behavior of disclination pairs was similar to that for point defects in small molecule liquid crystals. The pair separation distance, D, decreased with annihilation time t_0 as $D \sim (t_0-t)^{0.5}$. The coarsening behavior of the schlieren textures we observed is in good agreement with the scaling prediction of asymptotic behavior of disclination density $\rho(t) \sim t^{-1}$.

We characterized the structure of both Néel-bend walls (bend-splay) and Néel-splay (splay-bend) walls, and presented the formation mechanism of inversion wall loops, and

their interaction dynamics. The director patterns of Néel bend and Néel splay inversion walls, which had not been well distinguished before, were identified and imaged at high resolution via a lamellar decoration technique using atomic force microscopy. These inversion walls are metastable, and may shrink, smooth, coalesce, and split into a wall terminated by two opposite sign disclinations to reach the uniform orientation equilibrium state. We gained insight to the inversion wall dynamics and shape evolution of wall loops from the energy calculation of inversion walls with elastic anisotropy.

A solution of the director orientation across Néel inversion walls in a liquid crystal placed in a magnetic field for different values of the elastic anisotropy was also presented. We redefined an appropriate characteristic length, containing the bend, k_{33}, and splay, k_{11}, elastic constants, for the Néel type inversion walls as $1/H((k_{11}+k_{33})/\chi_a)^{0.5}$. The elastic anisotropy of liquid crystal polymers may be obtained directly from microscopic images of inversion walls by measuring the director orientation with the lamellar decoration technique. Combined with the measurement of the wall width, the absolute value of elastic constants, k_{11} ad k_{33}, can be obtained with knowledge of the magnetic susceptibility anisotropy.

5.2 Future work

Although the physics of nematics has been well studied, there are still numerous opportunities for fruitful work. As mentioned, the liquid crystal state of the crystallizable TLCPs can be revealed by SEM and AFM using the lamellar decoration technique. TLCPs are of interest to researchers because of the potential high resolution studies of the transitional states during magnetic orientation. A short section on future work is intended to serve as a general guide in the area of defects in TLCPs, including wall dynamics, the relationship between structure and property, and identification of high strength disclinations.

In view of equal probability of thermal fluctuations in forming the Néel bend wall and the Néel splay wall, transient textures in response to a magnetic reorientation should also have a periodic texture for Néel splay wall along the field. The evolving inversion wall dynamics needs to be explored more. It is interesting to further study such questions as:

1. Does a secondary periodic texture during magnetic reorientation exist? Why not? A periodic transient texture of the Néel splay wall may exist if the bend elastic constant is larger than the splay elastic constant.
2. How does film thickness affect the periodicity of the Néel bend wall and the Néel splay wall?
3. Does the proposed mechanism for interacting inversion walls fit for various times of alignment?
4. Based on the concept of line tension for the inversion wall, does the decrease of total *length*, l, of the inversion wall possess a power law, such as $l \sim t^{-\alpha}$? Here, α is the power law exponent, which may give more information on defect dynamics.
5. Does the breakdown position of an inversion wall segment with production of a pair of disclinations prefer to locate at the Néel bend wall, which is easier through twist wall transition, or at the Néel splay wall, which may possess higher energy?
6. Through the measurement of the motion of a disclination along an inversion wall, it may obtain possible to obtain the rotational viscosity of the polymer. Film thickness, substrate and superstrate may affect the defect motion and should be explored.

We developed a direct method to measure the bend constant and the splay constant for crystallizable thermotropic liquid crystal polymers in chapter 4. If a series of polymers with different types of spacer, spacer length, backbone rigidity and molecular weight were available, this approach provides a direct method to investigate:

1. How the spacer length and backbone rigidity affect both bend constant and splay constant.
2. The influence of molecular weight on the splay constant. Does k_{11} continue to increase or does it level off as the molecular weight increases? If the splay constant levels off, does this imply the presence of main chain hairpin folds?

Because the order parameter strongly depends on temperature and reaches zero at the nematic-isotropic transition temperature, it is also interesting to study the influence of temperature and order parameter on both splay and bend elastic constants. To our knowledge, there have been no studies of this type for TLCP or LLCP materials.

Disclinations with strengths ±1/2 and ±1 in lyotropic or thermotropic nematic polymers have been observed and well characterized through optical *and* electron microscopy. Recently, some higher strength (s=±3/2, 2, 3) disclinations in liquid crystal polymers have been claimed using optical microscopy.[1-3] In my opinion, more careful work is needed to make such claims. The apparent unusual high strength disclinations may result from air bubbles or impurities, which anchor director fields in a specific way. Also, a cluster of disclinations may appear under low resolution observation like a new high strength disclination with the strength the sum of the strengths of the disclinations in the cluster. It is inadequate to claim high strength disclinations with blurred core structures simply by polarized light microscopy observations. The best way to definitively prove the occurrence of high strength disclinations is by the combination of polarized microscopy and a higher resolution microscopy, such as TEM, SEM or AFM.

Since the microstructural scale affects physical properties profoundly, the density of defects and scale of domain size are very important. The defect density, in general, is related to the degree of thermal quenching. In this study, the samples showed no difference in the disclination density among different degrees of thermal quenching. It may be due to very fast annihilation rate and instrumental limitations. It is fundamental to know if disclination density depends on the degree of thermal quenching.

To summarize, this study has explored a few new aspects of structures and dynamics of disclinations and inversion walls. It is still a fruitful area for both fundamental liquid crystal physics and basic polymer science.

References

(1) Viney, C.; Brown, D. J.; Dannels, C. M.; Twieg, R. J. *Liquid Crystals* **1993**, 13, 95.

(2) Witteler, H.; Lieser, G.; Wegner, G.; Schulze, M. *Makromol. Chem., Rapid Commu.*, **1993**, 14, 471.

(3) Zhou, Q.; Wan, X.; Zhang, F.; Zhang, D.; Wu, Z.; Feng, X. *Liquid Crystals* **1993**, 13, 851.